Report No. CDOT-DTD-R-2003-2
Final Report

THREE-DIMENSIONAL LOAD TRANSFER OF COLORADO TYPE 7 AND TYPE 10 RAILS ON INDEPENDENT MOMENT SLAB UNDER HIGH TEST LEVEL IMPACT LOAD

Authors
Nien-Yin Chang, Principal Investigator
Fatih Oncul, Co-Investigator



April 2003

COLORADO DEPARTMENT OF TRANSPORTATION
RESEARCH BRANCH

The contents of this report reflect the views of the author(s), who is(are) responsible for the facts and accuracy of the data presented herein. The contents do not necessarily reflect the official views of the Colorado Department of Transportation or the Federal Highway Administration. This report does not constitute a standard, specification, or regulation.

Technical Report Documentation Page

1. Report No.	2. Government Accession No.	3. Recipient's Catalog No.
CDOT-DTD-R-2003-2		

4. Title and Subtitle	5. Report Date
THREE-DIMENSIONAL LOAD TRANSFER OF COLORADO TYPE 7 AND TYPE 10 RAILS ON INDEPENDENT MOMENT SLAB UNDER HIGH TEST LEVEL IMPACT LOAD	April 30, 2003
	6. Performing Organization Code CGES-0301
7. Author(s) Nien-Yin Chang, Fatih Oncul	8. Performing Organization Report No.
9. Performing Organization Name and Address Center for Geotechnical Engineering Science University of Colorado at Denver Campus Box 113, P. O. Box 173364 Denver, CO 80271-3364	10. Work Unit No. (TRAIS)
	11. Contract or Grant No.
12. Sponsoring Agency Name and Address Colorado Department of Transportation - Research 4201 E. Arkansas Ave. Denver, CO 80222	13. Type of Report and Period Covered
	14. Sponsoring Agency Code

15. Supplementary Notes
Prepared in cooperation with the US Department of Transportation, Federal Highway Administration

16. Abstract

The AASHTO LRFD Bridge Specifications changed the rail impact load requirement ranging from TL1 to TL6 with progressively increasing loads to accommodate heavier vehicles traveling at higher speeds to assure the safety of all traveling motorists and reduce maintenance time. Safety rails are usually top-mounted on retaining walls with independent moment slab and crashing vehicles can severely damage the retaining walls. Besides the safety concerns, the 2000 specs intend to mitigate the severe damage to rails and walls to facilitate cost-effective and speedy repair or reset. In the United States, over two million walls are MSE wall with modulus block facings, which are weaker than the reinforced concrete wall facings in hybrid walls. The Federal Highway Administration recommended the implementation of the 2000 Specs. The AASHTO Specs provide no design details or guidelines, but recommend the use of finite element analysis as a design tool. The consensus from the survey of all state DOT's indicates that the inertia resistance of rail-slab-wall systems should be included as resistance to the rail movement under high impact loads. Finite element analyses were performed to assess the need for design guidelines revisions to address the need for the high impact loads resistance enhancement. This study uses the three-dimensional nonlinear finite element program, NIKE-3D, to assess the performance of Colorado Type 7 and Type 10 rails under different impact loads. Results show that the 200-ft length is the minimum length requirement and the rail end (or edge) needs strong foundation support.

Implementation:
CDOT has already begun the implementation of the 200-ft minimum rail length requirement and the examination of of the need for foundation improvement at the rail end and the anchor for rail stability enhancement and displacement reduction. The research proposal for further study of rail stability enhancement submitted by CDOT has been recommended for funding by the NCHRP advisory committee.

17. Keywords	18. Distribution Statement
safety rails, high test level loads, influence length, MSE walls, geogrid, Type 7, Type 10, moment slab, backfill, FEM, stresses, displacements	No restrictions. This document is available to the public through the National Technical Information Service 5825 Port Royal Road Springfield, VA 22161

19. Security Classif. (of this report)	20. Security Classif. (of this page)	21. No. of Pages	22. Price
None	None	135	

Form DOT F 1700.7 (8-72) Reproduction of completed page authorized

THREE-DIMENSIONAL LOAD TRANSFER OF COLORADO TYPE 7 AND TYPE 10 RAILS ON INDEPENDENT MOMENT SLAB UNDER HIGH TEST LEVEL IMPACT LOAD

by

Principal Investigator
Nien-Yin Chang, Professor
Center for Geotechnical Engineering Science
University of Colorado at Denver
Co-Investigator
Fatih Oncul, Assistant Professor
Fairleigh Dickinson University

Report No. CDOT-DTD-R-2003-2

Prepared by
Colorado Department of Transportation
Research Branch

Sponsored by the
Colorado Department of Transportation
In Cooperation with the
U.S. Department of Transportation
Federal Highway Administration

April 2003

Colorado Department of Transportation
Research Branch
4201 E. Arkansas
Denver, CO 80222
(303) 757-9506

ACKNOWLEDGEMENTS

The study addresses the problem associated with the implementation of the new Test Level impact loads for the highway safety rail design in the AASHTO 2000 LRFD Bridge Design Specifications. The difficulty arises from the lack of detailed design specifications in the AASHTO 2000 code to serve as the design guide for bridge design engineers. The members of the study panel including Trever Shing-Chun Wang[1], Michael McMullen[2], Naser Abu-Hejleh[3], Richard Griffin[4], and Matt Greer[5], have provided a genuine collaborative effort in guiding the direction of this research as demonstrated in the evolution process of this research. Their contribution toward the successful conclusion of the research is hereby acknowledged. Also acknowledged is Dr. Trever Wang's insight and research idea for the rail design under high impact loads. The Colorado Department of Transportation and the Federal Highway Administration sponsored the study. This joint sponsorship is greatly appreciated.

[1] Senior Bridge Engineer, CDOT, 4021 E. Arkansas Ave., Denver, CO 80222, Tel: 303-512-4072; Email: ShingChun.Wang@dot.state.co.us

[2] Senior Bridge Engineer, CDOT, 4021 E. Arkansas Ave., Denver, CO 80222, Tel: 303-757-9587; Email: Michael.McMullen@dot.state.co.us

[3] Research Engineer, CDOT, 4021 E. Arkansas Ave., Denver, CO 80222, Tel: 303-757-9522; Email: naser.abu-hejleh@dot.stte.co.us

[4] Director, CDOT Research Branch, 4021 E. Arkansas Ave., Denver, CO 80222, Tel: 303-757-9522; Email: Richard.Griffin@dot.state.co.us

[5] Colorado Regional Manager, FHWA, Tel: 303-969-6730, Email: matt.greer@fhwa.dot.gov

EXECUTIVE SUMMARY

The AASHTO 2000 LRFD Bridge Specifications raise the rail impact load requirement to TL1 to TL6 with progressively increasing magnitude to accommodate heavier vehicles traveling at higher speeds to prevent an errant vehicle from leaving the road and serious injury or death to the occupants. This is to assure the safety of all traveling motorists and to reduce the maintenance time required to fix any damage caused by crashing vehicles. Safety rails are usually top-mounted on retaining walls and crashing vehicles can severely damage the retaining walls. Besides the safety enhancement, the new design specifications intend to mitigate the severe damage to rails and supporting retaining walls so that rail-wall system can be repaired and/or reset with minimal time and cost.

In the United States, more than 7,500,000 square feet of MSE walls with precast panel facings are constructed annually, equivalent to about half of all retaining walls for transportation applications. Out of these walls, more than 2,000,000 square feet have modular concrete block facings, which by nature are not as strong as the reinforced concrete wall facings in hybrid walls. To avoid severe wall damage during the vehicle crashing, top-mounted traffic barrier rails are connected monolithically to continuous footings (named anchor slab, moment slab, or sleeper slab). However, the AASHTO 2000 LRFD Specifications provide no design details or guidelines for the top-mounted rails on MSE walls under high impact loads, but recommended using finite element analysis as a design tool.

Through Dr. Naser Abu-Hejleh's initiative, CDOT queried the other 49 states, FHWA, and AASHTO regarding this problem and the design specifications as approved in the AASHTO 2000 LRFD specifications. The consensus is that the current design specifications do not account for the added resistance from the additional stiffness and mass inertia of a continuous

three-dimensional rail-wall system, which can add significantly to the system's ability to resist the impact forces. The latest version of LRFD recommends the FE solution.

Following the AASHTO design procedures for 10 kips impact load does not yield reasonable and economical designs for the high impact load. In practice, the wall system suppliers provide most of the designs for the traffic barrier/anchor slab systems during the submittal of shop drawings. Since the AASHTO LRFD 2000 Specification are **silent** on the rail impact load distribution and transfer, the design details provided by vendors are both non-uniform and incomplete. Thus, design details backed by comprehensive research are urgently needed and this study is important to public highway safety and maintenance operations.

This CDOT-sponsored project aims to assess the sufficiency of the current rail-wall system design specifications for the high impact load situation and, if found insufficient, to provide the enhancement mechanism for implementation in the state for the design of rail-wall systems under high impact loads as specified by AASHTO and mandated by FHWA. CDOT elected to study the performance of its Type 7 rail with Jersey concrete barriers and Type 10 rail with steel traffic barriers under high impact loads.

Initially the CDOT study panel and the CU-Denver research personnel agreed to perform the finite element analysis on 20-ft rails on MSE walls. In all analyses, the rail impact load was applied to the rail system as specified by AASHTO in terms of magnitude and its point of application. In a pseudo static condition, the soil-moment slab interface frictional resistance (or soil-slab interface frictional resistance or SSIFR) and the moment resistance constitute the

resistance to impact load, and under a dynamic impact condition, the rail-slab inertia force is added to resist the rail movement. The following analyses were performed in this study:

- Pseudo static analyses of 20-ft Type 7 and Type 10 rails under TL4 load.
- Pseudo static and impact analyses of 40-ft Type 7 and Type 10 rails under TL4 load.
- Pseudo static analyses of 400-ft Type 7 and Type 10 rails on the SGI workstations at the University of Colorado at Denver for influence length evaluation under TL5a.
- Pseudo static analyses of 200-ft Type 7 and Type 10 rails under TL5a on the Cray T90 supercomputer at the University of California at San Diego.

The analysis results showed gross instability of both 20-ft and 40-ft rails under TL-4. In fact, the rails, upon application of either pseudo-static or dynamic impact load as specified in the AASHTO 2000 LRFD Bridge Design Specifications, first rotate about their heels and eventually gain momentum and fly off the MSE walls. To investigate the effect of the dynamic impact load, the analysis uses the time history of the impact load extracted from the results of the field crash tests performed by the Texas Transportation Institute (TTI). The results of analysis show that the rails suffer the similar fate, gross displacement and flying off.

A decision was then made jointly to assess the influence length under TL-5.A using 400-ft rails. In the case of Type 7 rail, at 100 feet from the point of application of the pseudo-static impact load at its mid-span, the transverse displacements become tolerable, and the rails are resetable and no longer fly off the wall. Thus, the length of 200 feet is chosen as the influence length for Type 7 rail subjected to the impact load at the mid-span. Under the same loading condition, the Type 10 rail suffered a larger rotation, rail bending, transverse displacement and

base lifting than the Type 7 rail. When the impact load is applied at an end of either rail types, the rail rotation, bending, twisting, transverse displacement, and base lifting are found to be excessive and unacceptable with the Type 7 rail being less severe. To maintain consistency in analysis, the research group chose 200 feet as the influence length for both rail types and additional analyses were performed on the 200-ft rails.

Pseudo static analysis results show that the rotation, twisting, transverse displacement, and base lifting displacement of the 200-ft Type 7 and Type 10 rail systems sitting on 20-ft high MSE walls are close to the tolerable magnitude and the rails no longer fly off the wall when the impact load is applied at the mid-span of the rails. The rail-end application of the impact load still produces unacceptable performance with the Type 10 rail being more excessive. In the final analyses of 200-ft rail-wall systems, the problems became too large for the SGI workstations at the University of Colorado at Denver and all analyses require the Cray T90 supercomputer at the San Diego Supercomputer Center.

IMPLEMENTATION PLAN

The constant participation of the CDOT and FHWA research panel members and the PI's presentation of the research findings at the Annual Bridge Communication Week have contributed to the progressive implementation of the research findings before the completion of this study. CDOT had already begun the implementation of the 200-ft minimum rail length requirements and the examination of the need for the foundation improvement at the rail end and the anchor of the rail-system for the rail stability enhancement and displacement reduction. The research proposal for further study of rail stability enhancement submitted by CDOT has been recommended for funding by the NCHRP advisory committee.

TABLE OF CONTENTS

1.0 INTRODUCTION 1

1.1 Problem Statement 1

1.2 Objectives 2

1.3 Research Approach 3

1.4 Research Tasks 5

1.5 Projected Benefits 5

2.0 REVIEW OF PREVIOUS STUDIES 6

3.0 FINITE ELEMENT ANALYSES 18

3.1 Introduction and History of Analysis 18

3.2 Background Theory for NIKE3D Computer Code 19

3.2.1. Solution Procedure 19

3.2.2. Element Library 20

3.2.3. Interface Formulation In NIKE3D 20

3.3 Material Models and Model Parameters 23

3.3.1. Ramberg Osgood Non-Linear Model 23

3.3.2. Oriented Brittle Damage Model 25

3.4 AASHTO Rail Test Level Load and Transient Collision Load History 26

3.5 Moment Slab vs. Backfill Frictional Resistance 27

3.6 Finite Element Analysis for Performance of Rail and Load Transfer 29

3.6.1. 20-ft Rail with the Centrally Imposed TL4 Impact Load 29

3.6.2. 40-ft Type 7 Rail with Pseudo-Static and Dynamic TL4 or TL5a at Rail Center/Edge 33

3.6.2.1 40-ft Type 7 Rail under Static TL4 Load at Center 36

3.6.2.2 40 ft Type 7 Rail under TL4 Impact Load at Center 39

3.7 Conclusions 45

4.0 INFLUENCE LENGTH AND IMPACT PERFORMANCE OF RAILS 47

4.1 Influence Length Evaluation Using 400-ft Rails 47

4.2 Analysis Results and Discussions for the Influence Length of 400-ft Rails 48

4.2.1. Type 7 Rail with Static Center Load Application 50

4.2.2. Type 7 Rail with Static Edge Load Application 56

4.2.3. Type 10 Rail with Center Load Application, OBF Concrte, R-O Soil And EP Steel Rail 60
4.2.4. Analysis with E Concrete, R-O Soil, and EP Steel Rail 70
4.3 Analysis Program, Results, and Discussions for 200-ft Type 7 and Type 10 Rails on MSE Walls 72
4.3.1 Type 7 Rail with Jersey Barrier 73
4.3.2 Type 10 Steel Rail 76
5.0 RECOMMENDATIONS FOR IMPLEMENTATION AT CDOT 80
6.0 SUMMARY, CONCLUSIONS, AND RECOMMENDATIONS 82
6.1 Summary 83
6.2 Conclusions 84
6.3 Recommendations for Further Study 86
REFERENCES 87
APPENDIX A - FIGURES FOR 40-FT TYPE 7 RAIL A-1
APPENDIX B - FIGURES FOR 400-FT TYPE 7 & TYPE 10 RAILS B-1

LIST OF FIGURES

Fig. 1-1 CDOT Rail System....3
Fig. 2-1 Lateral Force on Wall Segment B for Test 3451-34....11
Fig. 2-2 Lateral Force on Wall Segment C for Test 3451-34....11
Fig. 2-3 Lateral Force on Wall Segment D for Test 3451-34....12
Fig. 2-4 Total Lateral Force on Wall for Test 3451-35....12
Fig. 2-5 Lateral Force on Wall Segment A for Test 3451-35....13
Fig. 2-6 Lateral Force on Wall Segment B for Test 3451-35....13
Fig. 2-7 Lateral Force on Wall Segment C for Test 3451-35....14
Fig. 2-8 Summary of Results for Test 3451-35....15
Fig. 2-9 New Jersey Shape Concrete Safety Barrier (Turner Fairbanks Highway Research Center)....16
Fig. 3-1 1-D, 2-D and 3-D Element library of NIKE3D....20
Fig. 3-2 Contact of node m with segment of jk[3]....21
Fig. 3-3 Penetrating of node m into the adjacent material boundary....23
Fig. 3.4 Test Load Location (AASHTO Table A12.2.1)....28
Fig. 3-5 Fictional resistance versus Length of Jersey Barrier....29
Fig. 3-6 Front view of conventional T wall and 20-ft long jersey barrier....30
Fig. 3-7 3-dimensional finite Element Modeling of Conventional T Wall w/o Tensile inclusions....31
Fig. 3-8 Gravitational load factor and impact load versus time....32
Fig. 3-9 Location of Node 158 selected for horizontal displacement time history....33
Fig. 3-10 Horizontal displacement time history of Node 158....33
Fig. 3-11 Front view of 40-ft long jersey barrier with MSE wall....34
Fig. 3-12 3-dimensional Finite Element Modeling for Type 10 (Steel) Impact Rail (backfill soil elements to be added)....35
Fig. 3-13 3-dimensional Finite Element Modeling for the Type 7 (Concrete) Impact Rail with tensile inclusions....35
Fig. 3-14 Gravitational acceleration load factor versus time....35
Fig. 3-15 Impact load factor versus time....36

Fig. 3-16 Transverse displacement of edge and corner nodes of Type 7 barrier under TL4 37
Fig. 3-17 Wall deflection (TL4, Center Hit, Static) 37
Fig. 3-18 Geogrid stresses along the wall connection (TL4, Center Hit, Static) 38
Fig. 3-19 Earth pressure distribution at four different locations (TL4, Center Hit, Static) 38
Fig. 3-20 Transverse displacement time history of edge and corner nodes of Type 7 Barrier (TL4, Center Hit, Impact) 40
Fig. 3-21 Final wall deflection after impact load (TL4, Center Hit, Impact) 40
Fig. 3-22 Min, Max and 1g geogrid stresses along the wall face (TL4, Center Hit, Impact) 41
Fig. 3-23 Min, Max and 1g earth pressure along the 1st column (TL4, Center Hit, Impact) 41
Fig. 3-24 Min, Max and 1g earth pressure along the 2nd column (TL4, Center Hit, Impact) 42
Fig. 3-25 Min, Max and 1g earth pressure along the 3rd column (TL4, Center Hit, Impact) 42
Fig. 3-26 Min, Max and 1g earth pressure along the 4th column (TL4, Center Hit, Impact) 43
Fig. 3-27 Min, Max and 1g vertical soil pressure along the1st column (TL4, Center Hit, Impact) 43
Fig. 3-28 Min, Max and 1g vertical soil pressure along the 2nd column (TL4, Center Hit, Impact) 44
Fig.3-29 Min, Max and 1g vertical soil pressure along the 3rd column (TL4, Center Hit, Impact) 44
Fig. 3-30 Min, Max and 1g vertical soil pressure along the 4th column (TL4, Center Hit, Impact) 45
Fig. 4-1 Front view of 400-ft long (a) Type 7 and (b) Type 10 guard rails 47
Fig. 4-2 Deformed shape of Type 7 rail under TL5a load. (Displacements are Scaled by 100 times) 48
Fig. 4-3 Three components of TL5a load for Type 7 Rail 48

Fig. 4-4 Reference locations for the data presentation of Type 7 barrier 50
Fig. 4-5 Normal Stress components along point A of Type 7 Rail (400-ft, Center Hit, Static, TL5a).....52
Fig. 4-6 Normal Stress components along point B of Type 7 Rail (400-ft, Center Hit, Static, TL5a).....52
Fig. 4-7 Normal Stress components along point C of Type 7 Rail (400-ft, Center Hit, Static, TL5a).....53
Fig. 4-8 Shear Stress components along point A of Type 7 Rail (400-ft, Center Hit, Static, TL5a).....53
Fig. 4-9 Shear Stress components along point B of Type 7 Rail (400-ft, Center Hit, Static, TL5a).....54
Fig. 4-10 Shear Stress components along point C of Type 7 Rail (400-ft, Center Hit, Static, TL5a).....54
Fig. 4-11 Displacement components at point A of Type 7 Rail (400-ft, Center Hit, Static, TL5a) 55
Fig. 4-12 Displacement components at point B of Type 7 Rail (400-ft, Center Hit, Static, TL5a) 55
Fig. 4-13 Displacement components at point C of Type 7 Rail (400-ft, Center Hit, Static, TL5a) 56
Fig. 4-14 Locations of A, B, C, and D for data presentation of Type 10 barrier.....60
Fig. 4-15 Normal Stress components at point A of Type 10 Rail (400-ft, Center Hit, Static, TL5a) 61
Fig. 4-16 Normal Stress components at point C of Type 10 Rail (400-ft, Center Hit, Static, TL5a) 62
Fig. 4-17 Normal Stress components at point D of Type 10 Rail (400-ft, Center Hit, Static, TL5a).....62
Fig. 4-18 Shear Stress components at point A of Type 10 Rail (400-ft, Center Hit, Static, TL5a) 64
Fig. 4-19 Shear Stress components at point C of Type 10 Rail (400-ft, Center Hit, Static, TL5a) 64

Fig. 4-20 Shear Stress components at point D of Type 10 Rail (400-ft, Center Hit, Static, TL5a) 65
Fig. 4-21 Displacement components at point A of Type 10 Rail (400-ft, Center Hit, Static, TL5a) 65
Fig. 4-22 Displacement components at point B of Type 10 Rail (400-ft, Center Hit, Static, TL5a) 66
Fig. 4-23 Displacement components at point C of Type 10 Rail (400-ft, Center Hit, Static, TL5a) 66
Fig. 4-24 Displacement components at point D of Type 10 Rail (400-ft, Center Hit, Static, TL5a) 67
Fig. 4-25 Axial force distribution in beam elements along point B of Type 10 Rail (400-ft, Center Hit, Static, TL5a)....67
Fig. 4-26 Shear force components in beam elements along point B of Type 10 Rail (400-ft, Center Hit, Static, TL5a)....68
Fig. 4-27 Front view of 200-ft long impact barrier with MSE wall 73
Fig. 4-28 Node reference for displacement time histories (Type 7) 64
Fig. 4-29 X Displacement time history of selected nodes (Type 7) 64
Fig. 4-30 Z Displacement time history of selected nodes (Type 7)....75
Fig. 4-31 Geogrid stresses along the wall face (Type 7) 75
Fig. 4-32 Earth pressure along the wall face (Type 7)....76
Fig. 4-33 Node reference for displacement time histories (Type 10) 77
Fig. 4-34 X Displacement time history of selected nodes (Type 10) 77
Fig. 4-35 Z Displacement time history of selected nodes (Type 10)....78
Fig. 4-36 Geogrid stresses along the wall face (Type 10) 78
Fig. 4-37 Earth pressure along the wall face (Type 10)....79

LIST OF TABLES

Table 2-1 Summary of Test on Instrumented Wall 9
Table 2-2 Vehicle Acceleration from Tests on Instrumented Wall 10
Table 2-3 Summary of Data from Instrumented Wall Test Series 10
Table 3.1 Material model parameters used in the analyisis 24
Table 3.2 Impact Load Definitions and Locations (AASHTO Table A13.2.1).....26
Table 3.3 Test conditions, Vehicles Weights and Velocity Definitions (AASHTO Table 3.7.2.1).....26
Table 4-1 Analyses performed for the evaluation of the influence length 50

1.0 INTRODUCTION

1.1 Problem Statement

The current CDOT impact rail design follows the rule specified in the AASHTO Standard Specification - bridge deck overhang design. It is designed to resist a 10-kips impact load. In the latest AASHTO LRFD specification, the impact load requirement was greatly increased. For instance the transverse component of rail impact loads was raised to the range of 13.5 kips in TL1 to 175 kips in TL6. Thus, the 10-kip impact load requirement used in Colorado no longer meets the AASHTO specifications. Unfortunately, the AASHTO LRFD Section 13 on Railing still lacks the design specifics required for a high impact load.

The AASHTO 2000 LRFD specifications state: "For use beyond the design of test specimens with expected failure modes similar to those shown in Figures CA 13.3.1-1 and CA 13.3.1-2, a rigorous yield line solution or a finite element solution should be developed. The procedures in Appendix A are not applicable to traffic railings mounted on rigid structures, such as retaining walls or spread footings, when the cracking pattern is expected to extend to the supporting components." Thus, the answers to the above questions through rigorous finite element analysis are needed for the design of the Colorado Type 7 and Type 10 rails as shown in parts a and b of Figure 1 under the high impact load.

This means the information needed for the design of traffic railings for high impact loads is lacking and there is an urgent need to answer the following critical questions:

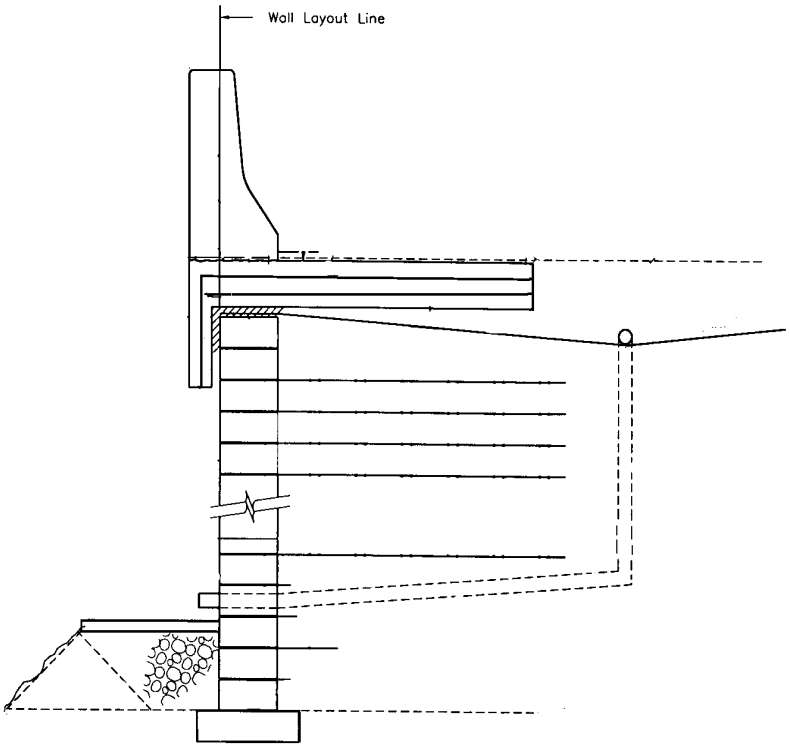
- The transfer of the impact load from rail to moment slab (or sleeper slab), backfill, and MSE walls.
- Effects of the impact load on earth pressure distribution and MSE wall design.
- The extent of damage to both concrete and steel railings under a high impact load.
- The sufficiency of the current CDOT traffic railing design practice in meeting the new AASHTO requirements.

This research examines the impact of the new AASHTO impact load requirement on the design of Colorado Type 7 and Type 10 rails as shown in Figures 1.1a and b.

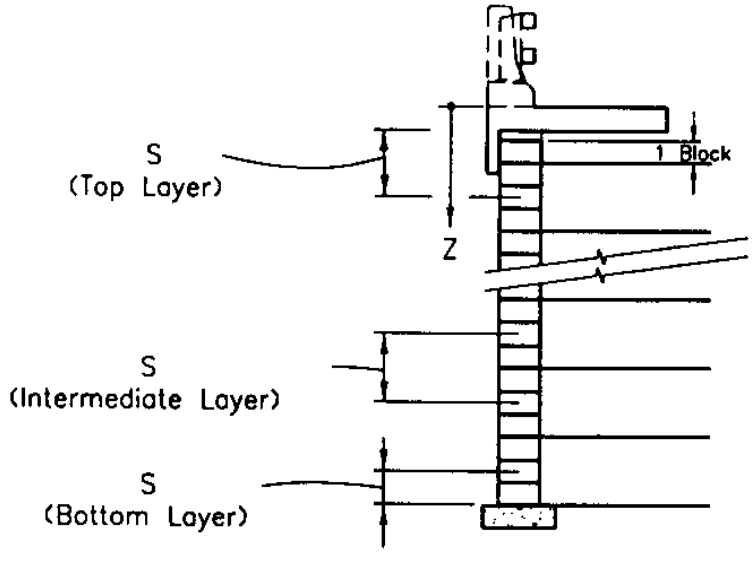
It is therefore proposed to perform a three-dimensional nonlinear finite element analysis to assess the performance of the above-said rails in terms of their stresses and displacements under AASHTO high impact loads. TL4 (kips) and TL5A as specified in the AASHTO 2000 LRFD Specifications are used in the analysis. Such severe impact loads do not apply to all rails but those seated on high bridge approaches or located above a deep canyon. The nonlinear finite element analysis computer code, NIKE3D developed at the Lawrence Livermore National Laboratory, was adopted in this analysis. This 3-dimensional analysis accounts for the added ability of a continuous three-dimensional system in resisting the impact load because of its added stiffness and mass inertia force.

1.2 Objectives

The major objectives of this proposed study are four fold: 1) to assess the ability of the Colorado Type 7 rail with concrete Jersey barrier and Type 10 rail with steel barrier to provide safety to the traveling public under the new AASHTO 2000 LRFD Specifications; 2) to examine the load transfer mechanism from rail to moment slab, backfills and MSE walls; 3) to examine the impact of this new impact load requirement on the design of MSE walls; 4) to recommend new design enhancements for aiding rail safety. In almost all CDOT sponsored research projects, the benefit of research is measured by the cost savings for very justifiable reasons. This research is, however, not going to save dollars in a conventional sense. Instead, safety enhancement is the major benefit of this research project because human life is precious. Besides, providing highway safety to the traveling public is the major CDOT mission.



(a) CDOT Type 7 Rail System (Concrete Barrier).



(b) CDOT Type 10 Rail System (Steel Barrier).

Figure 1: CDOT Rail Systems

1.3 Research Approach

In the past ten years, the NIKE/SSI (NIKE Soil-Structure Interaction) research group at the Center for Geotechnical Engineering Science (CGES) has utilized the NIKE-3D nonlinear finite element analysis computer code in its research efforts on the soil-structure interaction problems under both static and dynamic loads. The NIKE-3D program was developed at the Lawrence Livermore National Laboratory (LLNL) with over 30,000 man hours of highly qualified research scientists. To date, the development effort continues and CGES is collaborating with Dr. Michael Puso through a signed collaborative research agreement with LLNL. NIKLE3D was developed mainly for structural analysis. It is lacking in the constitutive models of soils although over 30 constitutive models are available in the code. Thus, CGES contribution in this collaborative agreement lies in the development of constitutive models and associated drivers. Three drivers for modified Cam Clay model, hybrid Mohr-Coulomb model, and Lade's model have been developed and the effort in their implementation in NIKE3D is progressing. Upon completion, the NIKE3D code will be much more versatile for the analysis of the static and dynamic soil-structure interaction problems.

The NIKE3D with its current capability is used in the study of the Colorado Type 7 and Type 10 rails under high impact load. The rails are integrated to the moment slab monolithically and the rail-slab units are then seated on the backfill of 20-ft high MSE walls with Colorado Class I backfill. Initially the analysis effort focused on the behavior of the rail-slab unit seated on level ground. First, the analysis on 20-ft long rails yielded totally unacceptable performance with the rail simply flying away from the supporting soil. Then the analysis evolved into 40-ft, 200-ft and 400-ft rails. The 400-ft rails were analyzed to determine the appropriate length, named influence length, for use in further study. Beyond the influence length, the impact load causes negligible effect on rail stresses and displacements. The influence was found to be 200 feet. In the final analysis, the 200-ft rail systems were analyzed with the monolithic rail-slab unit seated on the MSE wall backfill. The process was somewhat evolutional because of the lack of knowledge of the appropriate influence length for each rail system of interest.

NIKE3D was chosen for the following capability:

1. Its implicit formulation guarantees the best stable solution.
2. Over 30 material models for different materials.
3. The interface boundary formulation allowing the interface slippage, debonding (separation), and rebonding (re-attachment).
4. The double precision formulation and the capability in solving problems in parallel processors.

1.4 Research Tasks

The performance of the railing systems shown in Figures 1.a (Type 7) and 1.b (Type 10) was analyzed under TL4 and TL5.a impact loads. Major tasks are outlined as follows:

- 3-D finite element models of Colorado Type 7 and Type 10 rail systems
- Selections of material properties and impact load history
- Execution of nonlinear finite element analyses using NIKE3D
- Interpretation of numerical analysis results, and
- Recommendation of new design guidelines for high impact loads.

1.5 Projected Benefits

The guidelines for the design of Colorado Type 7 and Type 10 traffic railings under high impact loads as specified in the AASHTO LRFD 2000 Design Specifications are the major benefit of this research. The research revealed that the current CDOT design guidelines practice for the above-said railings are insufficient in dealing with the design of the above-said railings under the impact load greater than probably TL2. Thus, some improvements are needed for the safe design of traffic railings and this study will provide some preliminary recommendations. Such improved design will result in higher construction costs but a much improved safety of traffic railings.

2.0 REVIEW OF PREVIOUS STUDIES

A literature review shows that most research on rail impact has focused on full-scale crash tests and the Texas Transportation Institute has been the major contributor in this area. To date very little information is found on the rail impact research using numerical analysis. Numerical analyses, when performed appropriately, will provide the assessment of the effect of high impact loads on traffic rail behavior and design and also will provide information on stress and strain distributions, which can assist in selecting appropriate types of and locations for instrumentation in the full-scale tests. This chapter summarizes the findings from an extensive review of literature.

The information from the review is synthesized to provide guidelines for the direction and extent of research on Colorado Type 7 and Type 10 safety rail upon the effect of high test-level impact loads as specified in the AASHTO 2000 LRFD Bridge Design Specifications. It also provides the impact load time history for use in both pseudo-static and dynamic impact load analyses of the above-said safety rails. The following are the major sources of information:

- American Association of State Highway and Transportation Officials (AASHTO).
- Federal Highway Administration (FHWA), U. S. Department of Transportation.
- Transportation Research Board (TRB), National Research Council (NRC).
- National Cooperative Highway Research Program (NCHRP)
- Texas Transportation Institute (TTI), Texas A and M University.
- Different State Departments of Transportation.

To assess the safety of railings and barriers, different research groups have performed many full-scale crash tests, particularly Texas Transportation Institute (TTI) at Texas A and M University. Three major NCHRP publications on the subject include: Reports 153, 230 and 350. The Highway Research Correlation Services Circular 482 published in 1962 provided the base for the uniformity of the crash test procedures and mechanism. The Southwest Research Institute further revised the procedures for crash tests in its

NCHRP Report 153 on "Recommended Procedures for Vehicle Crash Testing of Highway Appurtenances" for Project 22-2 in 1974. TRB through Committee A2A04 further addressed the procedures in its report on "Recommended Procedures for the Safety Performance Evaluation of Highway Safety Appurtenances" in Transportation Research Circular 191 (1980) and NCHRP Report 230 in 1979. In 1987, AASHTO updated NCHRP 230 in Report 350 on "Recommended Procedures for the Safety Performance Evaluation of Highway Features" for Project 22-7. The research was initiated and carried out by the Texas A &M University and Dynatech Engineering. The differences between Report 350 and Report 230 important to this study are as follows:

- Six different test level loads are recommended in the crash test procedures and specifications.
- The critical impact point is defined.
- Includes critical review of methods for safety performance including computer simulations

The NCHRP Report 350 is heavily referenced in this study on Colorado Type 7 and Type 10 rails. The major emphasis of this study is placed in incorporating the research results in the overall design and development of Type 7 and Type 10 rails using numerical analysis. TL4 and TL5 loads were used in the analysis.

Major contributors to the fifty-year effort to improve the crash test criteria and procedures are:

- Transportation Research Board (TRB)
- Texas Transportation Institute (TTI)
- National Crash Analysis Center (NCAC)
- Federal Outdoor Impact Laboratories (FOIL)
- Turner Fairbanks Highway Research Center (TFHRC)
- Lawrence Livermore National Laboratories (LLNL) and

- Four major universities: Texas A and M, Univ. of Nebraska, Univ. of Cincinnati, and Worcester Polytechnic Institute of Massachusetts.

TTI specializes in full-scale crash tests, while TFHRC specializes in the numerical simulation to mimic real crashes, intending to avoid the costly full-scale crash tests. Both approaches are critical to the successful evaluation of the vehicle crash phenomenon.

The NCHRP Report 350 identified six test levels, TL1 through TL6. The former three test level loads correspond to the lower service level roadways and the latter three to higher service level roads. The chief of the Federal-Aid and Design Division requested strict adherence to the FHWA's goal for the improvement of highway safety by meeting the requirements set forth by NCHRP Report 350. A partial list for rails with designated test level loads is provided as follows:

- New Jersey Concrete Safety Shape TL-4
- NJ Turnpike Heavy Vehicle Barrier TL-5
- Texas T5 Modified TL-6
- Michigan 10 gage Retrofit on curb/sidewalk TL-4
- Iowa Concrete Block Retrofit TL-4
- 32-in Vertical Concrete Parapet TL-4
- Pre-cast NJ or F-Shape bolted to deck TL-4
- Illinois 2399 2-Rail on Curb TL-4
- 42-in Vertical Concrete Parapet TL-5
- 42-in F Shape Concrete Barrier TL-5
- Texas Type HT and Modified Texas C202 Bridge Rail TL-5.

Efforts to establish performance standards were conducted through a series of tests performed at the Texas Transportation Research Center. In this series, five full-scale guardrails of various designs with walls instrumented with load cells and an accelerometer were tested. In the calibration, a controlled magnitude of load was

imposed. Table 2.1, Table 2-2, and Table 3-2 summarize the result of these tests. Among them, Test 3451-34 and Test 3451-35 represent what may be considered a TL5 condition with vehicular weight of 20,030 lbs and 32,020 lbs, respectively. As a vehicle impacted the wall, two peak major lateral forces were clearly identified. During the test, the initial impact was followed by a second impact when the test vehicle became parallel to the wall. The test results as shown in Figure 2-1 through Figure 2-9 show a higher peak force frequently occurring at the second impact and the 20,030-lb vehicle produced an average peak impact force of 73.8 kips, while the 32,020-lb vehicle produced a peak of 211 kips.

Table 2-1: Summary of Tests on Instrumented Wall

Test Number	Test Date	Test Conditions	Comments
3451-29	4/23/80	1,970 lb/59.0 mph/15.5 deg	Successful test.
3451-30	4/15/80	2,800 lb/58.3 mph/14.8 deg	Successful test.
3451-31	4/18/80	2,830 lb/56.0 mph/20.0 deg	Successful test.
3451-32	4/29/80	4,680 lb/54.6 mph/16.5 deg	Successful test.
3451-33	5/01/80	4,700 lb/58.9 mph/23.8 deg	Instrumentation failure.
3451-34	5/06/80	20,030 lb/57.6 mph/16.5 deg	Successful test.
3451-35	6/18/80	32,020 lb/56.9 mph/15.8 deg	Successful test.
3451-36	5/20/80	4,740 lb/59.8 mph/24.0 deg	Successful test.
3451-37	10/24/80	2,090 lb/58.5 mph/21.0 deg	Successful test.

1 lb = 0.4536 kg
1 mph = 1.609 kph

Table 2-2: Vehicle acceleration from Tests on Instrumented Wall

TEST DESIGNATION	TEST CONDITIONS	MAX. 0.050 SEC AVG VEHICLE ACCELERATION			
		Long.	Trans.	Vert.	Result.
3451-29	1,970 lb/59.0 mph/15.5 deg	-4.0	10.2	-1.2	11.0
3451-30	2,800 lb/58.3 mph/14.8 deg	-3.0	7.7	1.2	8.2
3451-31	2,830 lb/56.0 mph/20.0 deg	-3.6	8.1	1.8	8.7
3451-32	4,680 lb/54.6 mph/16.5 deg	-4.0	9.3	-1.5	10.1
3451-33	4,700 lb/58.9 mph/23.8 deg	**	--	--	--
3451-34	20,030 lb/57.6 mph/16.5 deg	-1.8	6.3	-1.5	6.4
3451-35	32,020 lb/56.9 mph/15.8 deg	-1.4	8.6	-1.7	8.7
3451-36	4,740 lb/59.8 mph/24.0 deg	-9.1	15.4	-2.3	17.7
3451-37	2,090 lb/58.5 mph/21.0 deg	-6.50	13.10	-1.0	14.6

** Instrumentation failure.

1 lb = 0.4536 kg
1 mph = 1.609 kph

Table 2-3: Summary of Data from Instrumented Wall Test Series

		Initial Impact				Final Impact			
Test Number	Test Conditions	Force (kips)	X dist. (in.)	Y dist. (in.)	Time (sec)	Force (kips)	X dist. (in.)	Y dist. (in.)	Time (sec)
3451-29	Honda 1,970/59.0/15.5	18.4	217	16.0	.034-.084	8.4	214	18.7	.113-.163
3451-30	Vega 2,800/58.3/14.8	18.5	225	17.7	.019-.069	13.9	227	16.0	.101-.151
3451-31	Vega 2,830/56.0/20.0	22.0	225	20.0	.034-.084	22.5	231	21.0	.119-.169
3451-32	Plymouth 4,680/54.6/16.5	52.5	260	21.2	.054-.104	28.3	252	24.1	.154-.204
3451-34	School Bus 20,030/57.6/16.5	63.7	203	28.5	.110-.160	73.8	153	33.0	.335-.385
3451-35	Inter-City Bus 32,020/56.9/15.8	85.0	174	26.3	.041-.091	211.0	171	28.0	.331-.381
3451-36	Plymouth 4,740/59.8/24.0	59.9	125	21.9	.047-.097	28.3	125	22.5	.158-.208
3451-37	Honda 2,090/58.5/21.0	21.1	232	18.8	.036-.086	13.1	231	20.7	.103-.153

1 kip = 4.448 kN
1 in. = 0.025 m

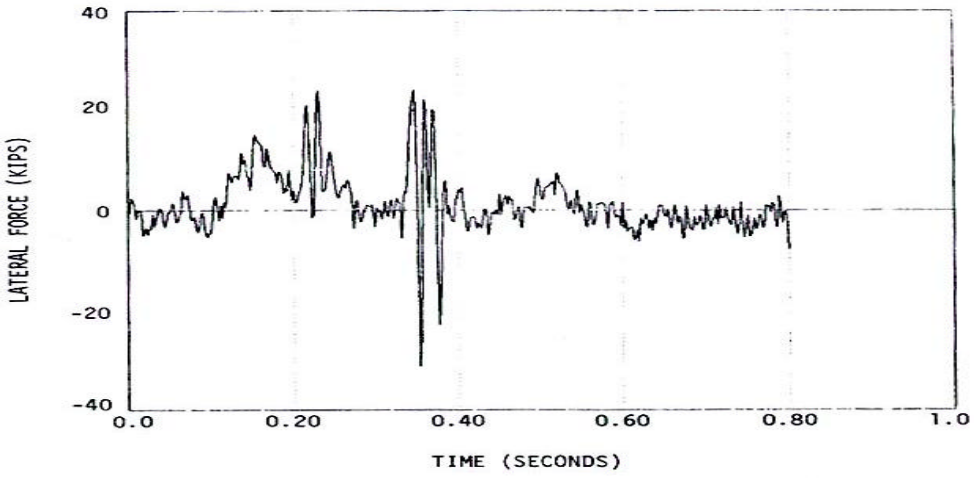


Figure 2-1: Lateral Force on Wall Segment B for test 3451-34

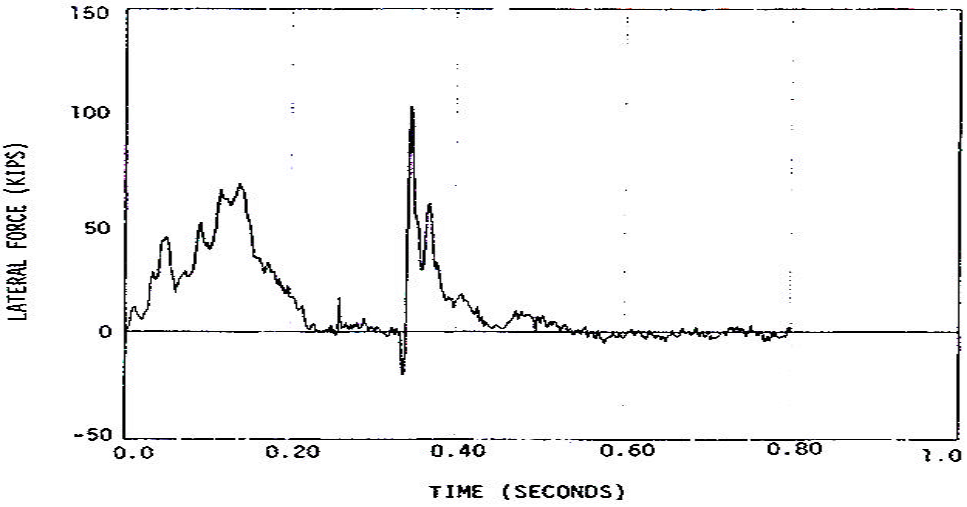


Figure 2-2: Lateral Force on Wall Segment C for test 3451-34

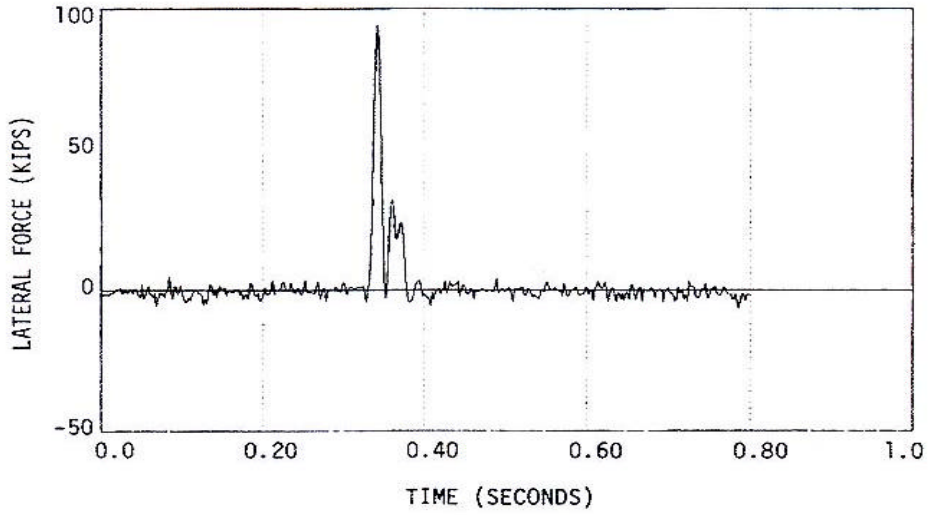


Figure 2-3: Lateral Force on Wall Segment D for test 3451-34

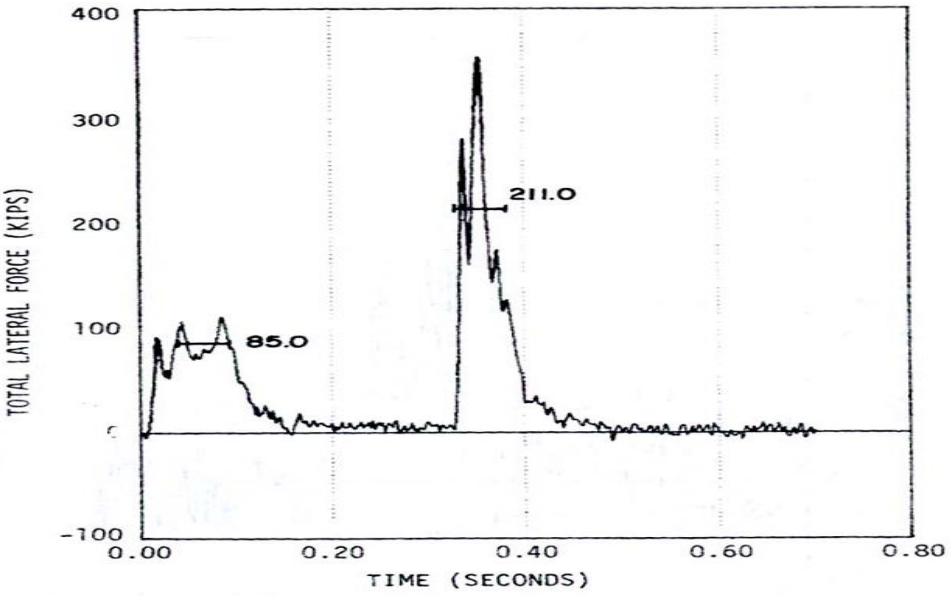


Figure 2-4: Total Lateral Force on Wall for test 3451-35

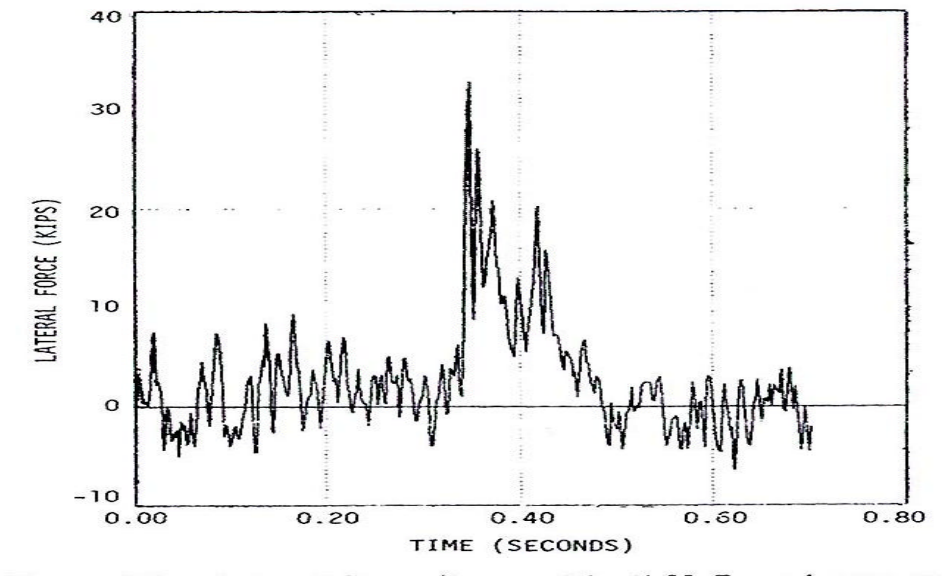


Figure 2-5: Lateral Force on Wall Segment A for test 3451-35.

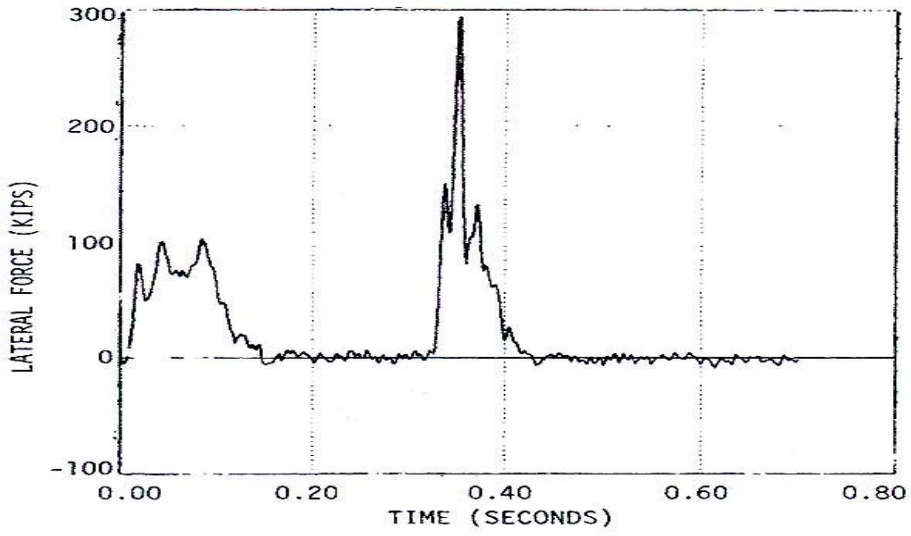


Figure 2-6: Lateral Force on Wall Segment B for test 3451-35

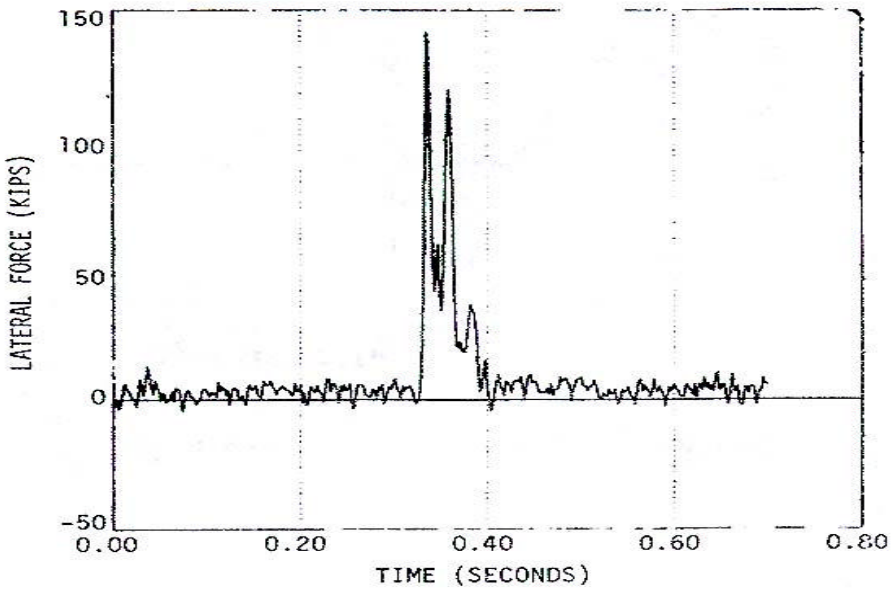
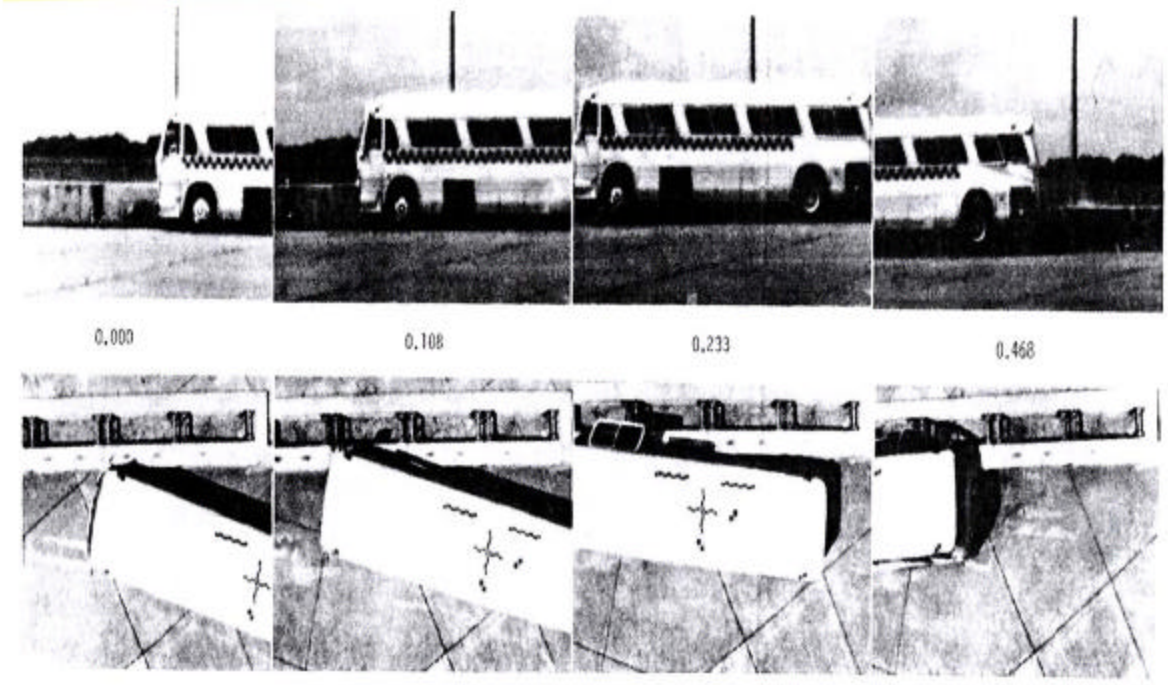
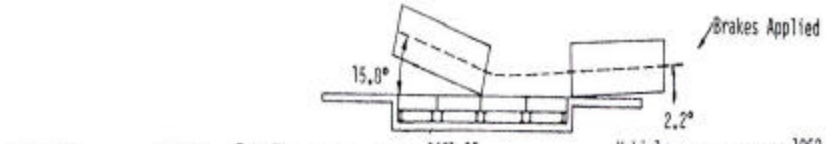
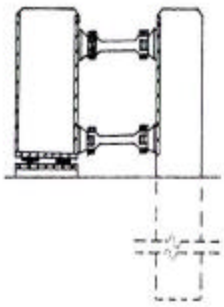


Figure 2-7: Lateral Force on Wall Segment C for test 3451-35







Test No.	3451-35
Date	6/18/80
Instrumented Wall	Four Blocks; 3.084 m x 1.067 m x .457 m (10 ft x 3.5 ft x 1.5 ft)
Instrumentation	Four load cells and one accelerometer per block
Length of Installation	22.88 m (75.08 ft)
Vehicle Damage	
TAD	1RFQ3
SAE	01FREE2
Maximum Roll	38.0 deg

Vehicle	1962 General Motors Inter-city Bus
Vehicle Weight (w/dummies, instr.)	14,524 kg (32,020 lb)
Dummy Restraints	
Driver	Lap Belt
Passenger	No Restraint
Impact Speed	91.6 kph (56.9 mph)
Impact Angle	15.8 deg
Exit Speed	83.7 kph (52.0 mph)
Exit Angle	2.2 deg
Vehicle Acceleration (Max. 0.050 sec avg)	
Longitudinal	-1.4 g
Transverse	8.6 g
Vertical	-1.7 g

INSTRUMENTED WALL

Figure 2-8: Summary of Results for Test 3451-35

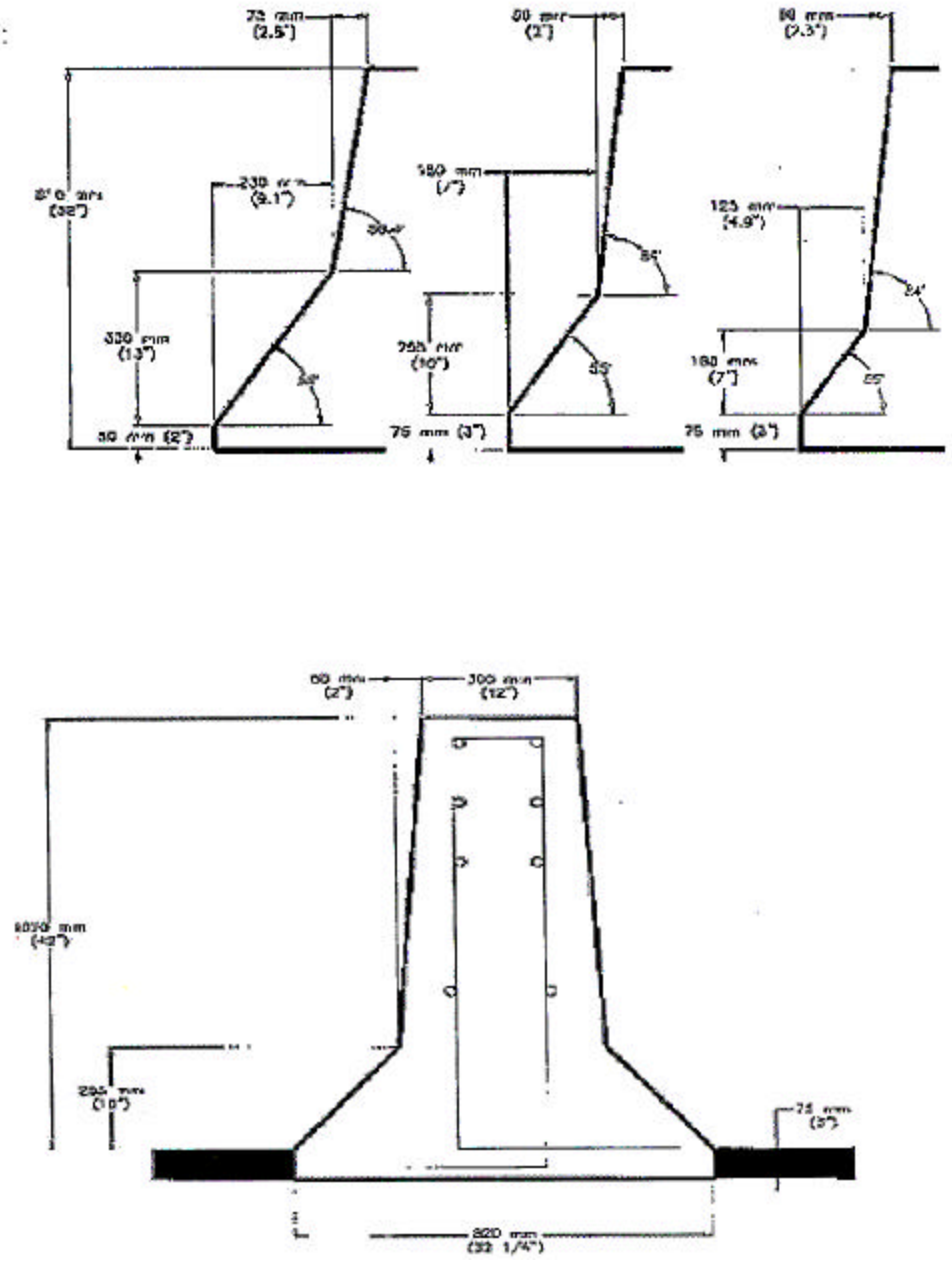


Figure 2-9: New Jersey Shape Concrete Safety Barrier (Turner Fairbanks Highway Research Center)

The height of a barrier and the geometry of a barrier is critical to its function of safe redirection of the impacted vehicle. Figure 2-9 shows the geometry of the Jersey barrier. During an impact, the front bumper first contacted the upper-sloped face of the barrier.

The impact lifted the vehicle barrier and as the vehicle became nearly parallel to the barrier, the wheel made the contact with the lower-sloped face compressing the front suspension and causing most of the additional lift. The process redirected and banked the vehicle and dissipated the energy and repeatedly converted the energy from kinetic to potential energies and visa versa.

While these test rails are different from the Colorado Type 7 and Type 10 rails, the data from the instrumented wall provides invaluable information about forces imposed on a barrier wall. These data also provide information and guidelines important to the study of Type 7 and Type 10 rails. In this study TL4 and TL5 (124 kips) are adopted by the Colorado DOT for the study of the "structural adequacy" and "load transfer mechanism" of the Colorado Type 7 and Type 10 longitudinal barriers. The strength of the barrier structure is defined by its ability to contain and redirect a vehicle upon impact.

3.0 FINITE ELEMENT ANALYSES

3.1 Introduction and Evolutional History of Analysis

Initially, the finite element analyses were to be performed on the 20-foot Colorado Type 7 and Type 10 rail systems resting on a 20-foot MSE wall with block facing. The initial analysis of the 20-ft rail, however, indicated the gross instability of both rail types without installation of restraining anchors or other stabilizing mechanisms. After the presentation of the first quarterly report to the CDOT study panel, the decision was made to increase to the length of rails to 40 feet. The analysis still showed that even the 40-ft rails were still unable to cope with the stability problems. The rail just could not handle either TL4 or TL5A load. During the presentation of the second and third quarterly reports, the decision was made to check the influence length of the rail, the rail length at which the displacement in the transverse direction is not excessive, using 400-ft rails. Until this point, SGI (Silicon Graphic) workstations were used in the analysis. However, when the analysis was expanded to cover the complete rail system, the rail sitting on top of the backfill of MSE block facing walls, the problem became too big for SGI and the Cray supercomputer at the San Diego Supercomputer Center was used in the analysis. The nonlinear analysis computer program, NIKE3D, was used in all analyses. The program was developed at the Lawrence Livermore National Laboratory under the direction of Dr. Michael Puso. To gain the privilege of using NIKE3D, the Center for Geotechnical Engineering Science at the University of Colorado at Denver entered a collaborative development agreement with Dr. Puso.

3.2 Background Theory for NIKE3D Computer Code

NIKE3D[1] developed at the Lawrence Livermore National Laboratory (LLNL) for structural analysis provides a powerful tool for the study of the response of various structures subject to static and/or transient loads. Computer simulation of nonlinear behavior is quite complex and the nonlinear finite element computer programs developed at the LLNL are among the most powerful programs in the world for nonlinear soil-structure interaction analysis. To allow readers a good understanding of the theoretical background of the NIKE3D program, its user's manual (Puso, etc. 2001) is **extensively referenced** and the authors of this report would like to acknowledge the original authorship and **disclaim** any credit for the information on THE NIKE3D program.

NIKE3D is an implicit three-dimensional finite element code for analyzing the finite strain static and dynamic response of structures of linear or nonlinear materials with or without interface between two distinctive materials. A great number of material models are incorporated to simulate a wide range of material behavior including, elastic, elasto-plastic, anisotropic, creep, and rate dependent behaviors, etc. Arbitrary contact between independent bodies is handled by a variety of slideline algorithms. These algorithms model gaps and sliding along material interfaces.

3.2.1 Solution Procedures

In NIKE3D, several nonlinear solution strategies are available, including Full-, Modified-, and Quasi-Newton method with the BFGS method being the default. An extensive set of diagnostic messages in the quasi-Newton solvers allows the monitoring of the progress of convergence.

NIKE3D uses the updated Lagrangian formulation, in which the nodal displacements that satisfy the equilibrium condition are calculated at the end of each load step to update the

[1] The NIKE3D user's manual is heavily quoted in this section of the report describing the NIKE3D program.

geometry. After obtaining the updated displacement increments, the displacement, energy, and residual norms are computed, and equilibrium convergence is tested using the user-defined tolerance. Once convergence is obtained, displacements and stresses are updated and the solution process proceeds to the next load step. If convergence is not achieved within the user-specified iteration limits, the optional automatic time step controller will adjust the time step size and the computation process continues.

3.2.2 Element Library

NIKE3D utilizes use low order interpolation, requiring no mid-side node definitions. This approach chooses highly efficient elements over more costly higher order elements. The available elements are solid, beam, and shell elements. Eight node solid elements are integrated with a 2x2x2 point Gauss quadrature rule. Four node shell elements use 2x2 Gauss integration in the plane, and one of many available schemes for integration through the thickness. Two node beam elements use one integration point along the length with many options for integration of the cross section.

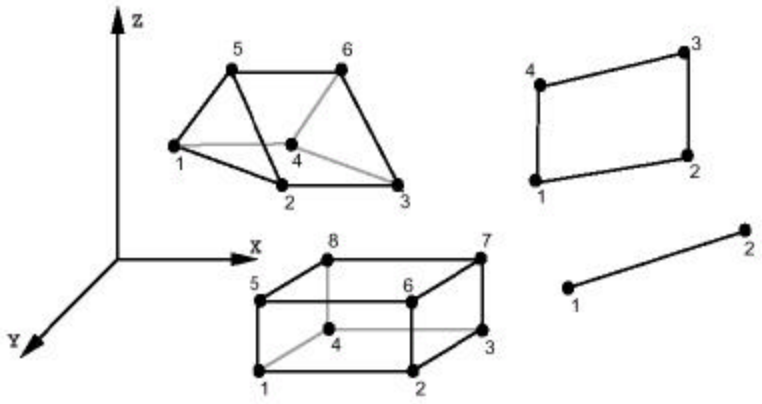


Figure 3-1: 1-D, 2-D and 3-D Element library of NIKE3D.

3.2.3 Interface Formulation

In NIKE3D the multi-body contact algorithms are based on a master-slave approach. Typically one side of a potential interface is identified as the “master” side and the other

as the “slave” side. Internal logic identifies a master facet for each slave node and a slave facet for each master node. This information is updated at each time step as the slave and master nodes slide along their respective surfaces. In this manner, a large relative motion between the two surfaces is allowed. Three types of interfaces are available: tied, sliding only, and frictional sliding with permission of gaps. Among the three types of interface algorithm, “frictional sliding with gaps” is most appropriate to simulate the behavior of soil-concrete interface. The frictional sliding with gaps provides general multi-body contact capability. Frictional behavior is modeled with Coulomb type friction. The surfaces need not be initially in contact. During execution the surfaces may close and subsequently separate as necessary to satisfy global equilibrium.

The following illustrates the NIKE3D's argumentation of stiffness matrix K and the internal nodal force F^s when penetration is detected. Figure 1 shows an isolated portion of the interface where node m penetrates through segment *jk*. A local equilibrium relationship can be written as:

$$K^s \Delta u^s = P^s - F^s$$

where Δu^s is the incremental displacement vector containing the degrees of freedom of the penalty spring, K^s is the spring stiffness, F^s is the spring internal force , and P^s is the external force arising from internal stress in the interface elements. The spring degrees of freedom are as;

$$\Delta u^s = \left[\Delta v_m \Delta w_m, \Delta v_j \Delta w_j, \Delta v_k \Delta w_k\right]$$

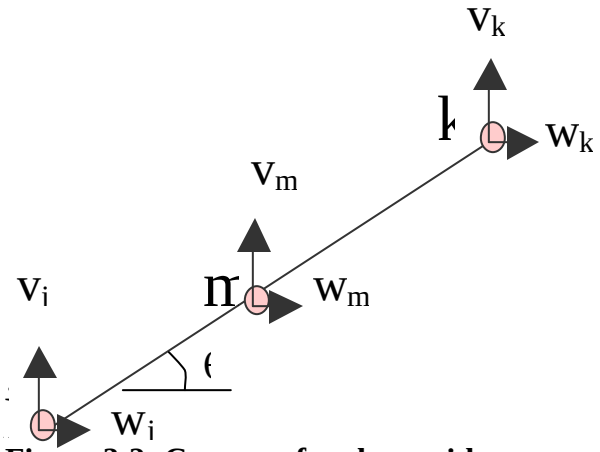


Figure 3-2: Contact of node m with segment of jk [3].

The spring stiffness matrix K^s is defined as

$$K^s = k\begin{bmatrix} s^2 & -sc & -(1-a)s^2 & (1-a)sc & -as^2 & asc \\ & c^2 & (1-a)sc & -(1-a)c^2 & asc & -ac^2 \\ & & (1-a)^2 s^2 & -(1-a)^2 sc & (1-a)as^2 & -(1-a)asc \\ & & & (1-a)^2 c^2 & -(1-a)asc & (1-a)ac^2 \\ & \text{Symm.} & & & a^2 s^2 & -a^2 sc \\ & & & & & a^2 c^2 \end{bmatrix}$$

where c = cos(θ), s = sin(θ), |jk| = L, |jm| = aL and k is the penalty stiffness and is a constant defined as

$$k = \frac{f_{SI} K_i A_i^2}{V_i}$$

where K_i, A_i, and V_i are bulk modulus, area and volume of the penetrated material, respectively. f_{SI} is called penalty scale factor, which allows the user to control the penalty spring stiffness.

The spring internal force F^s is defined by

$$F^s = -kd\begin{bmatrix} -s \\ c \\ (1-a)s \\ -(1-a)c \\ as \\ -ac \end{bmatrix}$$

where -δ is the amount of penetration of node m through segment *jk*. The spring stiffness K^s and force F^s are computed for all active slideline nodes and segments, and are assembled into the global finite element equations. Thus, the stiffness profile changes as analysis with slidelines evolves.

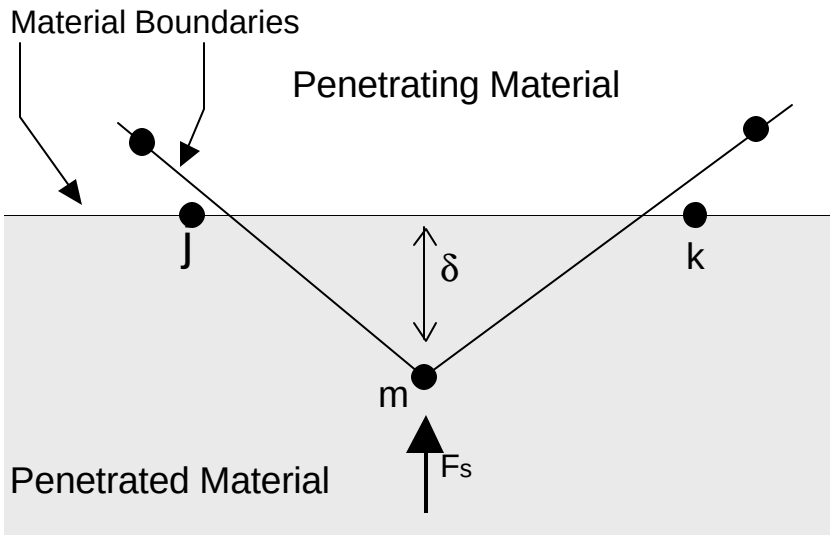


Figure 3-3: Penetrating of node m into the adjacent material boundary.

The penalty stiffness κ, is unique for each segment, and is based on the contact area and bulk modulus of the penetrated material. If noticeable penetration is observed, the penalty number should be increased. However high penalty numbers may cause divergence of global iterations. In NIKE3D the default value of *k* has been chosen to balance global convergence rate on a wide variety of problems.

3.3 Material Models and Model Parameters

In this study, the Ramberg-Osgood nonlinear material model is used to represent the Backfill, the Oriented Brittle model for concrete, and linear elastic model for geogrid. The first two models are further discussed.

3.3.1 Ramberg-Osgood Non-Linear Model

The equation for Ramberg-Osgood stress-strain relation used to model the backfill behavior is given by:

$$\frac{g}{g_y} = \frac{t}{t_y}\left(1 + a\left|\frac{t}{t_y}\right|^{r-1}\right)$$

where γ is shear strain, τ shear stress, γ_y reference shear strain, τ_y reference shear stress, α constant$\geq$0, and r constant$\geq$1.

The Ramberg-Osgood relations are inherently one-dimensional, and are assumed to apply to shear components. To generalize this theory to the multi-dimensional case, it is assumed that each component of the deviatoric stress and deviatoric tensorial strain is independently related by the one-dimensional stress-strain equations (Maker, 1995). Its material parameters are obtained using the computational procedure proposed by Ueng and Chen (Ueng et. al. 1992). This procedure calculates the Ramberg-Osgood parameters using G_{max} value, and Seed's average modulus and damping ratio versus shear strain curves (Seed, 1970). Table 3.1 shows all the material properties used in the parametric analysis.

Table 3.1 Material model parameters used in the analyses.

ELASTIC			
Material	**E (10^3 psi)**	n	g **(pcf)**
Concrete	3625	0.15	175
Backfill Soil	8	0.3	125
Foundation Soil	15.9	0.35	130
Inclusion	42	0.4	65

RAMBERG-OSGOOD				
Material	g_y **(10^{-4})**	t_y **(psf)**	a	**r**
Backfill Soil	1.052	1.6	1.1	2.35

ORIENTED BRITTLE FAILURE						
Material	**f_t (psf)**	h	**f_s (psf)**	**g_c**	**s_y (psf)**	b
Concrete	450	0.0	2100	0.872	3637	0.03

3.3.2 Oriented Brittle Damage Model

This model describes the anisotropic damage of brittle materials, and is designed primarily for application to concrete. The model admits the progressive degradation of tensile and shears strengths across the smeared cracks initiated under tensile loadings. Damage, the evolution of cracks, is handled by treating the fourth rank elastic stiffness tensor as an evolving internal variable. Softening induced mesh dependencies are addressed by a characteristic length method described by Oliver [1989].

The elastic properties, E (Young's modulus) and ν (Poisson's ratio), define the material response before damage occurs. Whenever the first principal stress reaches the initial tensile strength, f_T, a smeared crack is initiated in the plane normal to the first principal stress direction. The crack orientation is fixed in the material, rotating in space with the body. As the loading advances, the tensile traction normal to the crack plane is progressively degraded to a small machine-dependent constant. This occurs by reducing the material's modulus normal to the smeared crack plane according to a maximum dissipation law that incorporates exponential softening. The normal traction $t_n = (\boldsymbol{n} \otimes \boldsymbol{n}) \cdot s$ is restricted by the condition: $t_n \le f_T - (1 - \varepsilon) f_T [1 - \exp(-H\alpha)]$, where $\boldsymbol{n}$ is the smeared crack normal, ε is a small constant, σ is the stress, H is the softening modulus, and α is an internal variable. H is calculated automatically based upon the fracture toughness g_c and the element geometry.

3.4 AASHTO Rail Test Level Load and Transient Collision Load History

To provide some design guidelines for the highway safety rails, in AASHTO 2000 LRFD Bridge Design Specifications different test level loads are specified based on the vehicle speed and weight, traffic volume and the importance of roadway. The test level loads, components and point of application are defined in Table 3.2 and Figure 3.4. This specification came about through the contribution of the crash test research performed at the Texas Transportation Institute (TTI). The test conditions are specified in Table 3.3. The Federal Highway Administration (FHWA) requires the adoption of this specification in the design of safety rails at the state level. Because of the lack of design details in the AASHTO specifications for rails on important highways, AASHTO recommends the use of finite element analysis and the like to facilitate rail design. It is due to this recommendation that the Colorado Department of Transportation commissioned this study on "Colorado Type 7 and 10 Rails on Independent Moment Slab under High Test Level Impact Loads" to assess the sufficiency of its current design specifications and the three-dimensional load transfer mechanism under high impact loads, the need for the improvement in design mechanism and the effect of load transfer on MSE wall design. The TL-4 (53 kips) and TL-5A (124 kips) loads were chosen in this study.

Table 3.2 Impact Load Definitions and Locations (AASHTO TableA13.2.1)

Design Forces and Designations	Railing Test Levels						
	TL-1	TL-2	TL-3	TL-4	TL-5A	TL-5	TL-6
F_t Transverse (N)	60 000	120 000	240 000	240 000	516 000	550 000	780 000
F_L Longitudinal (N)	20 000	40 000	80 000	80 000	173 000	183 000	260 000
F_v Vertical (N) Down	20 000	20 000	20 000	80 000	222 000	355 000	355 000
L_t and L_L (mm)	1220	1220	1220	1070	2440	2440	2440
L_v (mm)	5500	5500	5500	5500	12 200	12 200	12 200
H_e (min) (mm)	460	510	610	810	1020	1070	1420
Minimum H Height of Rail (mm)	685	685	685	810	1020	1370	2290

Applications of the above test level loads are specified as:

- TL-1: generally acceptable for work zones with low posted speeds and very low volume, low speed local streets;
- TL-2: work zones and most local and collector roads with favorable site conditions as well as work zones and where a small number of heavy vehicles is expected and posted speeds are reduced;
- TL-3: a wide range of high-speed arterial highways with very low mixtures of heavy vehicles and with favorable site conditions;
- TL-4: the majority of applications on high speed highways, freeways, expressways, and Interstate highways with a mixture of trucks and heavy vehicles;
- TL-5.A: the same applications as TL-4 when site conditions justify a higher level of rail resistance;
- TL-5 and TL-6: the applications on freeways with high-speed, high-traffic volume and a higher ratio of heavy vehicles and a highway with unfavorable site conditions.

3.5 Moment Slab versus Backfill Frictional Resistance

In the current CDOT rail design method, the impact load transfers from the rail-moment slab unit to the MSE wall backfill mainly through the slab-backfill interface friction and the interface friction is further transferred to the MSE wall. Under the assumption of no backfill-slab separation under the TL-4 or TL-5.A test level load, the frictional resistance at different soil-backfill interface friction coefficient is calculated and summarized in Figure 3.5. The figure indicates that, under the assumption of full slab-backfill contact, a 100-foot long Type 7 rail with Jersey barrier with an interface friction coefficient of 0.5 is capable of resisting TL-5.A impact load. The finite element analysis result, however, shows that the rail-slab unit twists and rotates about the toe of the rail under the impact

Table 3.3 Test Conditions, Vehicle Weights and Velocity Definitions

(AASHTO Table13.7.2.1)

Vehicle Characteristics	Small Automobiles		Pickup Truck	Single-Unit Van Truck	Van-Type Tractor-Trailers		Tractor-Tanker Trailers
W (N)	7000	8000	20 000	80 000	220 000	355 000	355 000
B (mm)	1700	1700	2000	2300	2450	2450	2450
G (mm)	550	550	700	1250	1630	1850	2050
Crash angle, θ	20°	20°	25°	15°	15°	15°	15°
Test Level	TEST SPEEDS (km/h)						
TL-1	50	50	50	N/A	N/A	N/A	N/A
TL-2	70	70	70	N/A	N/A	N/A	N/A
TL-3	100	100	100	N/A	N/A	N/A	N/A
TL-4	100	100	100	80	N/A	N/A	N/A
TL-5A	100	100	100	N/A	80	N/A	N/A
TL-5	100	100	100	N/A	N/A	80	N/A
TL-6	100	100	100	N/A	N/A	N/A	80

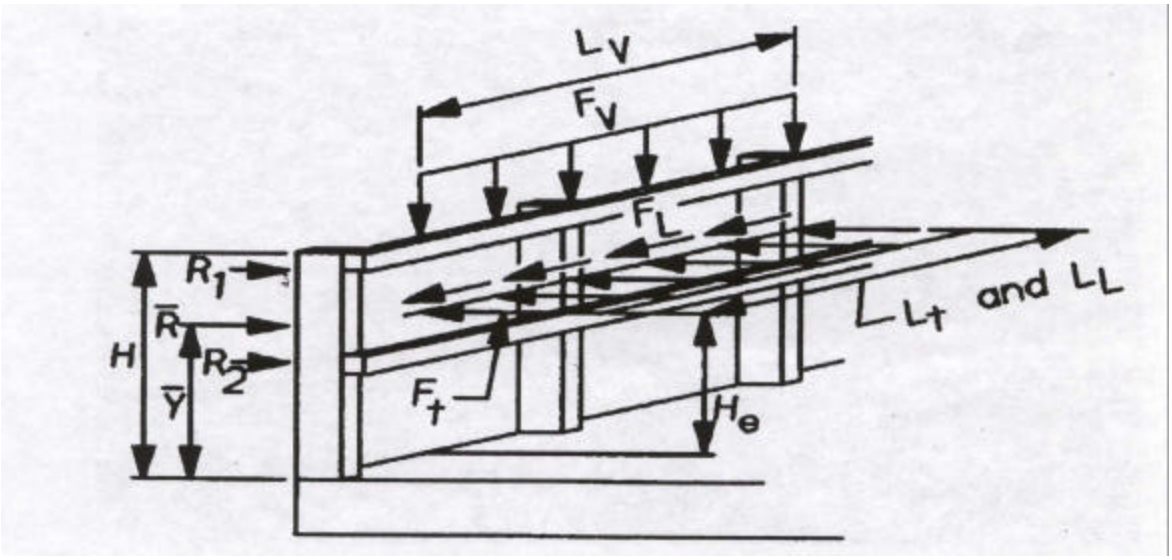


Figure 3.4 Test Load Locations (AASHTO Table A13.2.1)

load and, during the process a major portion of the slab separates from the backfill. This separation grossly reduces the slab-backfill interface friction and the resulting rail resistance. This causes the rail to rotate and move excessively. To stabilize the rail system requires the improvement mechanism that enhances its resistance through the increase of interface friction and the additional horizontal resistance provided by the improvement mechanism.

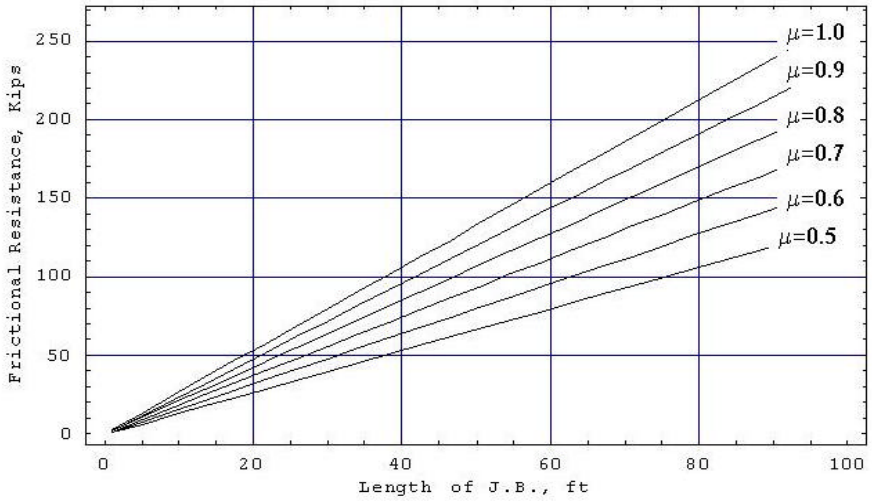


Figure 3.5 Frictional resistance versus Length of Jersey Barrier

3.6 Finite Element Analysis for Performance of Rail and Load Transfer

3.6.1 20-foot Rail with the Centrally Imposed TL4 Impact Load

In the first attempt to analyze the stability of the Colorado Type 7 rail with Jersey barrier, the finite element analysis was performed on a 20-foot rail under TL-4 and subsequently TL-5.A load. Figures 3.6 and 3.7 show the finite element model used in the analysis. Figure 3.6 shows the front view of the model with a conventional T wall without geosynthetic inclusions in the backfill. A 20-foot Jersey barrier is located on the wall top with 10-ft extensions on each side. A frictional interface is introduced between

extensions and the Jersey barrier. Figure 3-7 shows the 3-D finite element mesh of the model. Two types of analyses were performed, one pseudo-static analysis and another impulse load analysis. The analyses were performed before a realistic impulse load-time history was made available through literature review, and the load was assumed to have the same rise and decay time of 0.1 second as shown in Figure 3.8.

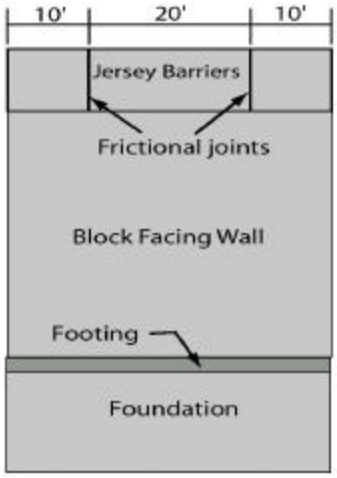


Figure 3.6 Front view of conventional T wall and 20-ft long Jersey barrier.

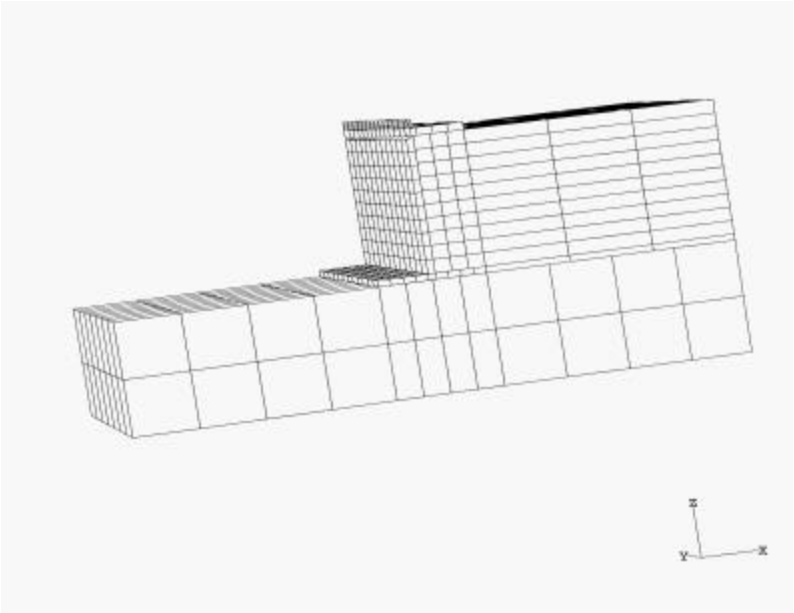
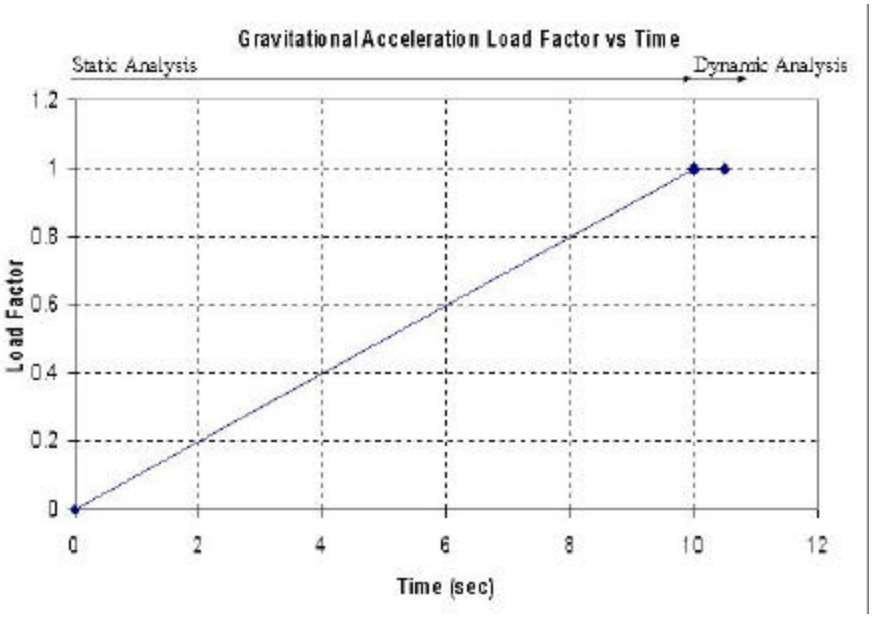
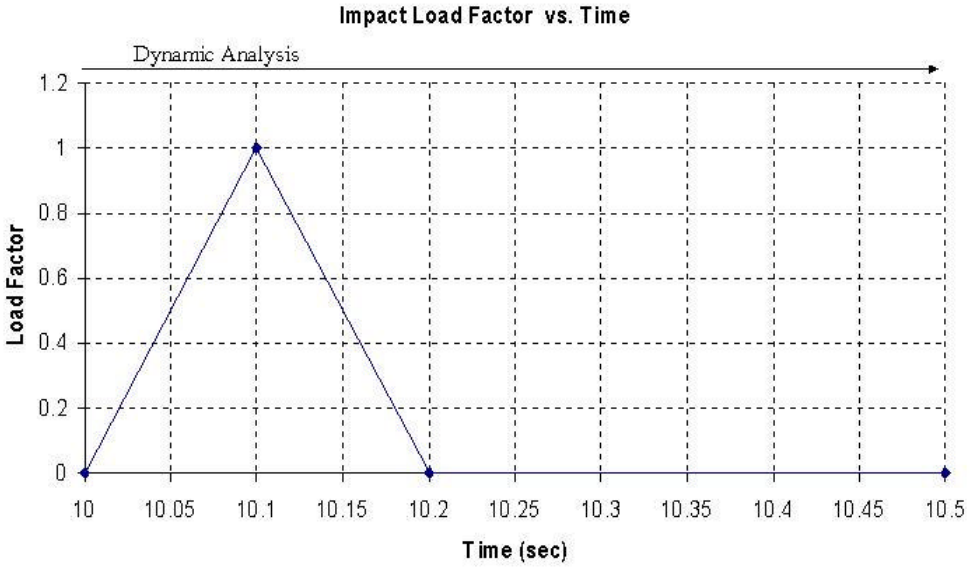


Figure 3.7 3-dimensional Finite Element Modeling of Conventional T Wall w/o tensile inclusions



(a)



(b)

Figure 3.8 Gravitational load factor and impact load factor versus time.

Pseudo-static analyses were attempted using both TL-4 and TL-5.A concentrated loads in transverse directions applied at the center of the 20-foot Jersey barrier. The static and

dynamic material properties are obtained for the backfill similar to the Colorado Class I material. Figure 3.9 shows the Type 7 Rail-MSE wall system and the location of Nodal Point (NP) 158 for the demonstration of the nodal point transverse displacement. Figure 3.10 shows the transient horizontal displacement of Type 7 Rail under TL4 impact load as shown in Figure 3.8. The analysis failed to complete due to the excessive wall displacement. The analysis result using TL4 shows that the rail gains momentum and flies off the wall.

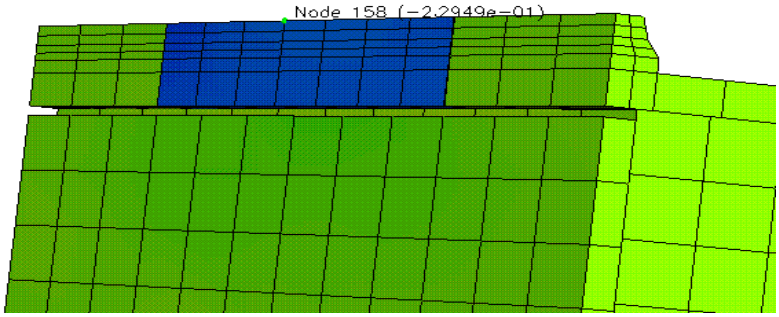


Figure 3-9: Location of Node 158 selected for horizontal displacement time history.

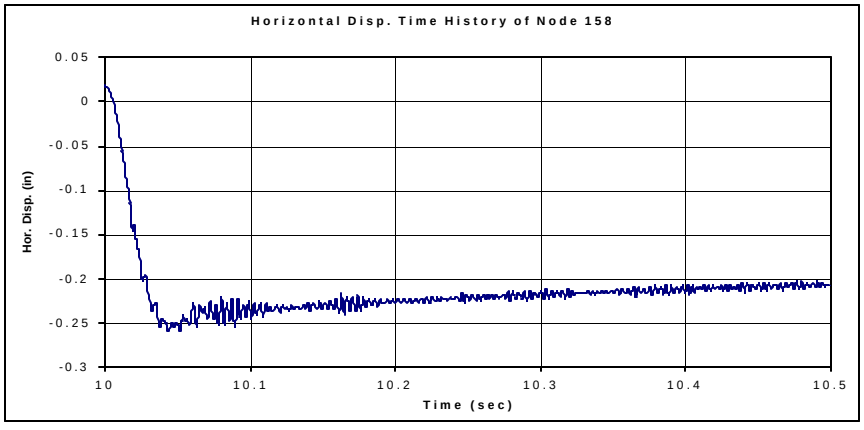


Figure 3-10: Horizontal displacement time history of Node 158.

3.6.2 40-ft Type 7 Rail with Pseudo-static and Dynamic TL4 or TL5a at Rail Center/Edge

In this model 40-ft long Jersey barrier was used with no extensions as shown in Figure 3.11. Tensile inclusions were modeled using 2-D shell elements. For simplicity the MSE wall was assumed to be sitting on stiff foundation, therefore foundation soil was not included in the model.

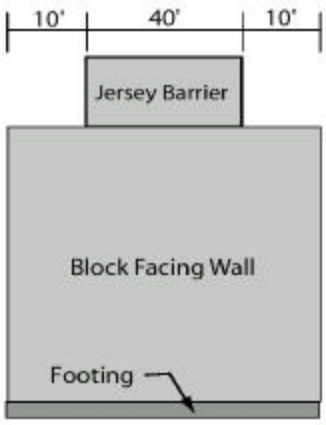


Figure 3.11 Front view of 40-ft long Jersey barrier with MSE wall.

Both pseudo-static analysis and impulse-load analyses were performed. In the impulse load analysis, the time history recommended by Professor Buth at TTI was used. Dr. Buth started the rail impact study way back in the early 1970's. The measured time histories of forces and acceleration are available in graphical form. The measurement indicates that the average peak impulse force remains on a rail for about 0.05 second.

The load was distributed uniformly over an area of 3 ft by 6 ft. In these preliminary analyses, all materials were assumed to be elastic. A 40-ft long rail-slab-wall system (3 ft high Jersey barrier monolithically attached to the moment slab 8-ft wide and 1-ft thick) seats on an MSE block-facing wall (20 ft high, 60 ft long and 40 ft deep) with a 14-ft long geogrid reinforcement attached to the facing blocks. For illustration purpose, Figure

3.12 shows the finite element mesh exposing geogrids by hiding backfills. Figure 3.13 shows the finite element mesh used in the actual analyses.

Gravitational load was applied incrementally in pseudo time domain in 10 seconds as shown in Figure 3.14. Then either static or impact load was applied at the desired load levels. Figure 3.15 shows the time history of impact load factor.

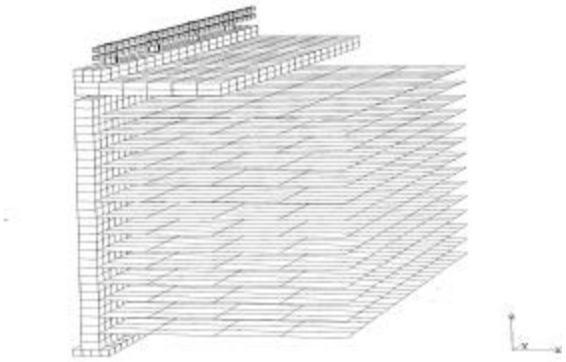


Figure 3.12 3-dimensional Finite Element Modeling for Type 10 (Steel) Impact Rail (backfill soil elements to be added)

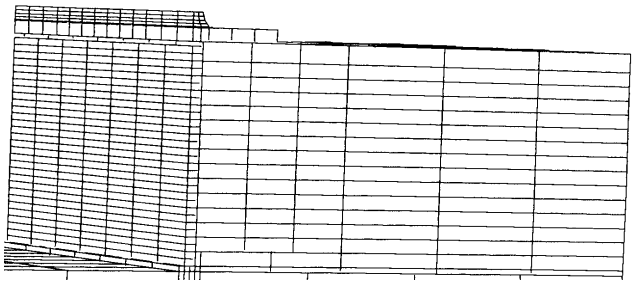


Figure 3.13 3-dimensional Finite Element Modeling for the Type 7 Impact Rail with tensile inclusions.

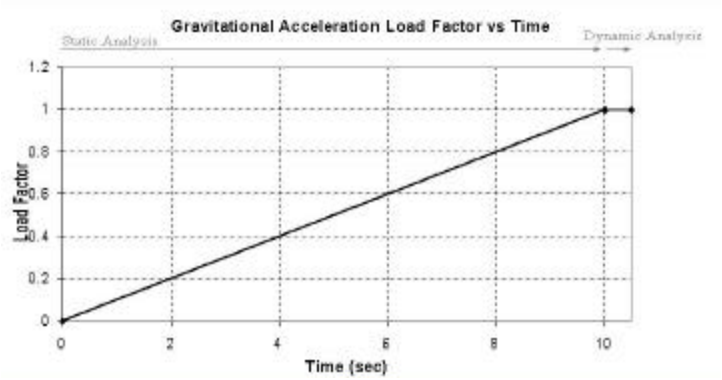


Figure 3.14 Gravitational acceleration load factor versus time.

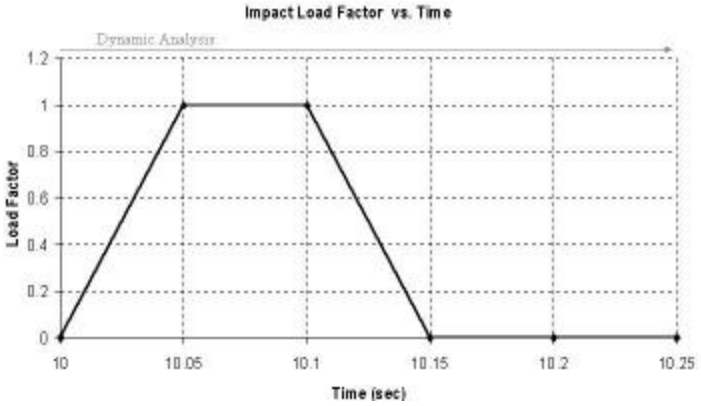


Figure 3.15 Impact load factor versus time.

3.6.2.1 40-ft Type 7 Rail under Static TL4 Load at Center

Figures 3.16 thru 19 show the result of the static analysis when the transverse load is applied at the center of the rail. The displacement achieves a maximum value at the center, point of load application, and both ends move by a near equal amount during the process of load application, which was never completed because of the instability of the rail-slab unit. The application of the transverse load causes the rail-slab unit to rotate about its toe and further causes the slab to separate from the wall backfill. Once the separation takes place the soil-backfill interface friction that provides the resistance to the rail movement decreases drastically and thus causes the instability of the rail system and

the automatic termination of the analysis. The wall displacement decreases from a maximum value at the wall top to zero at the wall base, Figure 3.17. Figures 3.18 and 3.19 reflect the changes, while small, in geogrid stresses and earth pressures. The wall experiences the maximum change in earth pressure at the wall top. The change decreases with the depth.

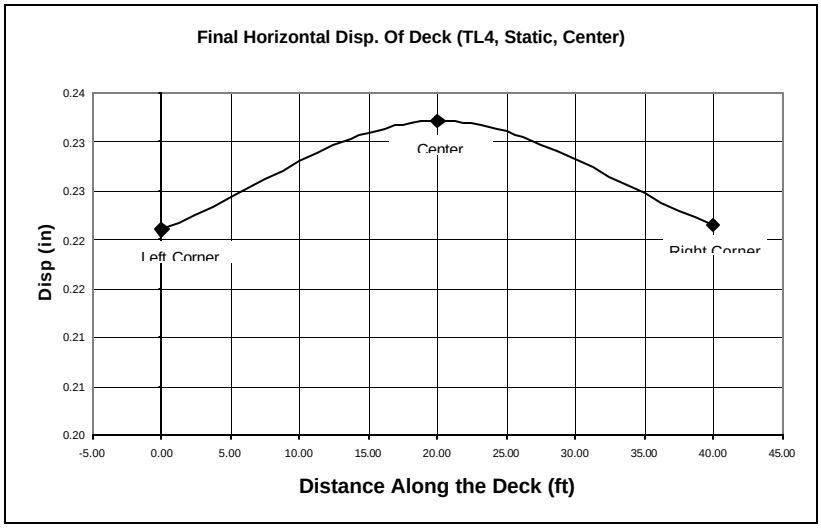


Figure 3-16: Transverse displacement of edge and corner nodes Of Type 7 barrier under TL4.

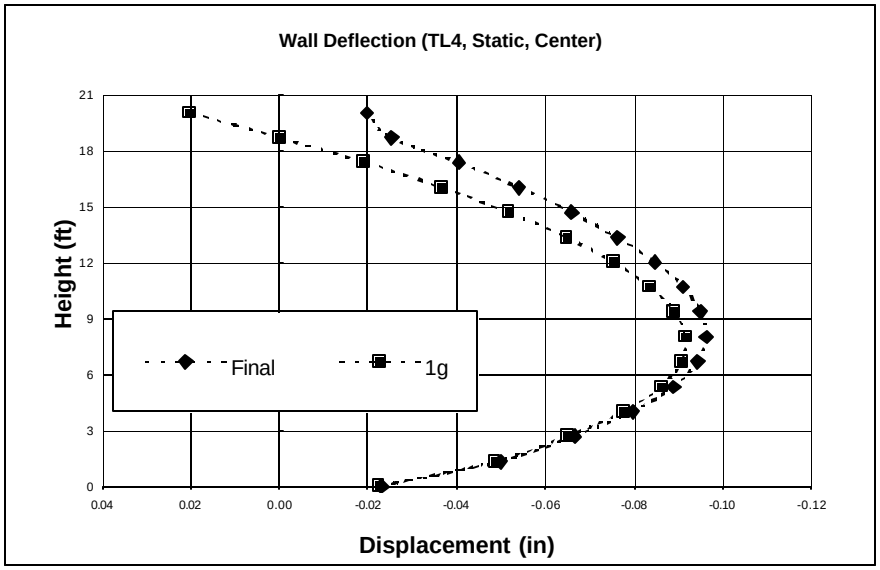


Figure 3-17: Wall deflection (TL4, Center Hit, Static).

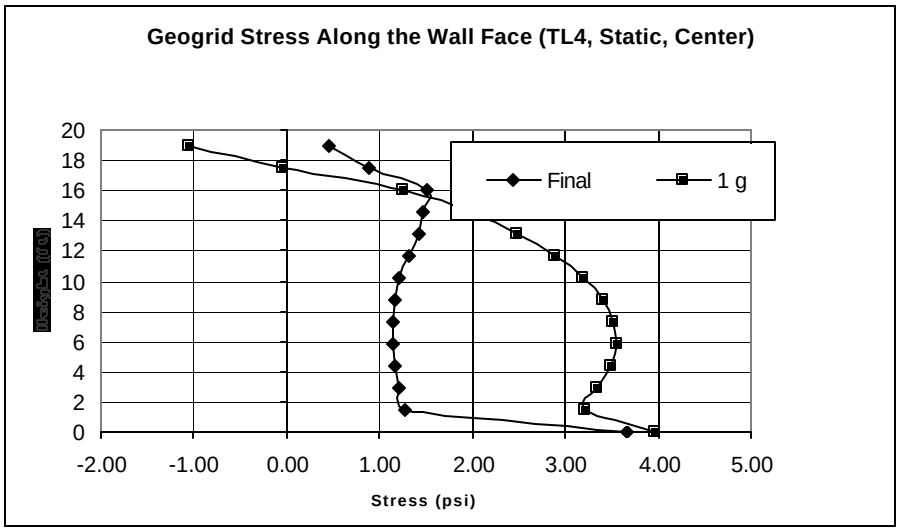


Figure 3-18: Geogrid stresses along the wall connection

(TL4, Center Hit, Static).

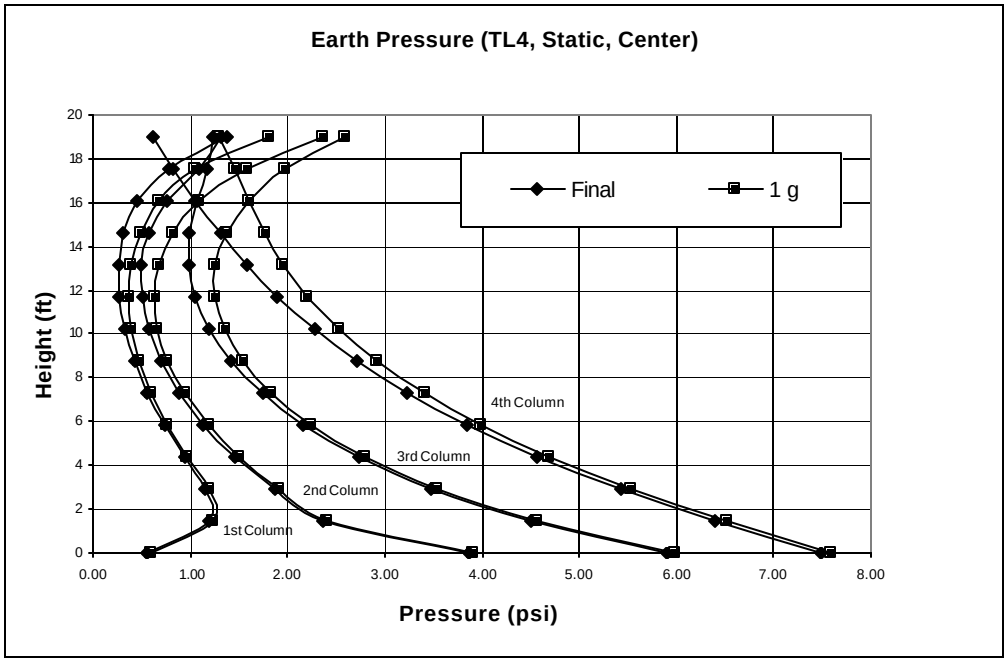


Figure 3-19: Earth pressure distribution at four different locations

(TL4, Center Hit, Static).

3.6.2.2 40-ft Type 7 Rail under TL4 Impact load at center

The analysis using the TL4 impact load shown in Figures 3.14 and 15 demonstrates the effect of impact load on the rail-slab-wall system behavior. Figure 3.20 shows that, when the impact is applied at the center of the rail, the rail-slab and wall system undergoes oscillation even after the termination of impact load with the amplitude at both ends being much larger than the center amplitude. Figure 3.21 shows that the forward wall displacement attains a maximum value near the wall top, drastically decreases with depth, and remains near a constant value at a depth greater than 5 feet. Figure 3.22 shows that the impact load causes the geogrid stress to increase from its static value by a maximum of 6 psi near the wall top. Figure 3.23 shows that the impact causes the earth pressure along the wall back to increase by a maximum of 6.5 psi and the change decreases drastically until a depth of 6 feet. Figures 3. 24, 25 and 26 show that the impact-load-induced earth pressures along the 2^{nd}, 3^{rd}, and 4^{th} column nodes decrease with depth and the distance from the wall back. Figure 3. 27, 28, 29 and 30 show the vertical stress distribution along the 1^{st}, 2^{nd}, 3^{rd} and 4^{th} column nodes, respectively. The impact load causes the vertical stress to change. The difference between the static and dynamic stresses is largest near the wall back and wall top, decreases with depth and the distance from the wall back, and becomes insignificant along the 3^{rd} and 4^{th} column nodes. The vertical stress distribution shifts from nonlinear to linear from the 3^{rd} column nodes and beyond.

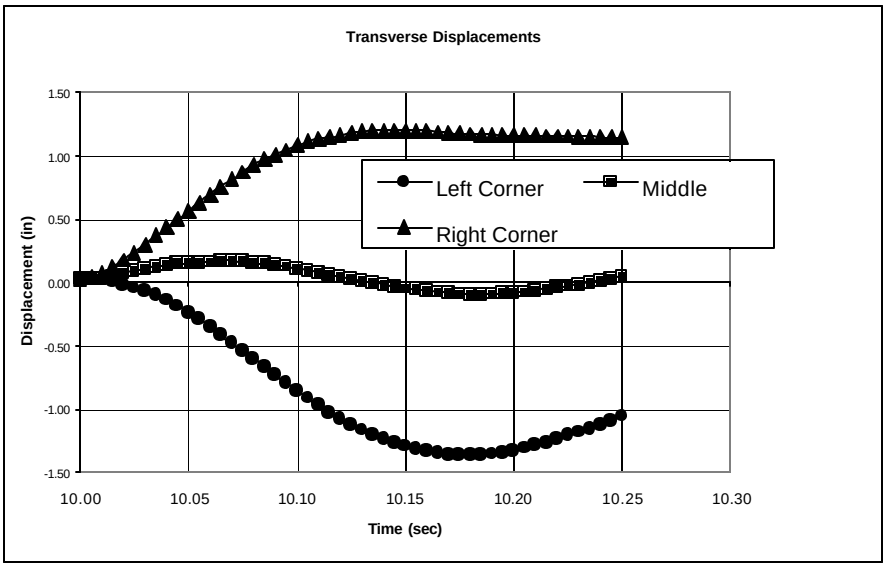


Figure 3-20: Transverse displacement time history of edge and corner nodes of Type 7 barrier (TL4, Center Hit, Impact)

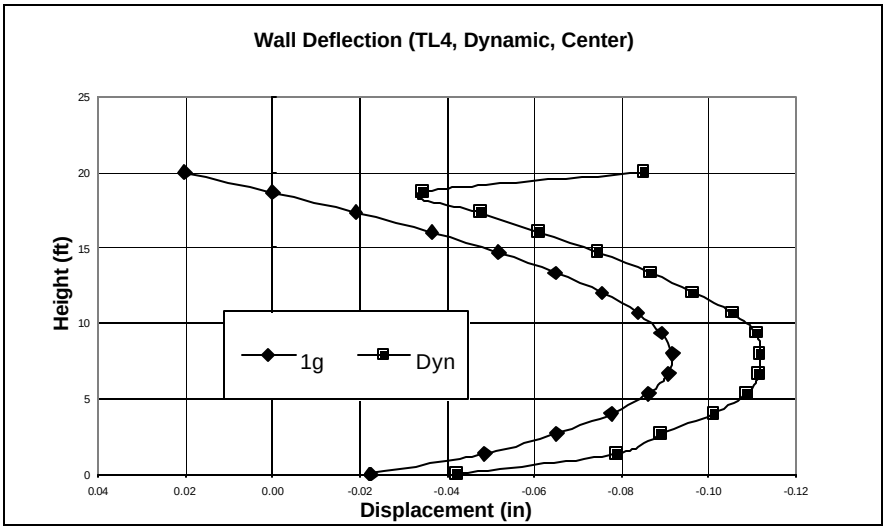


Figure 3-21: Final wall deflection after impact load (TL4, Center Hit, Impact)

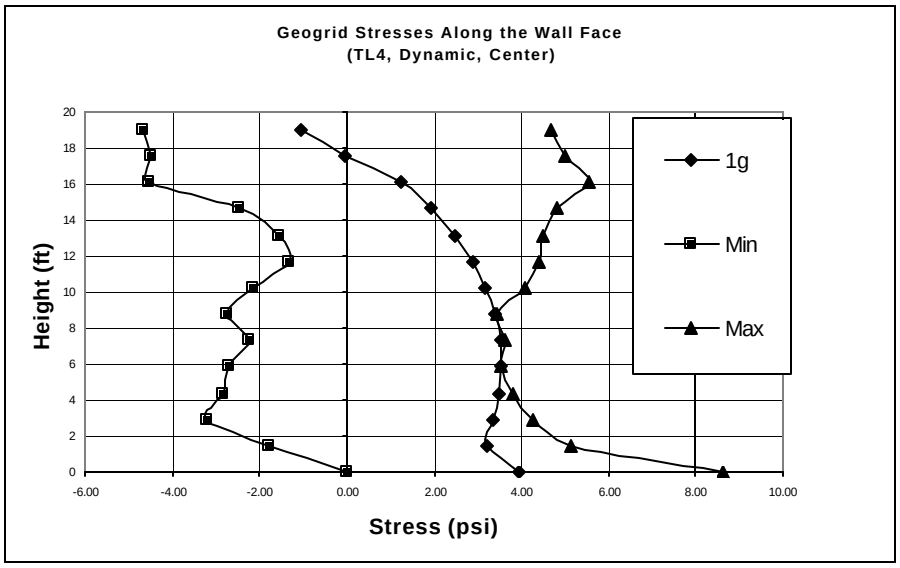


Figure 3-22: Min, Max and 1g geogrid stresses along the wall face (TL4. Center Hit, Impact)

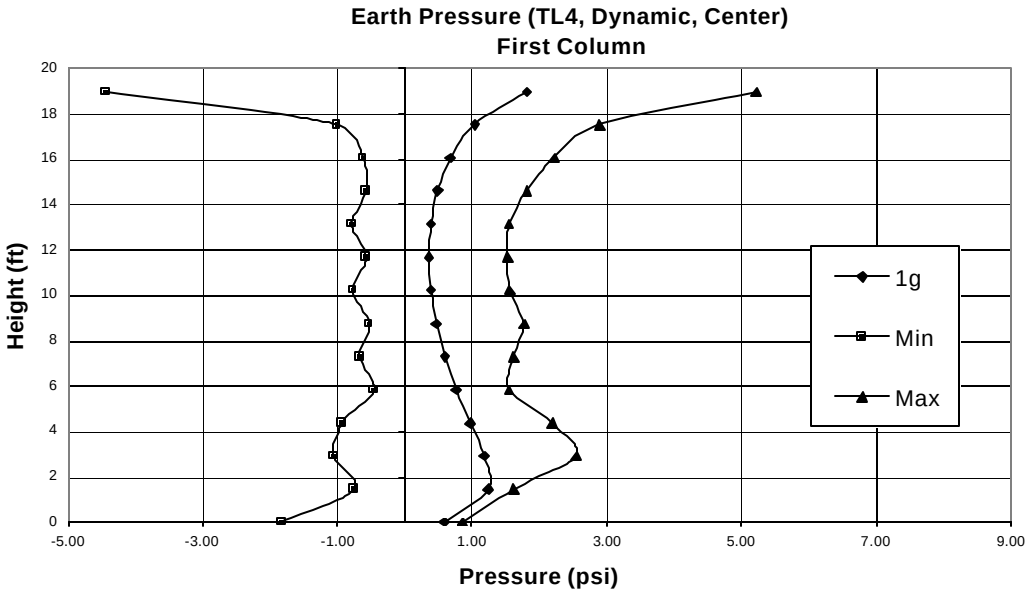


Figure 3-23: Min, Max and 1g earth pressures along the first column (TL4, Center Hit, Impact).

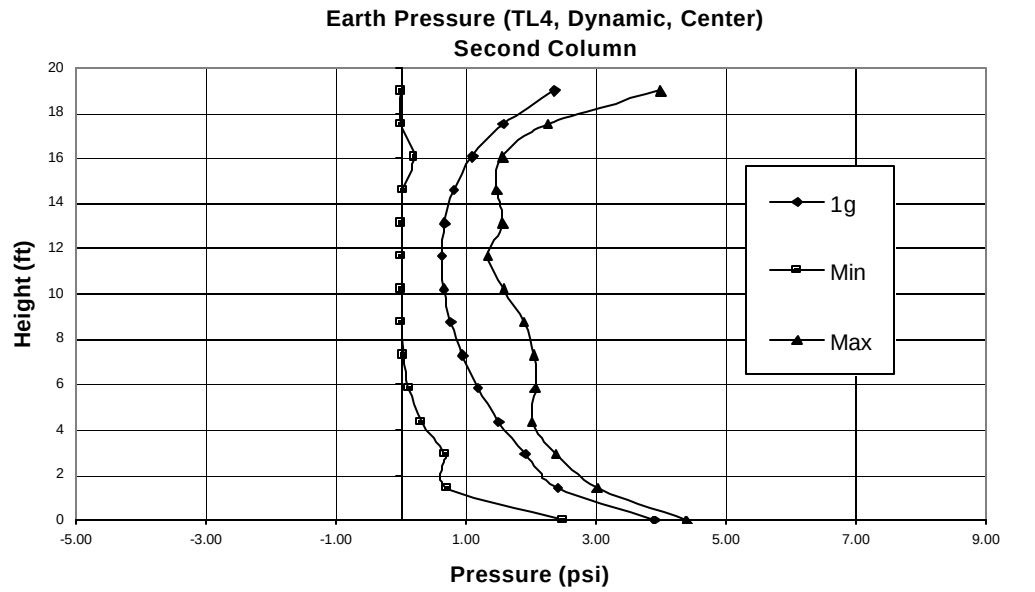


Figure 3-24: Min, Max and 1g earth pressure along the second column (TL4, Center Hit, Impact).

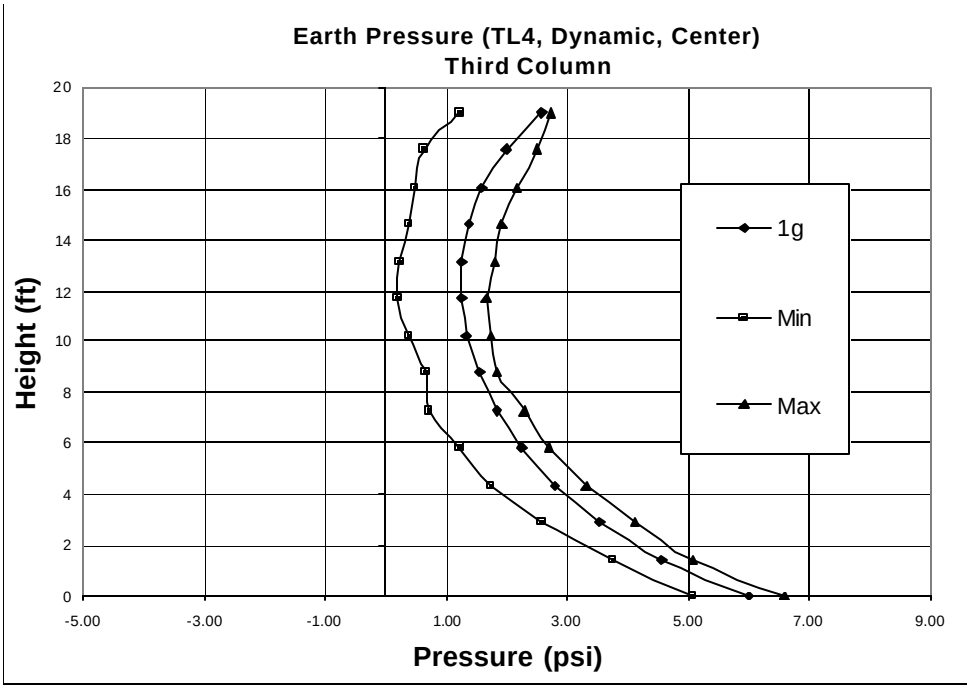


Figure 3-25: Min, Max and 1g earth pressure along the third column (TL4, Center Hit, Impact).

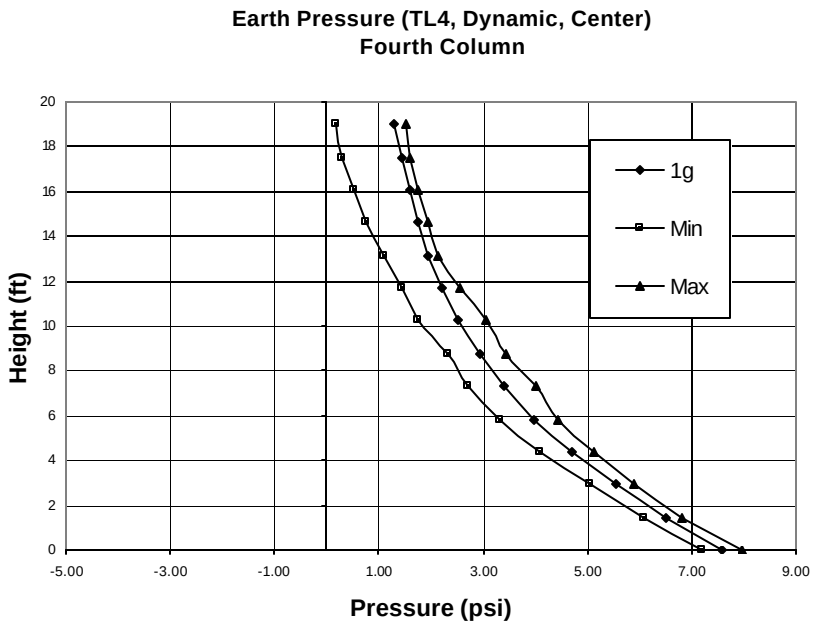


Figure 3-26: Min, Max and 1g earth pressure along the fourth column (TL4, Center Hit, Impact).

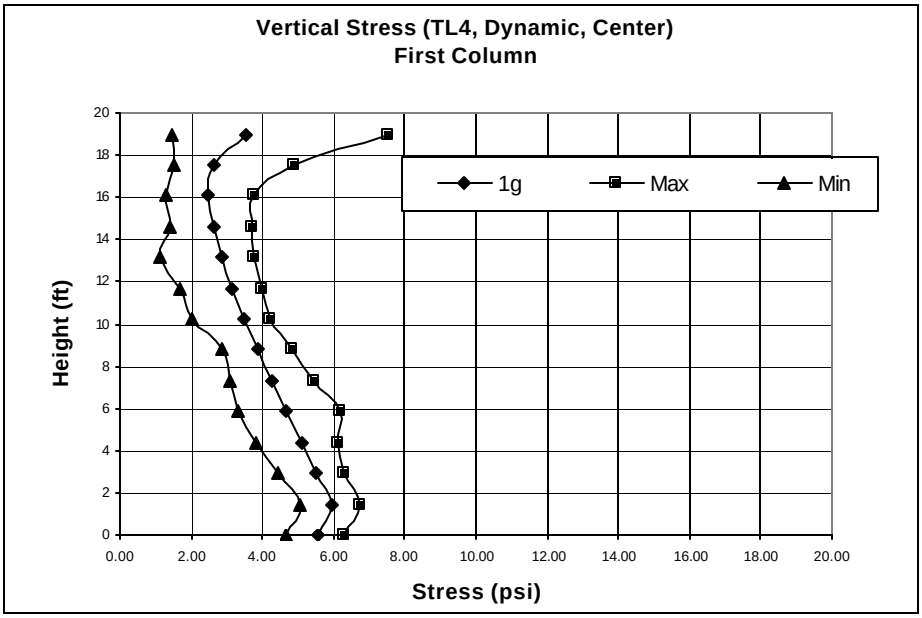


Figure 3-27: Min, Max and 1g vertical soil pressure along the 1st column (TL4, Center Hit, Impact).

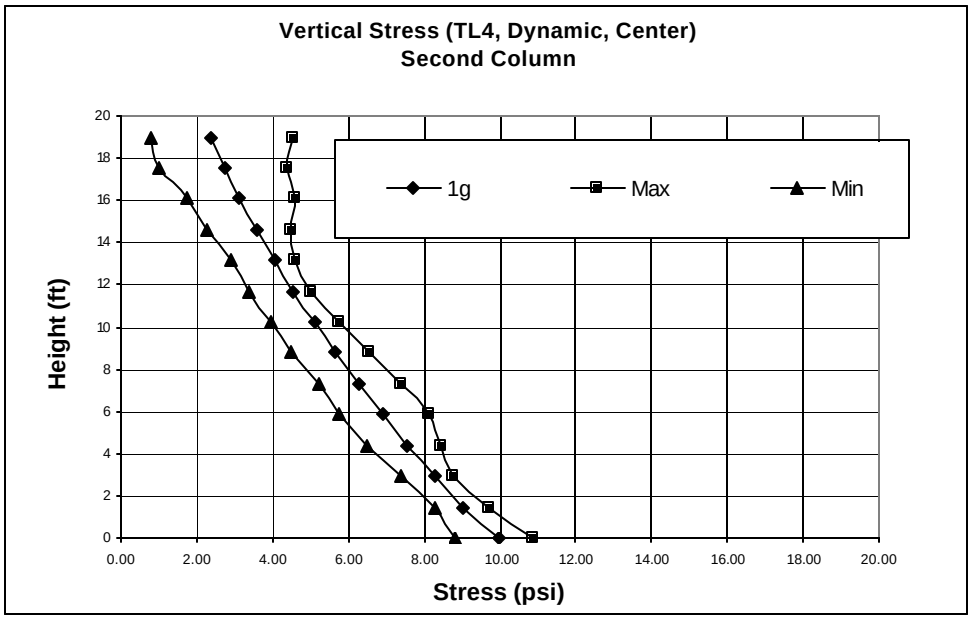


Figure 3-28: Min, Max and 1g vertical soil pressure along the 2nd column (TL4, Center Hit, Impact).

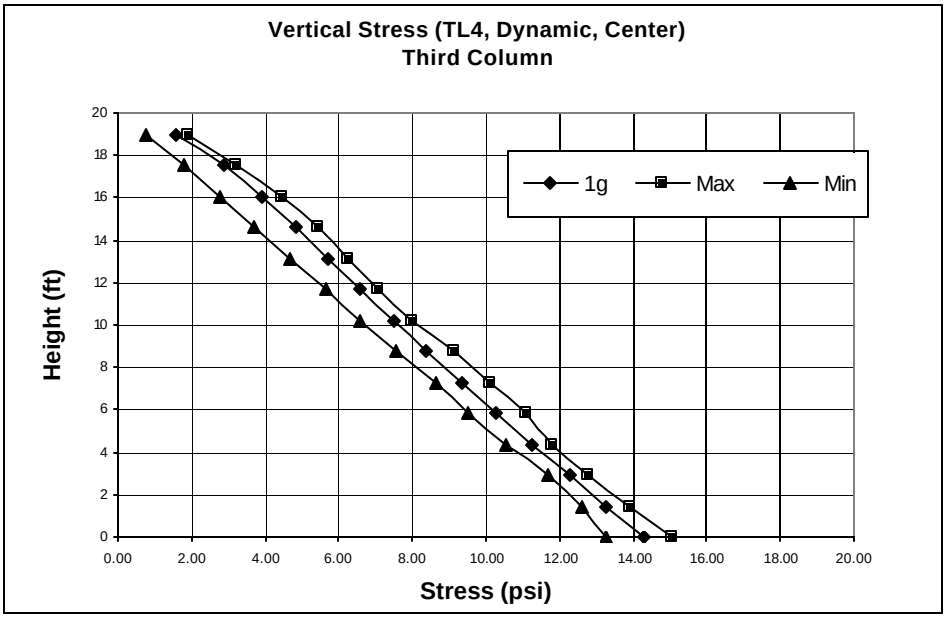


Figure 3-29: Min, Max and 1g vertical soil pressures along the 3rd column (TL4, Center Hit, Impact).

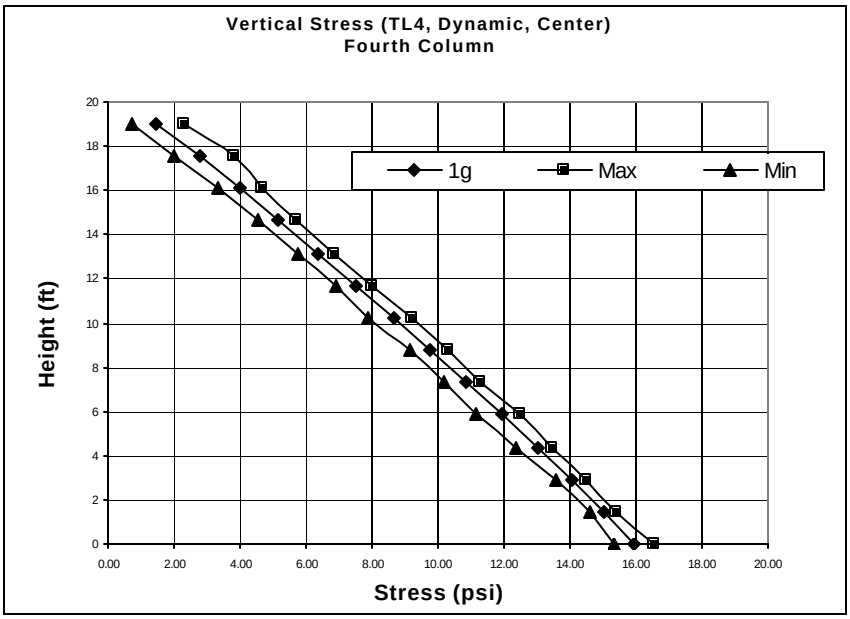


Figure 3-30: Min, Max and 1g vertical soil pressures along the 4th column (TL4, Center Hit, Impact).

3.7 Conclusions

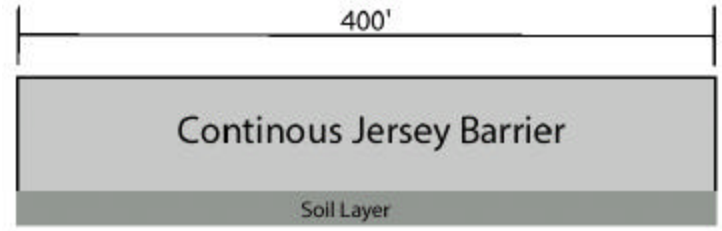
The TL4 impact load imposes great influences on the behavior of 20-ft and 40-ft Type 7 rails. All analyses were terminated prematurely because the rail and slab rotated, twisted and partially lifted off the backfill, and eventually gained momentum and tended to fly off the wall. The influence of impact on MSE wall performance is, generally speaking, small regardless of its ample reserved strength to resist the impact because of the loss of the slab-backfill interface frictional resistance. Without implementation of any improvement mechanism, it is necessary to evaluate the length of the rails required to prevent excessive movement. In Chapter 4, finite element analyses were performed to assess the influence length of both rail types at which the displacements become insignificant. The influence length was found to be 200 feet and 200-ft rails were then analyzed for their impact performance.

To determine the appropriate length for the analysis of the rail-MSE wall interaction and the rail-stability, the length of the rail analyzed evolved from 20, to 40, 200 and 400 feet. From the 400-ft analysis it was found that, at a distance of 100 feet away from the point of impact load application, stresses and displacements, particularly those in the transverse direction, become negligible. It was decided to choose the length of 200 feet as the influence length and use the length in further analysis. The results of all analyses are presented and discussed in details in Chapter 4.

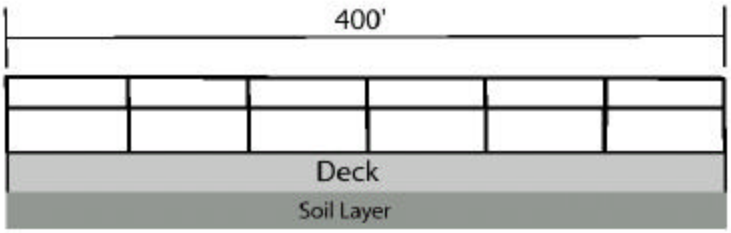
4.0 INFLUENCE LENGTH AND IMPACT PERFORMANCE OF RAILS

4.1 Influence Length Evaluation Using 400-ft Rails

To evaluate the minimum length required to achieve acceptable impact displacement, finite element analyses were performed on 400-ft Type 7 and Type 10 rails to determine the influence length. 400-ft long impact barriers were assumed to sit on a 1-ft thick foundation soil layer. Front views of both Type 7 and Type 10 rails are shown in Figure 4.1a and 4.1b, respectively. Finite element mesh of Type 7 rail is shown in Figure 4.2 in deformed shape right after the completion of TL-5a load. In all FEM analyses TL-5a load was used. All three components of TL-5a load as specified in the AASHTO LRFD Bridge Design Specifications 2000 (briefed as AASHTO 2000 Specs) were applied simultaneously in the analysis as shown in Figure 4. 3.



(a)



(b)

Figure 4.1 Front view of 400-ft long (a) Type 7 and (b) Type 10 guardrails.

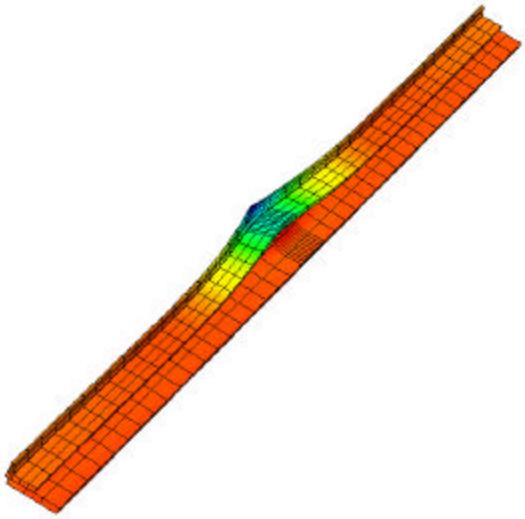


Figure 4.2 Deformed shape of Type 7 rail under TL5a load.

(Displacements are scaled by 100 times)

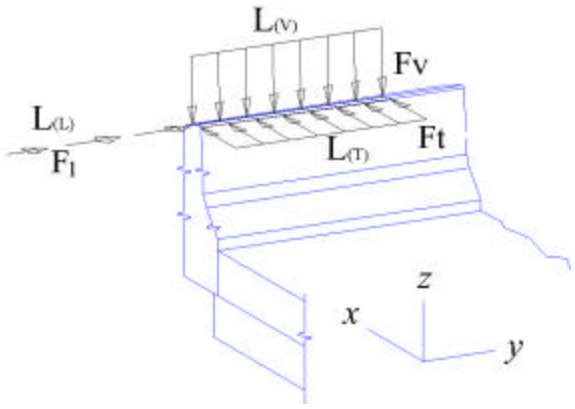


Figure 4.3 Three components of TL-5a load for Type 7 Rail.

4.2 Analysis Results and Discussions for the Influence Length of 400-ft Rails

Per the agreement set forth in the study panel meeting, analyses were performed for the following four different combinations of the impact load location and rail types to assess the influence length (IL) of impact rails:

- Colorado Type 7 Center Load,
- Type 7 Edge Load,
- Type 10 Center Load, and
- Type 10 Edge Load.

Table 4.1 summarizes the analysis cases. The influence length is defined as the length of impact rail at which a performance measure becomes negligible. The influence length will then be used in the subsequent three-dimensional analysis of the load transfer mechanism from the rail to the supporting retaining walls.

All analyses use the TL-5a load. Figure 4.4 shows the locations of the reference nodes of the Colorado Type 7 Rail and Figure 4.14 for the Colorado Type 10 Rail. Table 4.1 shows the analyses performed for the evaluation of the influence length. Concrete is modeled as an oriented brittle failure material (OBF) or linear elastic material whenever appropriate. In case of Type 10 rail, the steel rail is modeled as an elastic-perfect plastic material. In all analyses the rail is considered continuous.

4.2.1 Type 7 Rail with Static Center Load Application

When the oriented brittle failure model is used to model the concrete behavior (OBF concrete) and the Ramberg-Osgood the soil (R-O soil), the analysis was successfully completed for the case of Type 7 rail under TL-5a at center. The analysis results are briefly summarized. All six stress components (σ_x, σ_y, σ_z, τ_{xy}, τ_{yz} and τ_{zx}) and three displacement components (δ_x, δ_y and δ_z) at Points A, B, and C are plotted against the

Table 4.1 Analyses performed for the evaluation of the influence length

	TYPE 7		**TYPE 10**	
	Center	Edge	Center	Edge
STATIC FORMULATION	C=OBF, S=R-O Complete with full TL5a load	C=OBF-S=R-O Terminated at 55% if TL5a load	C=OBF, S=R-O, ST=EL-PL Complete with full TL5a load	C=OBF, S=R-O, ST=EL-PL Terminated at 55% of TL5a load
DYNAMIC FORMULATION		C=ELAS, S=R-O Complete C=OBF, S=R-O Terminated at 55% of TL5a load		C=ELAS, S=R-O, ST=EL-PL Terminated at 85% of TL5a load C=OBF, S=R-O, ST=EL-PL Terminated at 55% of TL5a load
C= Concrete, **S**= Soil, **OBF**= Oriented Brittle Damage material madel, **R-O**= Ramberg Osgood material model, **ST**= Steel, **ELAS**= Elastic material model, **EL-PL**= Elastic-Plastic Material model				

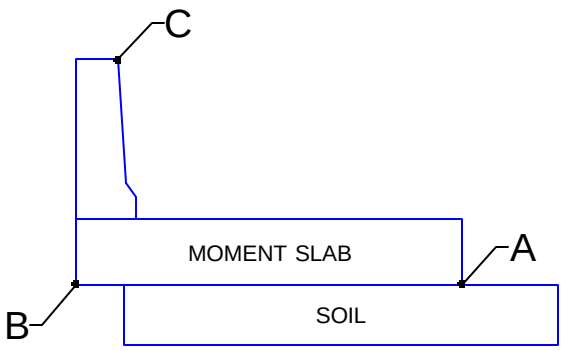


Figure 4.4 Reference locations for data presentation of Type 7 barrier.

distance from the left end of the rail in Figure 4.5 thru 10 and Figure 4.11 thru 13, respectively, and results are presented in the sequence of normal stresses, shear stresses and displacements.

Normal Stresses As shown in Figure 4.5 the maximum normal stress at Point A (briefed as A) is compressive σ_y of 200 psi, which is much smaller than the compressive strength of concrete. It becomes tensile at 35 feet and negligible at 100 feet from both sides of the center. σ_x and σ_z are much smaller than σ_y. Thus, the influence length is estimated at

200 feet. Figure 4.6 and 4.7 show the maximum normal stresses are 47 psi (tension) at B and over 200 psi at C. The IL is also estimated at 200 feet. In short, all normal stresses become negligible at a distance of 100 feet from both sides of the center and the influence length is selected as 200 feet.

Shear Stresses Shear stress components at A, B, and C are shown in Figures 4.8, 4.9 and 4.10, respectively. The maximum shear stress at A is τ_{xy} of 125 psi. It reverses the direction at both sides of the center. The influence length is approximately 200 feet. The maximum shear stress at B is τ_{yz} of 75 psi and the influence length is 100 feet. The maximum shear stress at C is τ_{yz} of 60 psi and the influence length is 100 feet. In short, all shear stresses become small at 100-ft distance from the center and the IL is also 200 feet and shear stresses are not critical to the IL selection.

Normal Displacements Figures 4.11, 4.12, 4.13 show the maximum displacements at A, B and C when the analysis is terminated are δ_x of 0.24, 0.4 and 0.24 inches, respectively. The displacements δ_y and δ_z are much smaller and the influence length is 150 feet.

General Conclusions

- All maximum stresses at A, B, and C are much smaller than the corresponding concrete strengths.
- The maximum normal displacement in the transverse direction is less than 0.5 inches.
- The influence length is determined to be 200 feet.
- The rail slightly rotates about B, the moment slab is not in full contact with the supporting soil, and the vertical normal stress is concentrated near B.

It must be noted that the analysis is performed under the assumption of continuous rail. This would mean that all performance factors vary when short sections are used. For instance, if 40-foot sections are used, the displacements are expected to be much larger.

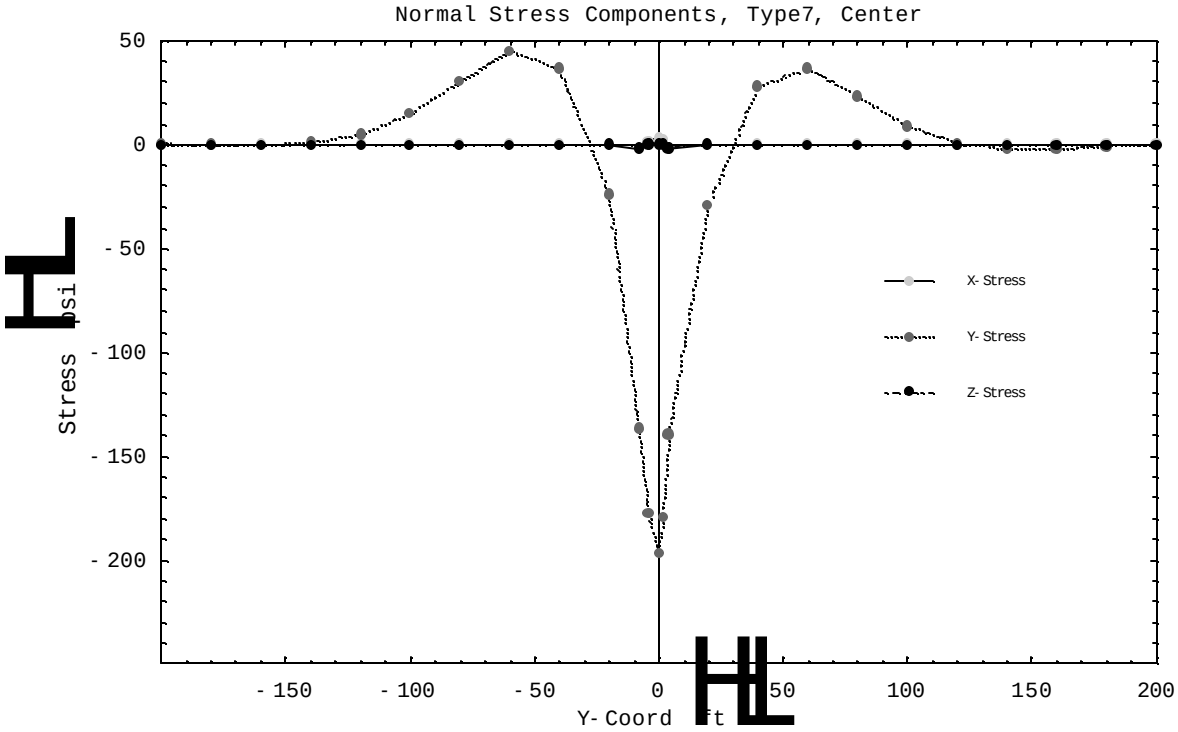


Figure 4.5 Normal Stress components along point A of Type 7 Rail (400-ft, Center Hit, Static, TL5a).

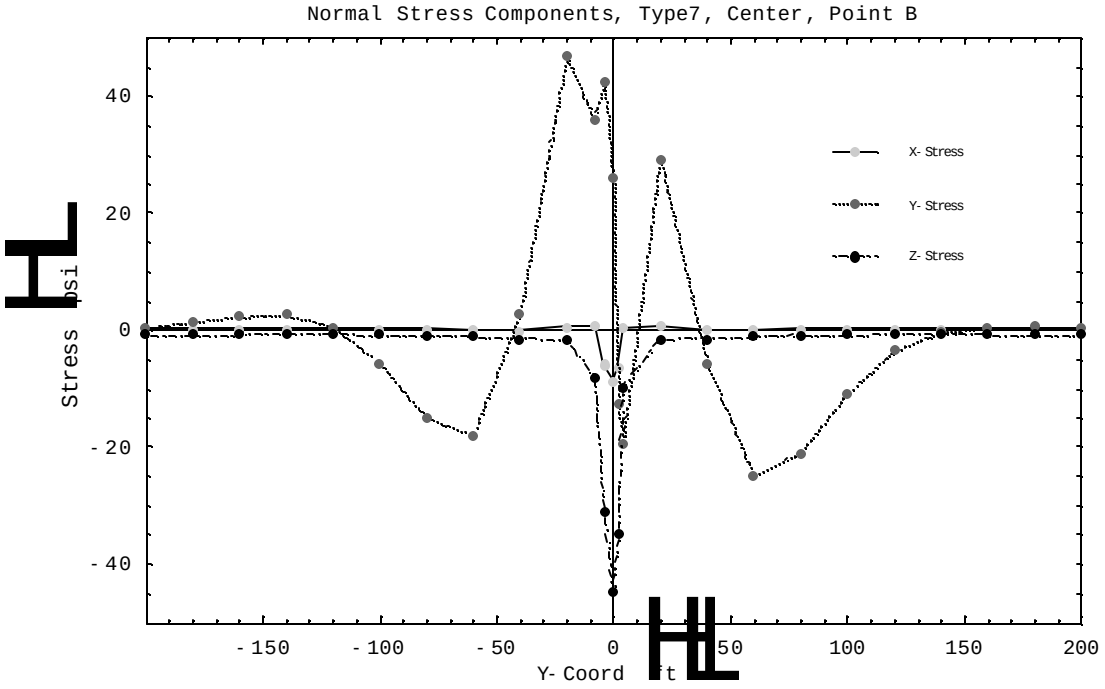


Figure 4.6 Normal Stress components along point B of Type 7 Rail (400-ft, Center Hit, Static, TL5a).

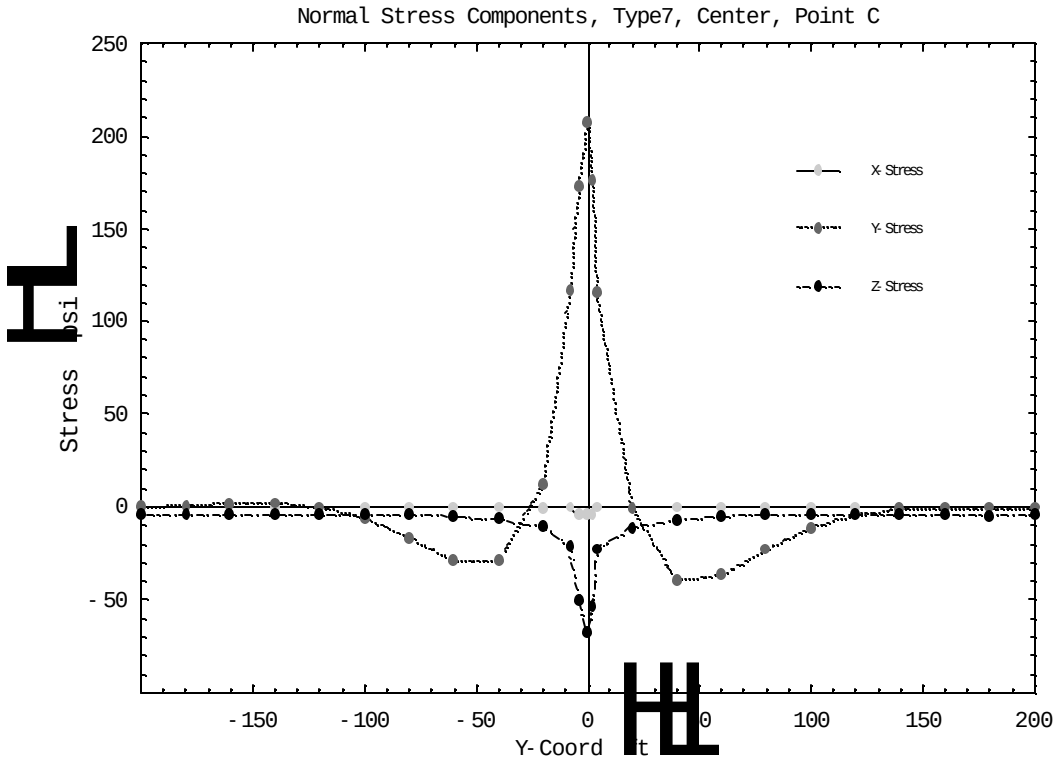


Figure 4.7 Normal Stress components along point C of Type 7 Rail (400-ft, Center Hit, Static, TL5a).

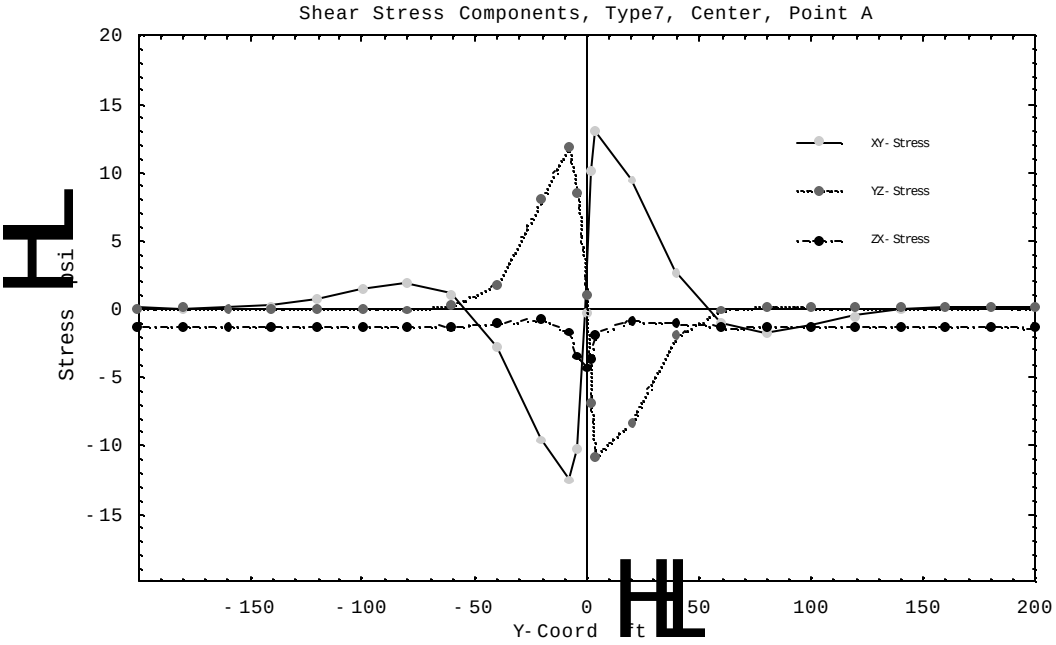


Figure 4.8 Shear Stress components along point A of Type 7 Rail (400-ft, Center Hit, Static, TL5a).

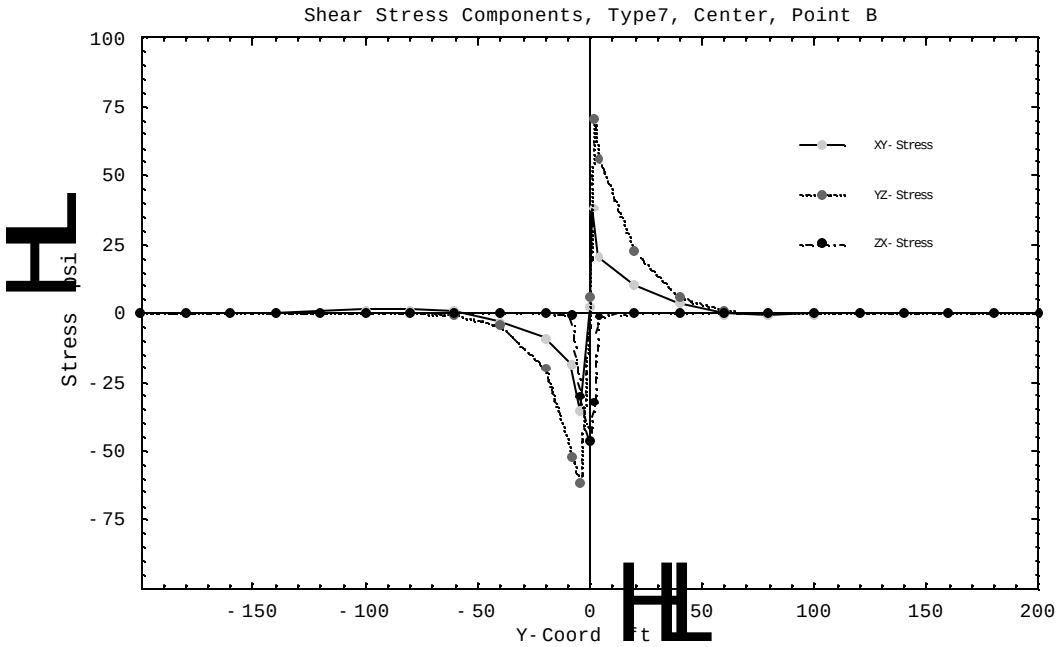


Figure 4.9 Shear Stress components along point B of Type 7 Rail (400-ft, Center Hit, Static, TL5a).

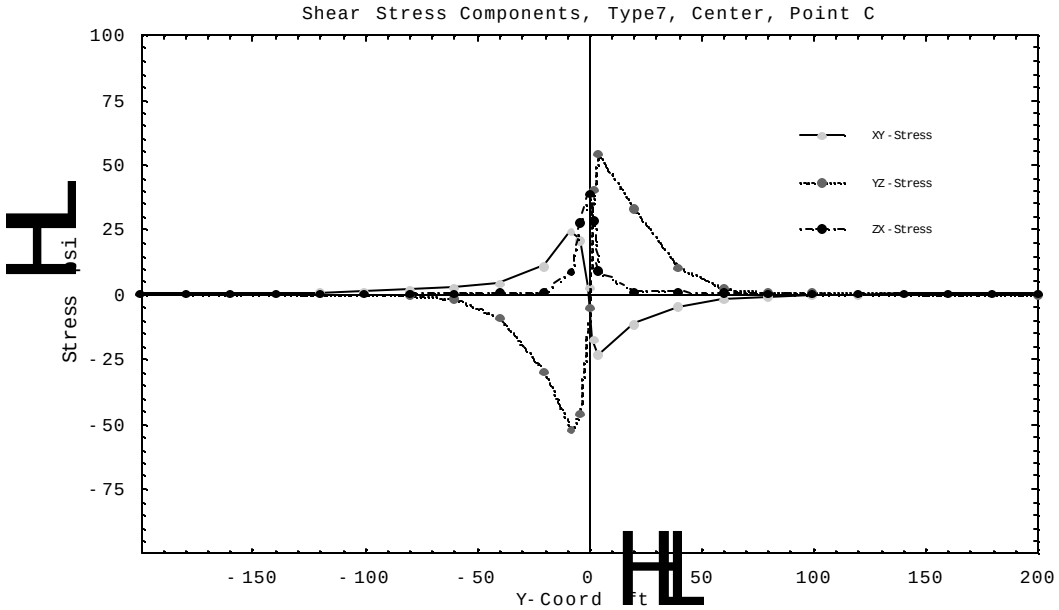


Figure 4.10 Shear Stress components along point C of Type 7 Rail (400-ft, Center Hit, Static, TL5a).

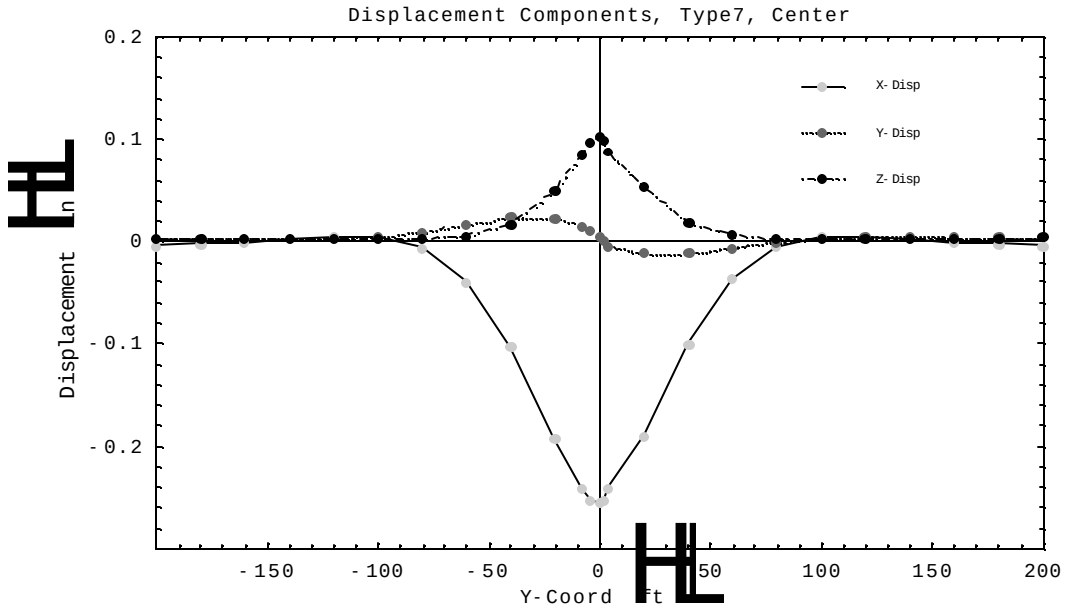


Figure 4.11 Displacement components at point A of Type 7 Rail (400-ft, Center Hit, Static, TL5a).

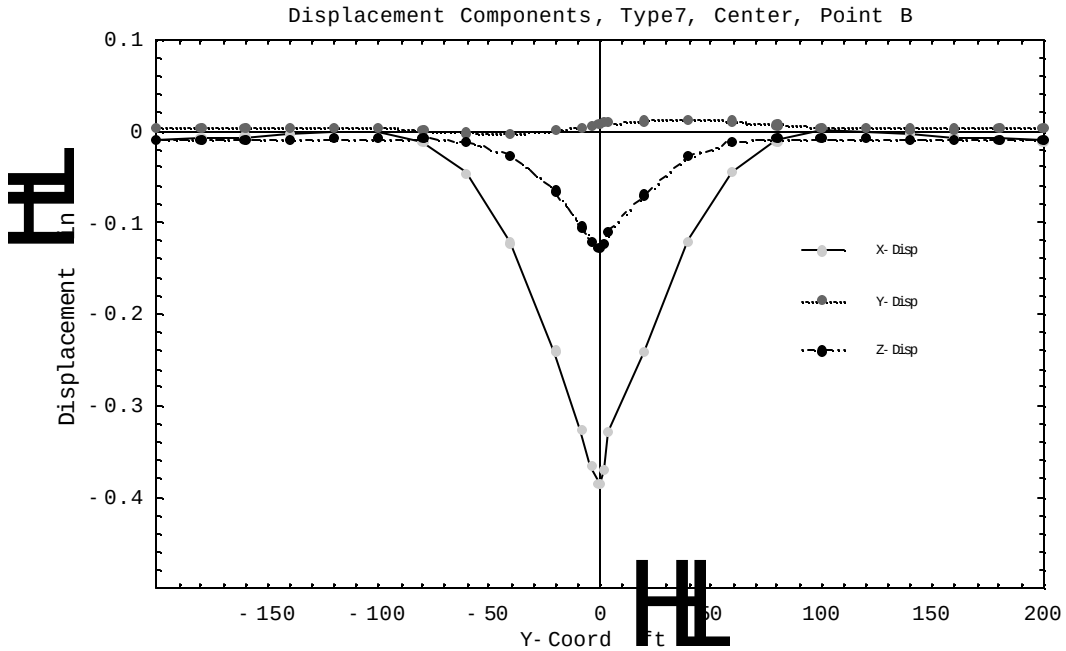


Figure 4.12 Displacement components at point B of Type 7 Rail (400-ft, Center Hit, Static, TL5a).

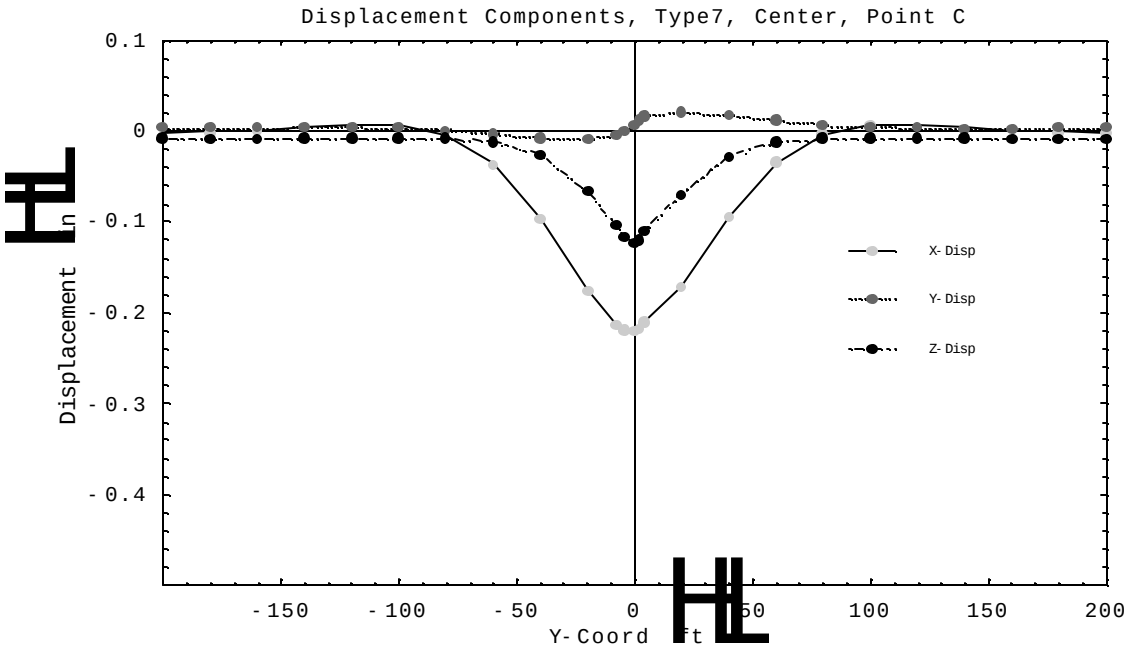


Figure 4.13 Displacement components at point C of Type 7 Rail (400-ft, Center Hit, Static, TL5a).

4.2.2 Type 7 Rail with Static Edge Load Application

The analysis was not successful with the OBF concrete and R-O soil using the static formulation. It was terminated at 55% of the full TL-5a load. The decision was made to pursue the analysis with dynamic formulation because of its ability in accommodating the rigid body rotation. The first trial using the OBF concrete and R-O soil was also terminated at 55% of the full TL-5a load. Then, it was decided to perform another analysis using elastic concrete (E-concrete) and R-O soil using dynamic formulation. The analysis was successfully carried out to the full TL-5a load. The end displacement was found to be extremely large at about 280 inches or over 23 feet as will be discussed later. Both sets of analysis results are briefly summarized. All six stress and three displacement components at A, B, and C are plotted against the distance from the left edge of the rail. All figures for this section are shown in Appendix B.

Normal Stresses with OBF Concrete and R-O Soil The analysis was terminated at 55% of TL-5a load and the analysis results are summarized as follows:

- Maximum normal stress at A is σ_y of 340 psi (tensile) at 75 feet from the left edge of the rail and it becomes very small at a distance of 150 feet. σ_x and σ_z are much smaller than σ_y.
- Maximum normal stress at B is σ_y of –245 psi (compressive). The maximum σ_x and σ_z are also compressive and are much smaller than σ_y. All normal stresses become negligible at a distance of L = 150 feet from the left edge.
- Maximum normal stress at C is σ_y of –230 psi (compressive). σ_x and σ_z are also compressive but are much smaller than σ_y. All normal stresses become negligible at a distance of 150 feet from the left edge.

In short normal stresses are smaller than the concrete strength at all points investigated and the influence length is estimated at 150 feet.

Normal Stresses with E (elastic) Concrete and R-O Soil The analysis was successfully performed to 100% TL-5a load and the observations are summarized as follows:

- Maximum normal stress at A is σ_y of 3600 psi (tensile) at 150 feet from the left edge of the rail. This tensile stress remains quite large throughout the whole length of the rail except near both ends. σ_x and σ_z are much smaller than σ_y.
- Maximum normal stress at B is σ_y of –3700 psi (compressive) at 150 feet from the left edge. σ_x and σ_z are insignificant compared to σ_y.
- The normal stress at C is σ_y of 1000 psi (tension) at 130 feet and –1900 psi (compression) at 300 feet from the left edge. σ_x and σ_z are insignificant as compared to σ_y, which remained significant throughout almost the whole length of the rail.

In short all stress components and transverse displacements are quite large and the rail stability analysis should engage the whole length of the rail. Even then the rail fails under both tension and compression.

Shear Stresses with OBF Concrete and R-O Soil

- All shear stresses at A are quite small compared to the shear strength of concrete. The maximum τ_{xy} is 22 psi at 20 feet, which is larger than τ_{zx} and τ_{yz}. τ_{xy} reverses its direction at around 60 feet from the edge and eventually becomes insignificant at 170 feet.
- At B and C, the maximum shear stress is τ_{yz} = 75 psi and it becomes insignificant at 100 feet.

In short all shear stresses are much smaller than the shear strength and become negligible at 100 feet from the edge. Thee shear stress is not the governing factor.

Shear Stresses with E Concrete and R-O Soil Shear stresses are in general much larger than those of the OBF concrete and R-O soil and are approaching the shear strength of concrete. They are briefed as follows:

- At A, τ_{xy} peaks at 365 psi at 150 feet, τ_{yz} varies between –300 psi to +200 psi, and τ_{zx} is very small in comparison.
- At B, τ_{xy} varies from –100 psi at edge to –1100 psi at 170 feet, τ_{yz} from +50 psi at edge to +900 psi at 200 feet, and τ_{zx} is very small in comparison.
- At C, τ_{yz} varies between +130 psi to +720 psi at 170 feet and the other two components are much smaller.

In short some components of shear stresses are quite large and approaching shear resistance of concrete with little buffer for safety.

Normal Displacements with OBF Concrete and R-O Soil

- The maximum displacement component is δ_x, about 2 inches. Since the analysis was terminated at 55% of the full TL5a load, the actual displacement is expected to be much larger.
- Another analysis was successfully performed to the full TL5a load using the E concrete and R-O soil and the dynamic formulation. To check the difference between the two analyses, the normal displacements from the two analyses were compared and the difference was found to be insignificant for the displacement at the same load level of 55% of the full TL5a load.
- At the full TL5a load, the maximum displacement in the x direction at A is δ_x = 285 inches (or over 23 feet.) This implies that the end of the Type7 rail needs a strong end support to minimize transverse displacement.
- At the full TL5a load, about 200 feet of the moment slab is lifted and separated from the foundation soil. This implies that a proper anchorage is required along the longitudinal edge of the moment slab.

Normal Displacement with E Concrete and R-O Soil

- At all points, the displacement in the x direction (transverse direction), δ_x, dominates and it is excessively large. The end of the rail will move around 23 feet away from the supporting MSE wall and the influence become an unrealistic term.
- The end of the rail is lifted off the ground by about 12 feet over 280 feet of the rail. This shows that without improvement under the current AASHTO code, the rail is unsafe under TL-5a load applied at the rail edge.

General Conclusions for Type 7 Rail under TL5a Load Applied to the Edge

- The normal displacements are unacceptably large with a maximum of over 23 feet at the left edge where the load is applied.

- About 200 to 300 feet of the moment slab is lifted off the foundation. This indicates that the rail system requires improvement mechanisms at the rail edge to prevent rotation and separation.
- Some normal and shear stress components approach the respective strengths of concrete.

Colorado Type 7 rail will require a strong end support to resist the displacements, rotation, twisting, and the stress-induced failure. It definitely requires some restraining mechanism to prevent the moment slab from being lifted off the foundation soil and to prevent the rotation of rail system. Without any improvement, the rail system will be unsafe in the situation where a vehicle impacts the end of the rail.

4.2.3 Type 10 Rail with Center Load Application, OBF Concrete, R-O Soil and EP Steel Rail

The analysis was successfully completed with OBF concrete, R-O soil and EP (elastic-plastic) steel for the Type 10 rail under the TL-5a load applied at the rail center. Briefly summarized are six stress components at A, C and D, three displacement components at points A, B, C, and D, and axial force and shear forces along the length of steel rail. Out of four analyses, only the case with the center load application, OBF concrete, R-O soil, and EP steel rail was completed to the full TL-5a load and the other three cases with the edge load application were not.

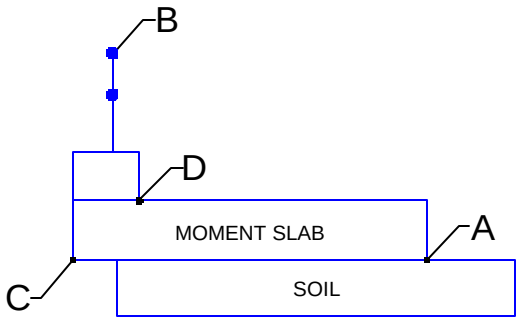


Figure 4.14 Locations of A, B, C and D for data presentation of Type 10 barrier.

Normal Stresses The analysis was completed to the full TL-5a load with the following observations from Figures 4.16, 17 and 18:

- At A, σ_y has a maximum compressive stress of 400 psi at the center of impact. The compressive stress gradually decreases to zero at ±50 feet from the center, then it reaches a maximum tensile stress of 165 psi at ±90 feet and becomes zero at both ends. σ_x and σ_z are much smaller than σ_y. The influence length based on σ_y is 400 feet.
- At C, σ_y reaches a maximum of +450 psi at the center of impact, it decreases to zero at ±50 feet, becomes compressive and eventually becomes zero at ±170 feet. σ_x and σ_z are much smaller than σ_y. Influence length is 350 feet.
- At D, σ_y reaches a maximum of 130 psi at the center of impact, becomes compressive at ±50 feet and becomes zero at -125 feet and +165 feet. Influence length is 300 feet.

In short, the maximum tensile stress is 450 psi at C, the maximum compressive stress is -400 psi at A and the influence is 350 feet.

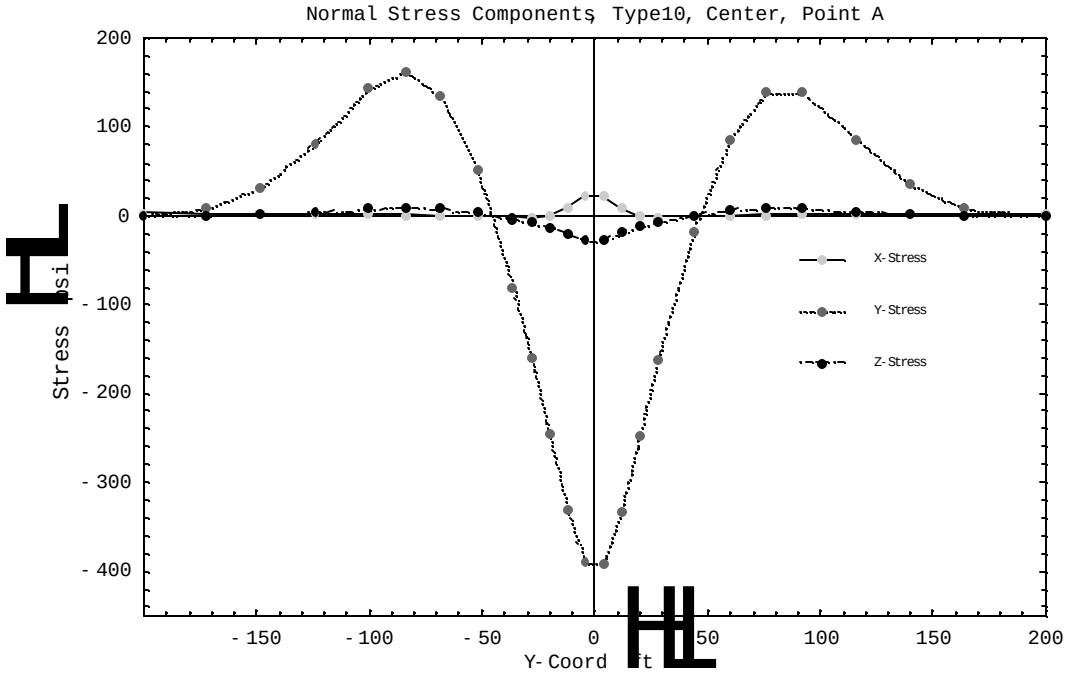


Figure 4.15 Normal Stress components at point A of Type 10 Rail(400-ft, Center Hit, Static, TL5a).

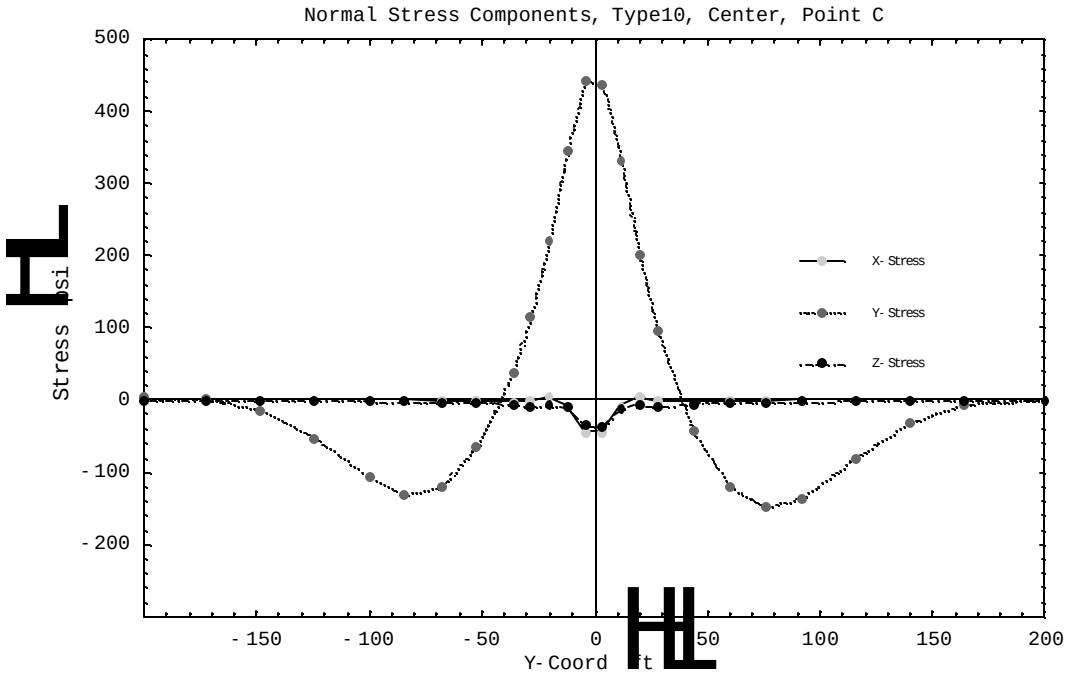


Figure 4.16 Normal Stress components at point C of Type 10 Rail (400-ft, Center Hit, Static, TL5a).

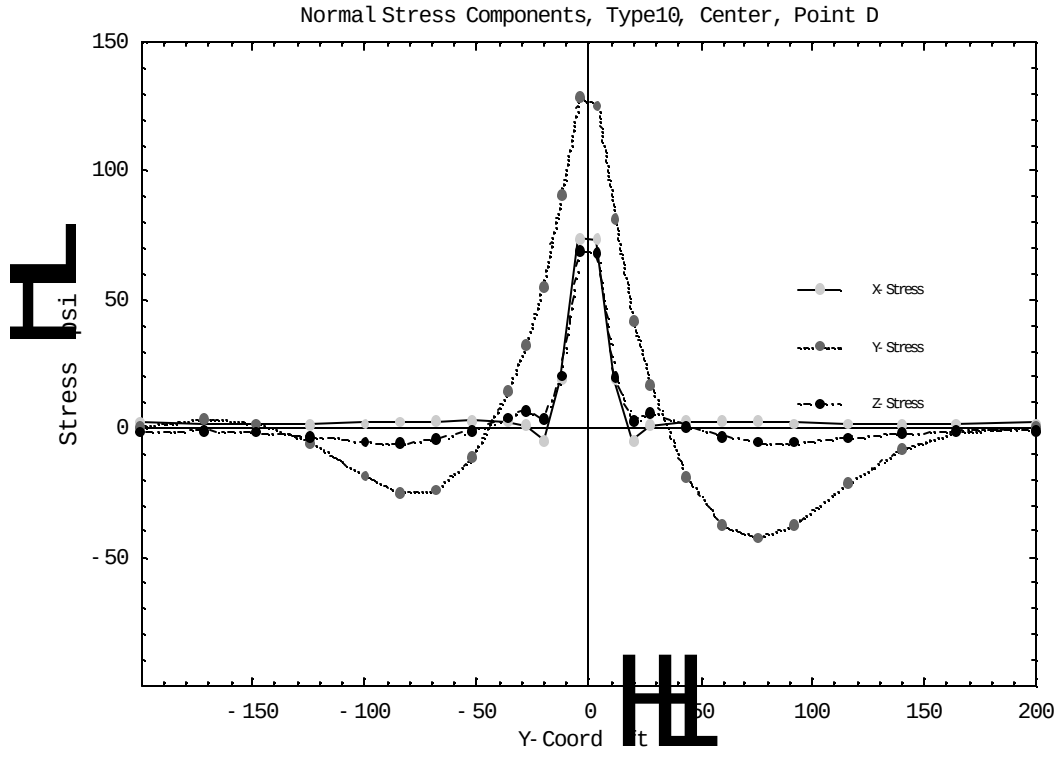


Figure 4.17 Normal Stress components at point D of Type 10 Rail (400-ft, Center Hit, Static, TL5a).

Shear Stresses (Figures 4.18, 19 and 20)

- At A, the maximum shear stress is ±15 psi near the center. At shear stresses becoming nearly zero at L = ±150 feet, the influence length = 300 feet.
- At C, the maximum shear stress is 100 psi. It occurs at L = ±25 feet. All shear stresses become negligible at L = ±75 feet. Influence length = 150 feet.
- At D, the maximum shear stress is 130 psi at L = ±20 feet. They become negligible at L = ±75 feet. Influence length is 150 feet.

In short shear stresses are small compared to the shear strength of concrete and the influence length is 300 feet.

Normal Displacements (Figures 4.21, 22, 23 and 24)

- The vertical displacement at A indicates the moment slab is lifted off the ground. At A, C, and D, however, the normal contact stress is zero near the edge of the moment slab and is maximum compressive near the block facing wall.
- The maximum displacement ranges from 1.0 to 1.5 inches.
- All displacements become negligible at ±100 feet.

In short the maximum displacement is δ_x = 1.5 inches at the point of contact and the influence length is 200 feet.

Axial and Shear Forces along the Rail (Figures 4. 25 and 26)

- The maximum shear force on the steel pipe is 20,000 lbs., and it becomes negligible at ±100 feet and the influence length is 200 feet.
- The maximum axial tensile force is 10,000 lbs at - 40 feet, maximum compressive forces are 3500 lbs at 100 feet and 5000 lbs. at ±100 feet and the influence length is 400 feet.

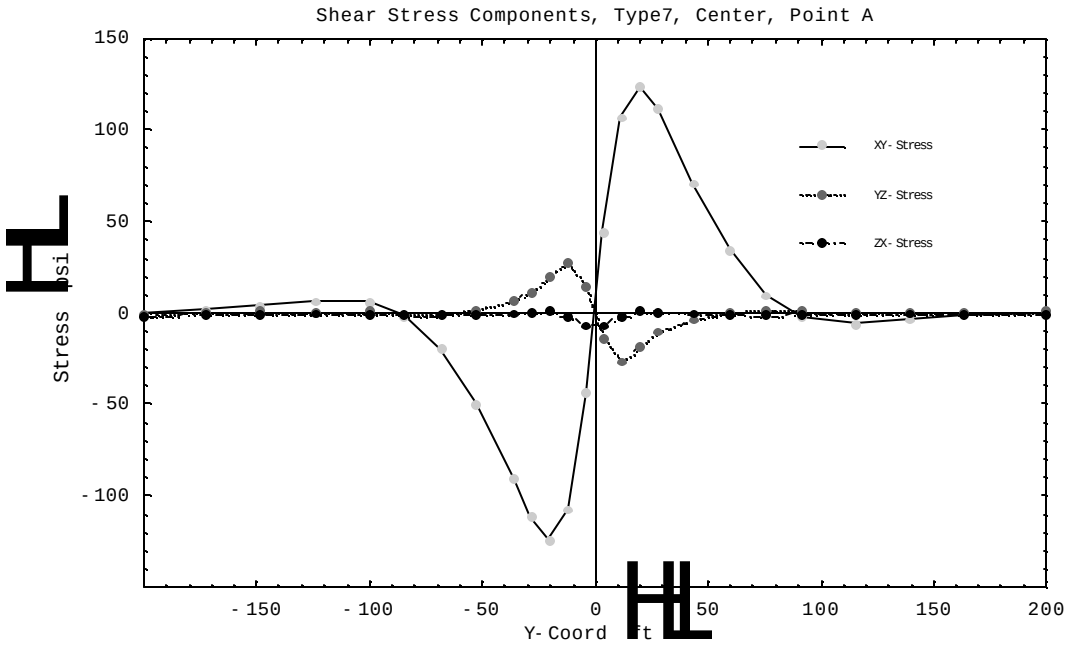


Figure 4.18 Shear Stress components at point A of Type 10 Rail (400-ft, Center Hit, Static, TL5a).

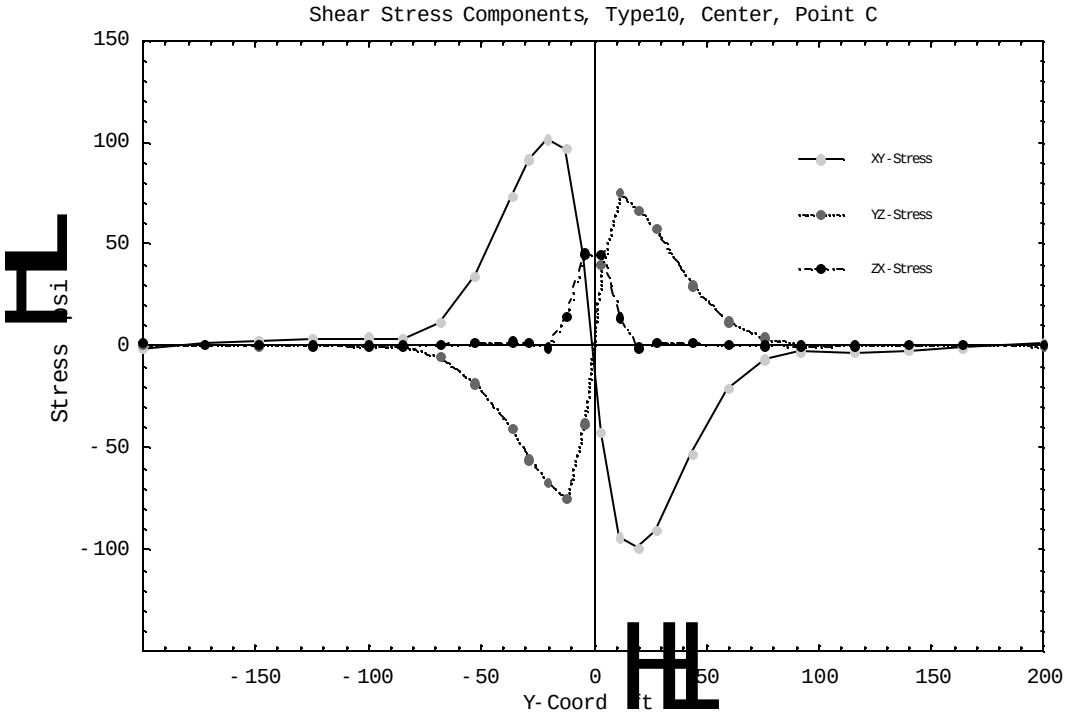


Figure 4.19 Shear Stress components at point C of Type 10 Rail (400-ft, Center Hit, Static, TL5a).

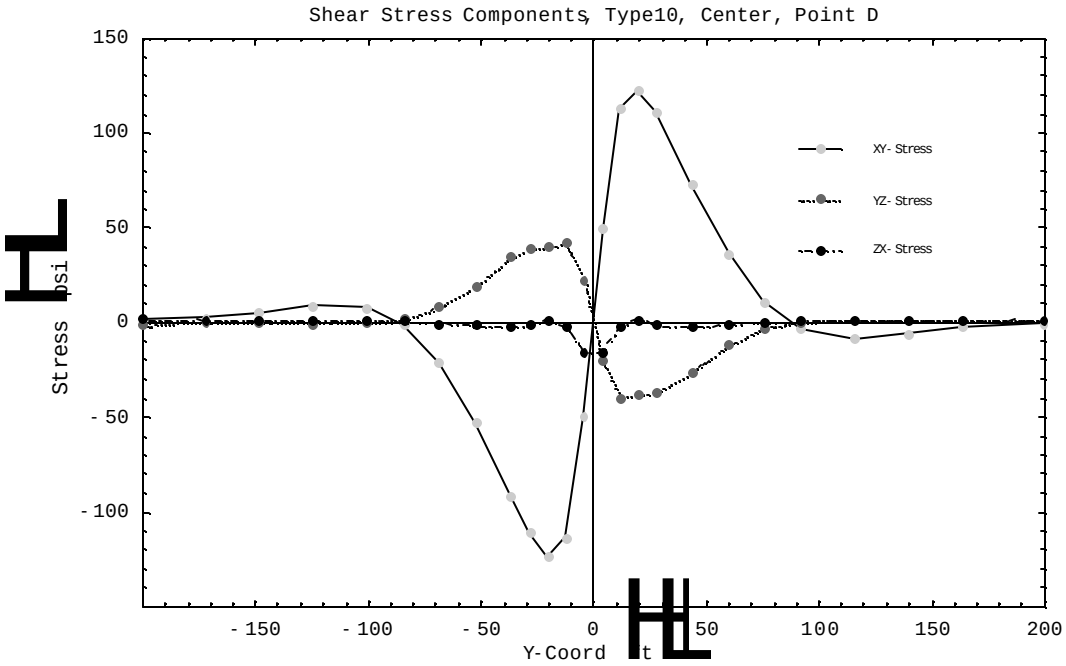


Figure 4.20 Shear Stress components at point D of Type 10 Rail (400-ft, Center Hit, Static, TL5a).

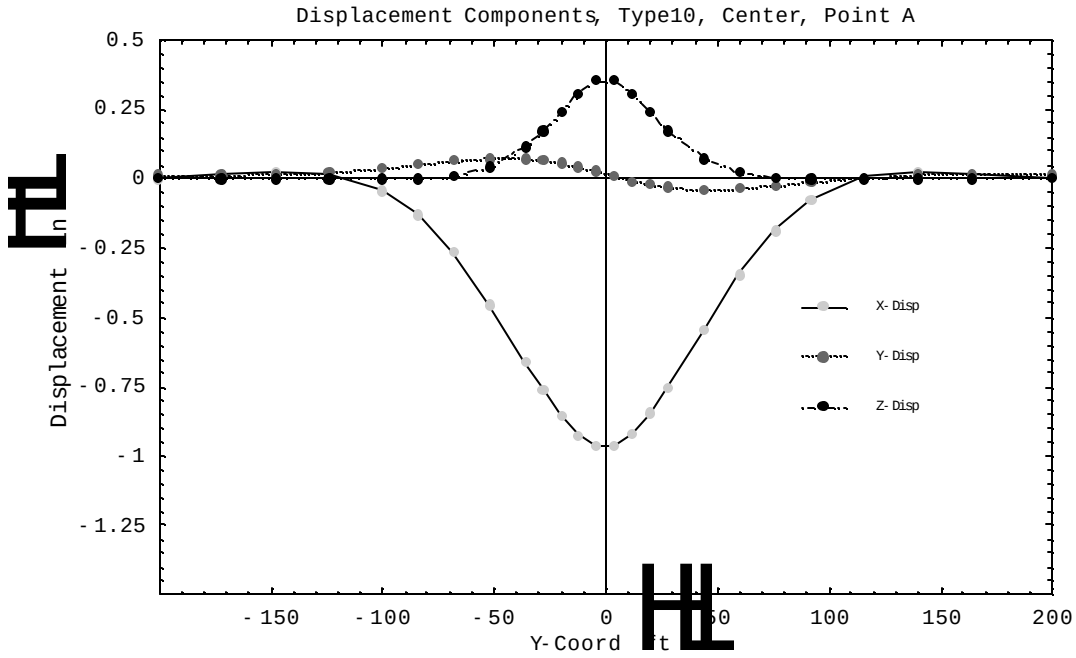


Figure 4.21 Displacement components at point A of Type 10 Rail (400-ft, Center Hit, Static, TL5a).

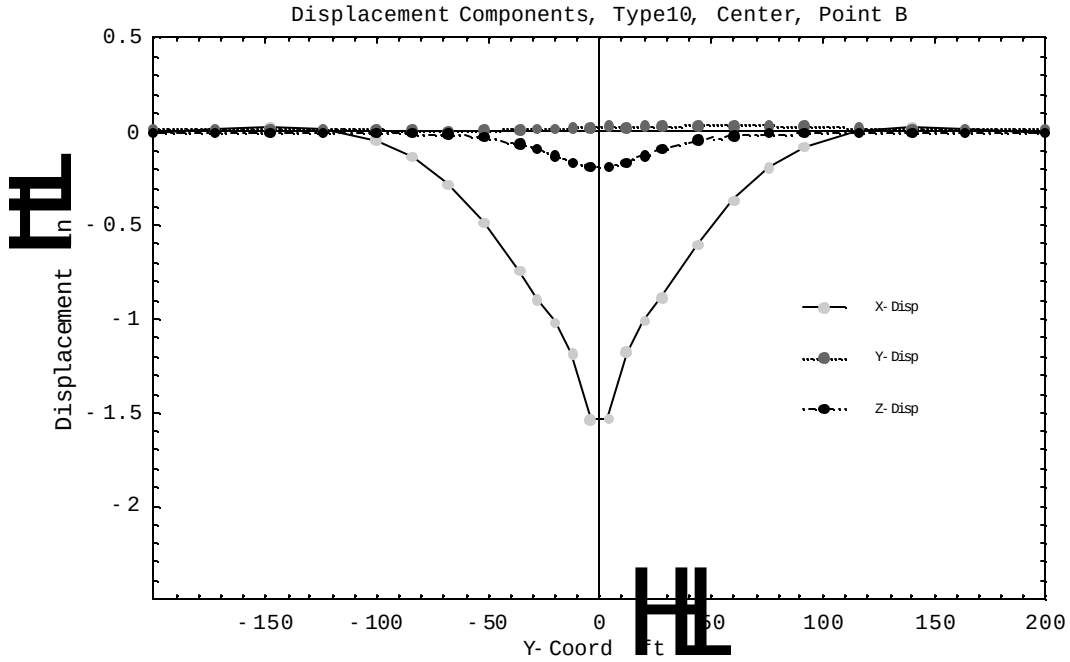


Figure 4.22 Displacement components at point B of Type 10 Rail (400-ft, Center Hit, Static, TL5a).

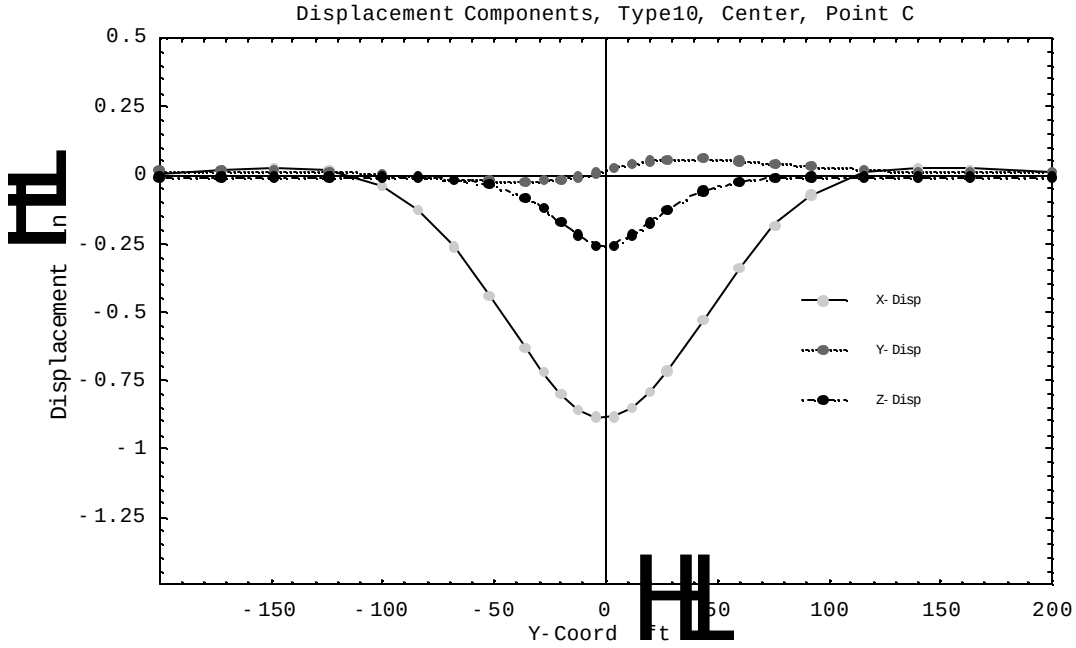


Figure 4.23 Displacement components at point C of Type 10 Rail (400-ft, Center Hit, Static, TL5a).

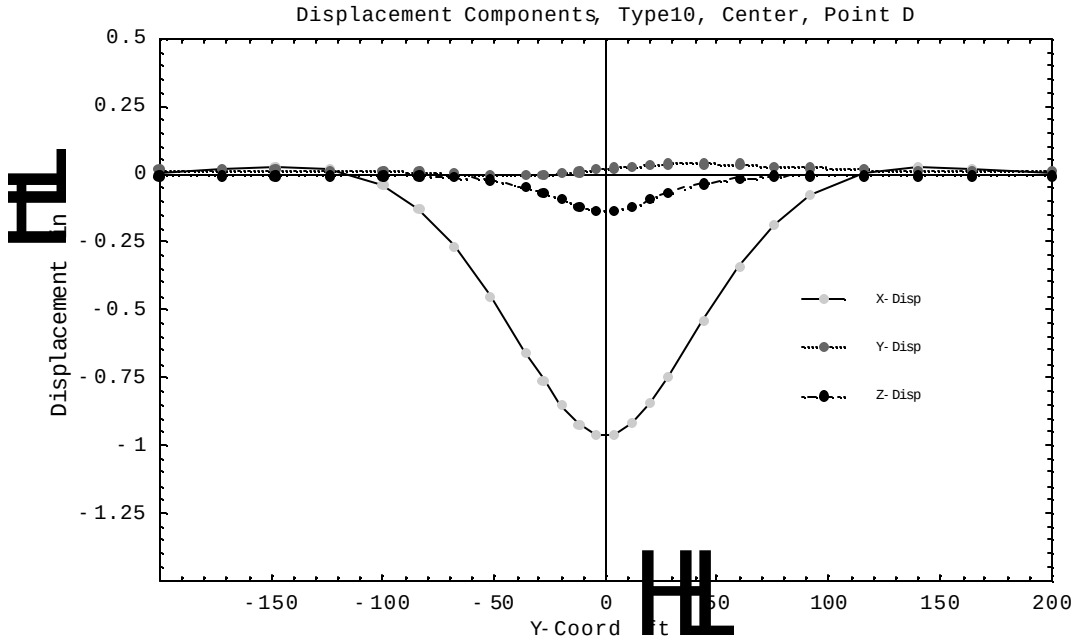


Figure 4.24 Displacement components at point D of Type 10 Rail (400-ft, Center Hit, Static, TL5a).

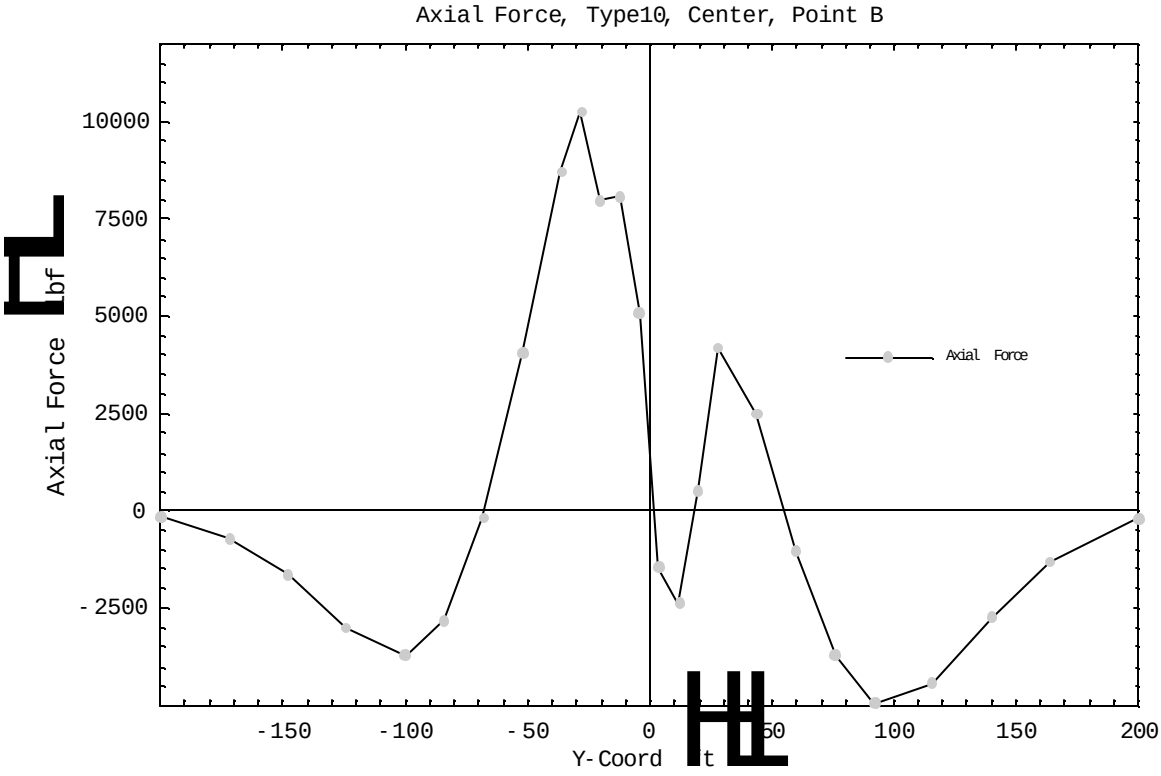


Figure 4.25 Axial force distribution in beam elements along point B of Type 10 Rail (400-ft, Center Hit, Static, TL5a).

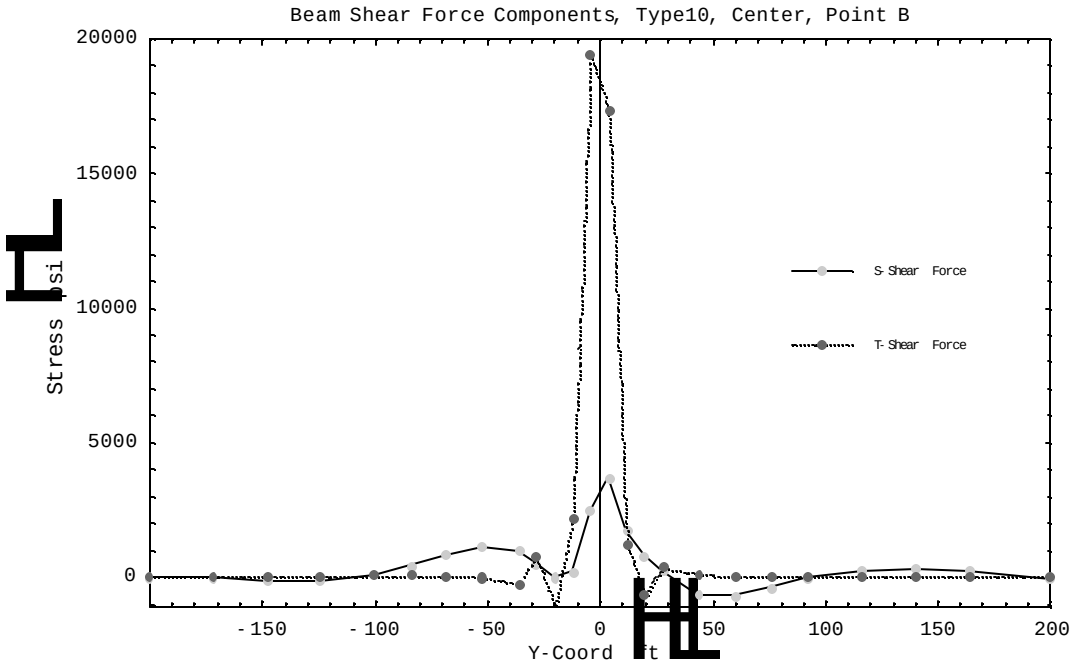


Figure 4.26 Shear force components in beam elements along point B of Type 10 Rail (400-ft, Center Hit, Static, TL5a).

General conclusions

- All stresses are small compared to the corresponding strengths and the influence length is estimated at 300 feet.
- The maximum displacement is less than 1.5 inches, and the influence length is 200 feet.
- Because of the nature of small stresses as compared to the strength, it is recommended to adopt the displacement as the criterion for determining the influence length of 200 feet.

4.2.4 Type 10 Rail with edge load application

The analysis was terminated at 55% of TL-5a load with the OBF concrete, R-O soil and EP steel (elastic plastic steel) using the static formulation. The decision was made to pursue the analysis with the dynamic formulation. The first trial using the OBF concrete, R-O soil and EP steel was also terminated at 55% of TL5a load. Then, it was decided to perform another analysis using elastic concrete (E-concrete), R-O soil and EP steel using dynamic formulation. The analysis was terminated at 85% of TL-5a load. The end displacement was found to be about 4 feet even at 85% load. Further analysis was deemed unnecessary because of the excessive displacements and stresses. The performance at the full TL-5a load is expected to be much more drastic. The results for the cases of static formulation with OBF concrete, R-O soil and EP steel rail and dynamic formulation with E concrete, R-O soil, and EP steel rail are briefly summarized. All six stress and three displacement components at A, C and D and the axial and shear forces of the steel rail at B are plotted against the distance from the left end of the rail in the figures shown in Appendix B.

4.2.4.1 Analysis with OBF concrete, R-O soil and EP steel rail

The analysis is terminated at 55% of the full TL-5a load and the observations are briefed as follows:

Normal Stresses

- At A, maximum stress is σ_y = 510 psi in tension at 60 feet from the edge. σ_y becomes compression at 170 feet and zero at 270 feet. σ_x and σ_z are minimal in comparison with σ_y. The influence length is 170 feet.
- At C, σ_y reaches -440 psi at 75 feet. It then reverses to small tension 170 feet and becomes near zero 300 feet. Both σ_x and σ_z are very small in comparison. The influence length is 170 feet.

- At D, all normal stresses are small comparing to those at A and C and are not considered in the influence length decision.
- In short, the influence length is controlled by stresses at A and C and is 170 feet.

Shear Stresses

- At A, maximum τ_{xy} is 133 psi at the left edge. It decreases to zero at 70 feet, reverses its direction, achieves a maximum of 30 psi at 120 feet and finally becomes negligible at 200 feet. Thus, the Influence Length = 200 feet. τ_{yz} and τ_{zx} are much smaller than τ_{xy} and do not affect the influence length decision.
- At C, τ_{xy} is larger than τ_{yz} and τ_{zx}, achieves a maximum of 110 psi at the left edge and sharply decreases to 10 psi, and subsides at 200 feet. Thus, the influence length = 200 feet.
- At D, τ_{xy} is larger than τ_{yz} and τ_{zx}. τ_{xy} achieves a maximum of 105 psi at left edge, becomes zero at 80 feet and subsides at 200 feet. Thus, the influence length = 200 feet.
- The analysis result indicates that, at all locations, A, C, and D, τ_{xy} controls and has a maximum of 133 psi. The influence length is 200 feet.

Normal Displacements

- The displacement in the x-direction, δ_x is much larger than those in the y and z directions. δ_x at B is -4.7 inches, at C, -4.15 inches, at D, -4.22 inches, and at A, -3.30 inches. The displacement becomes negligible at 110 feet. Thus, the influence length is 110 feet.

Axial and Shear Forces along the Steel Rail

- Shear force in the y direction of the steel rail is dominant and shows a maximum force of 14,000 lbs at the edge, and decreases to zero at 55 feet.
- Axial force achieves a maximum compressive force of -20,000 lbs at 73 feet and becomes negligible at 220 feet.

4.2.4.2 Analysis with E Concrete, R-O Soil, and EP Steel Rail

The analysis is terminated at 85% of the full TL-5a load and the observations are briefed as follows:

Normal Stresses

- At A, σ_y reaches the maximum tensile stress of 2000 psi at 130 feet and becomes negligible at 280 feet. σ_x and σ_z are minimal in comparison with σ_y. The influence length = 280 feet.
- At C, σ_y reaches a maximum compressive stress of 1500 psi at 130 feet and becomes negligible from 270 feet. σ_x and σ_z are minimal in comparison with σ_y. The influence length = 270 feet.
- At D, σ_y reaches a maximum compressive stress of 300 psi at 110 feet and becomes negligible from 260 feet. σ_x and σ_z are minimal in comparison with σ_y. The influence length = 260 feet.
- The concrete will fail in tension along the longitudinal edge of the moment slab because of the high tensile stress at A. The influence length is 280 feet.

Shear Stresses

- The general trend for all shear stress components is the same as in the case with OBF concrete, R-O soil and EP steel except the maximum t_{xy} increases to 200 psi and the influence increases to 300 feet.

Normal Displacements

- At all points of interest, the displacement in the x-direction, δ_x, is much larger than those in the y and z directions. δx at A is –39.5 inches, at B, –45.5 inches, at C, –45.5 inches, and, at D, -44.5 inches. All displacements become negligible at 200 feet. Thus, the influence length is chosen as 200 feet.
- At all points of interest, the normal displacements and the influence length are much larger at 85% TL-5a load with e concrete than at 55% TL5a load with OBF concrete.

- If the computation were carried out till full TL-5a load, the displacement would have been even bigger.

Axial and Shear Forces

- Shear force in the y direction of the steel rail is again dominant and shows a maximum force of 22,000 lbs at the edge and decreases to at 30 feet.
- Axial force achieves a maximum compressive force of –85,000 lbs at 130 feet and subsides to zero at 300 feet.
- Shear and axial forces and the influence are much larger at 85% TL-5a load with E concrete than at 55% TL-5a load with OBF concrete.

General Conclusions

- The stresses and displacements at 85% TL-5a are several times larger than those at 55% TL5a. It is believed that at the full TL-5a load the performance will be even more drastic. This indicates that the rail will fail and/or have excessive displacements when the full TL-5a load is applied at the edge of the Type 10 Rail. The influence length no longer has any physical meaning.
- Further analysis of the rail system under edge impact will not serve any useful purpose without strengthening the end with a strong foundation support.
- It is strongly recommended that the rail end be supported by a strong foundation to meet the rail safety requirement.

4.3 Analysis Program, Results and Discussions of 200-ft Type 7 and Type 10 Rails on MSE Walls

Based on the influence length (IL) determined in the previous analyses, 200-ft long Type 7 and Type 10 rails sitting on 20-ft high MSE walls were analyzed with the TL-5a load applied at the center of the rail. The simplified front view of the model is shown in Figure 4.27. The analysis uses OBF concrete, R-O soil and EP steel rail when required. Because of the expected unacceptable performance of rails subjected to TL-5a load applied at the edge rails without strong foundation support, the rails with the center load application are analyzed.

4.3.1 Type 7 Rail with Jersey Barrier

The 200-ft Type 7 Rail sitting on top of a 20-ft high MSE wall as shown in Figure 4.27 is subjected to a centrally applied dynamic TL-5a load. The transverse and vertical displacement-time histories, geogrid stresses and earth pressures at Nodal Points 230, 538, and 588 are shown in Figure 4.28. The rail continues to oscillate even after the termination of the impact load. Figure 4.29 shows the transverse displacement-time histories at the above-mentioned points and the displacements all asymptotically approach about 0.5 inches. Figure 4.30 shows that the heel of the slab (NP 588) moves upward, while the toe and rail top move downward. This indicates the partial separation of the anchor slab (moment slab or sleeper slab) from the retaining wall backfill. Figure 4.31 shows that the geogrid stresses are not affected much by the impact load. Figure 4.32 shows that the effect of earth pressure along the back of the retaining wall is insignificant beyond the depth of two and a half feet.

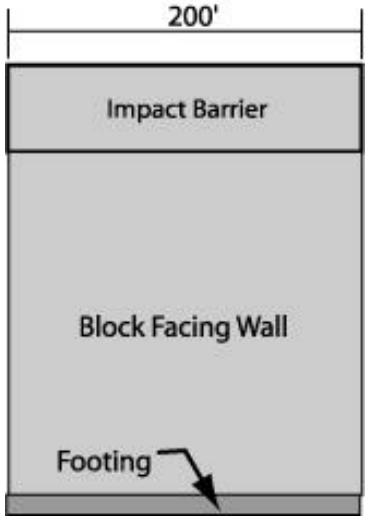


Figure 4.27 Front view of 200-ft long impact barrier with MSE wall.

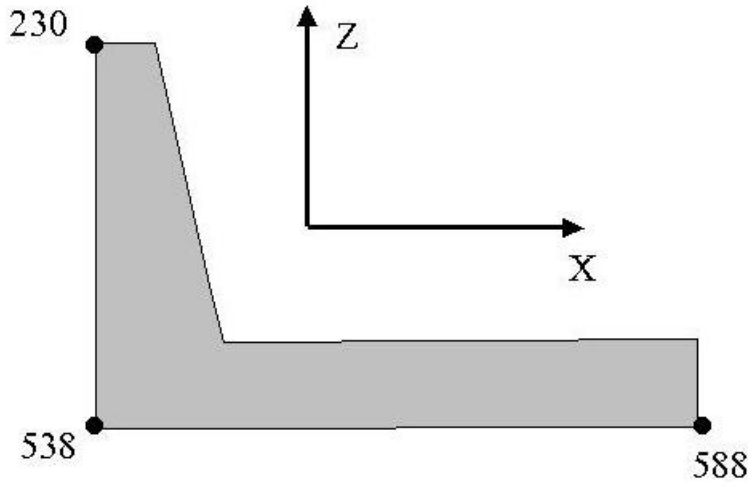


Figure 4.28 Node reference for displacement time histories (Type 7).

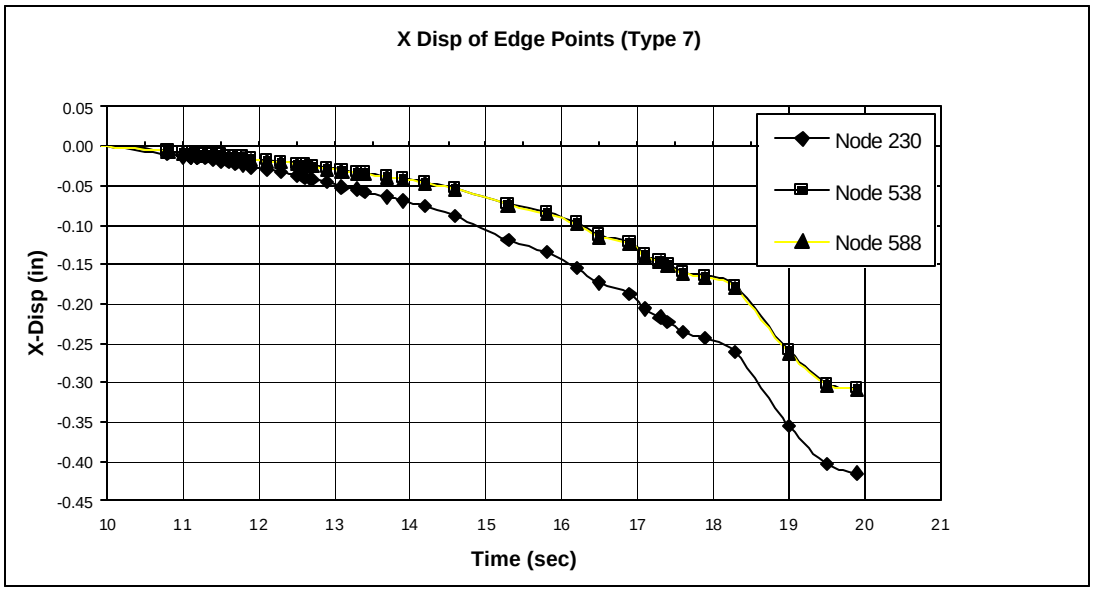


Figure 4.29 X Displacement time history of selected nodes (Type 7).

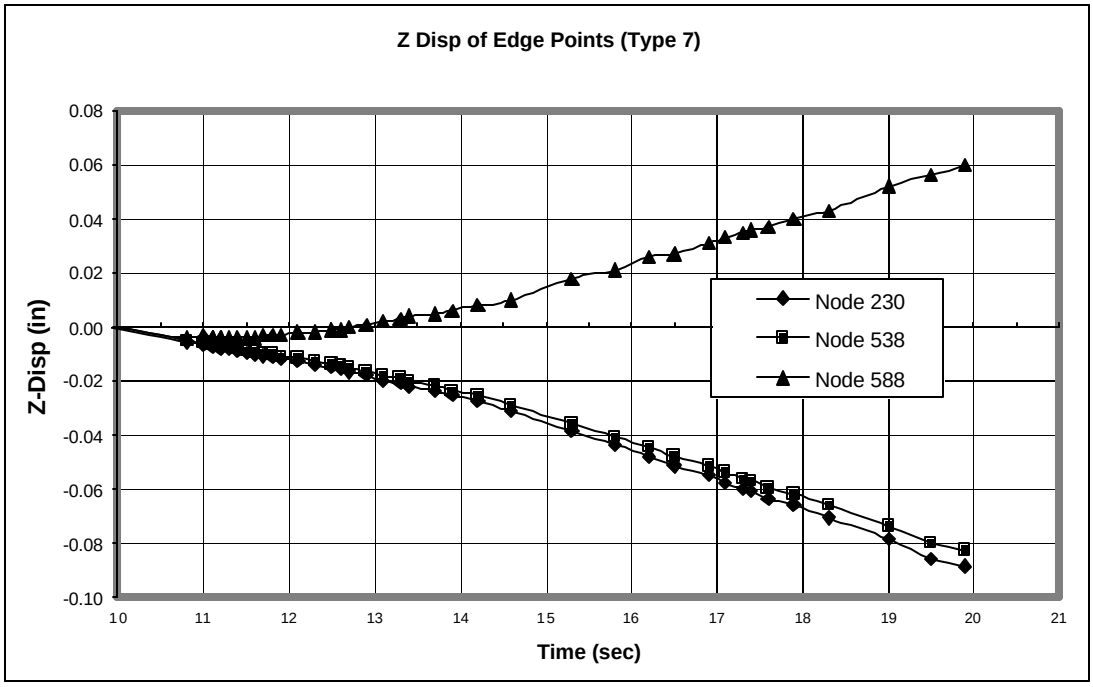


Figure 4.30 Z Displacement time history of selected nodes (Type 7).

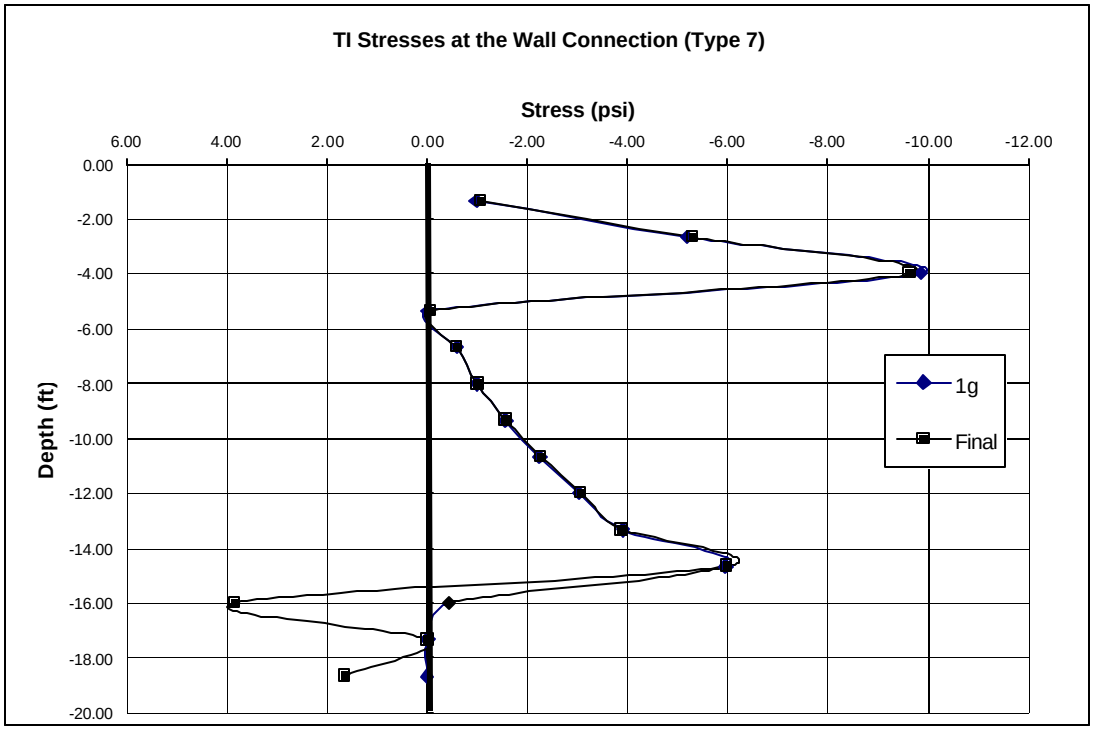


Figure 4.31 Geogrid stresses along the wall face (Type 7).

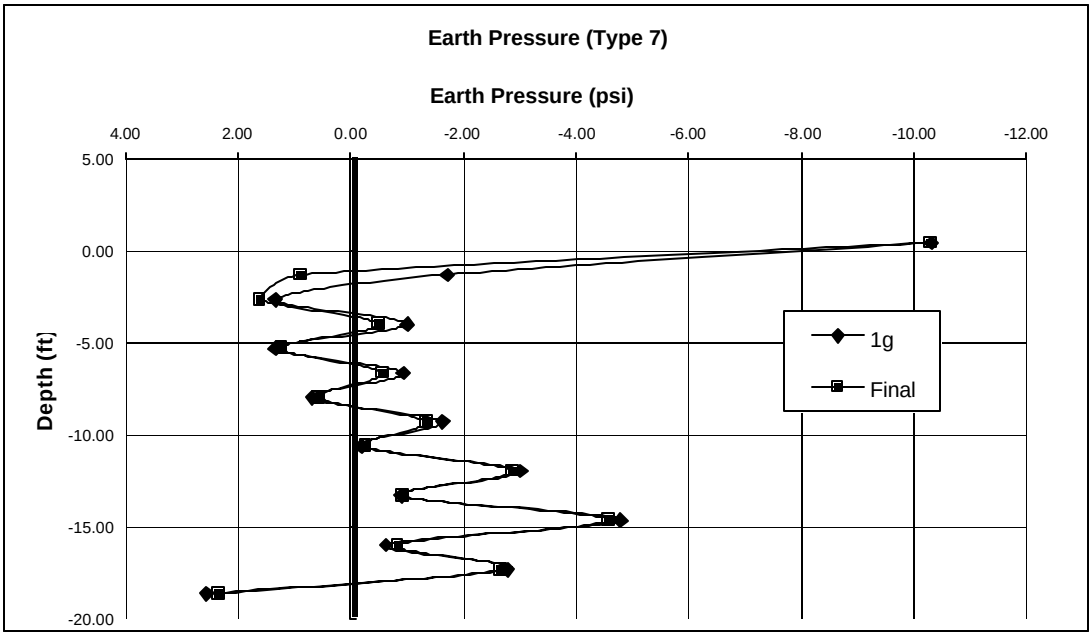


Figure 4.32 Earth pressure along the wall face (Type 7).

4.3.2 Type 10 Steel Rail

The 200-ft Type 10 Rail sitting on top of a 20-ft high MSE wall is subjected to a centrally applied dynamic TL-5a load. Presented are the transverse (x) and vertical (z) displacement-time histories at NP 73, 317, and 560 (figure 4.33), geogrid stresses and earth pressures along the back face to the retaining wall. The rail continues to oscillate even after the termination of the impact load. Figure 4.34 shows the transverse displacement-time histories at the above-mentioned NP and the displacements all asymptotically approach about 3.0 inches, which is much larger than those in Type 7 Rail. Figure 4.35 shows the upward heel (NP 560) movement and downward movement of the steel rail and the toe of the rail. This shows the partial separation of the anchor slab from the retaining wall backfill. Figure 4.36 shows virtually no influence of the impact load on the geogrid stresses beyond the depth of 2.5 feet. Figure 4.37 shows that the effect of the impact load on the earth pressure along the back of the retaining wall is insignificant beyond the depth of 5 feet. In general the rail-slab system of the Type 10 Rail displaces and rotates more than the Type 7 Rail. This can be attributed to the difference in the stiffness of the two rail types. The rails, however, no longer would fly off the MSE walls.

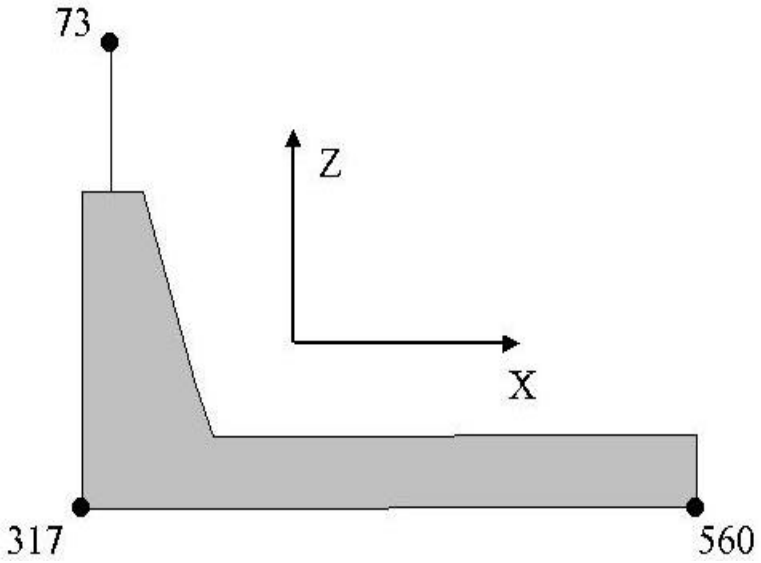


Figure 4.33 Node reference for displacement time histories (Type 10).

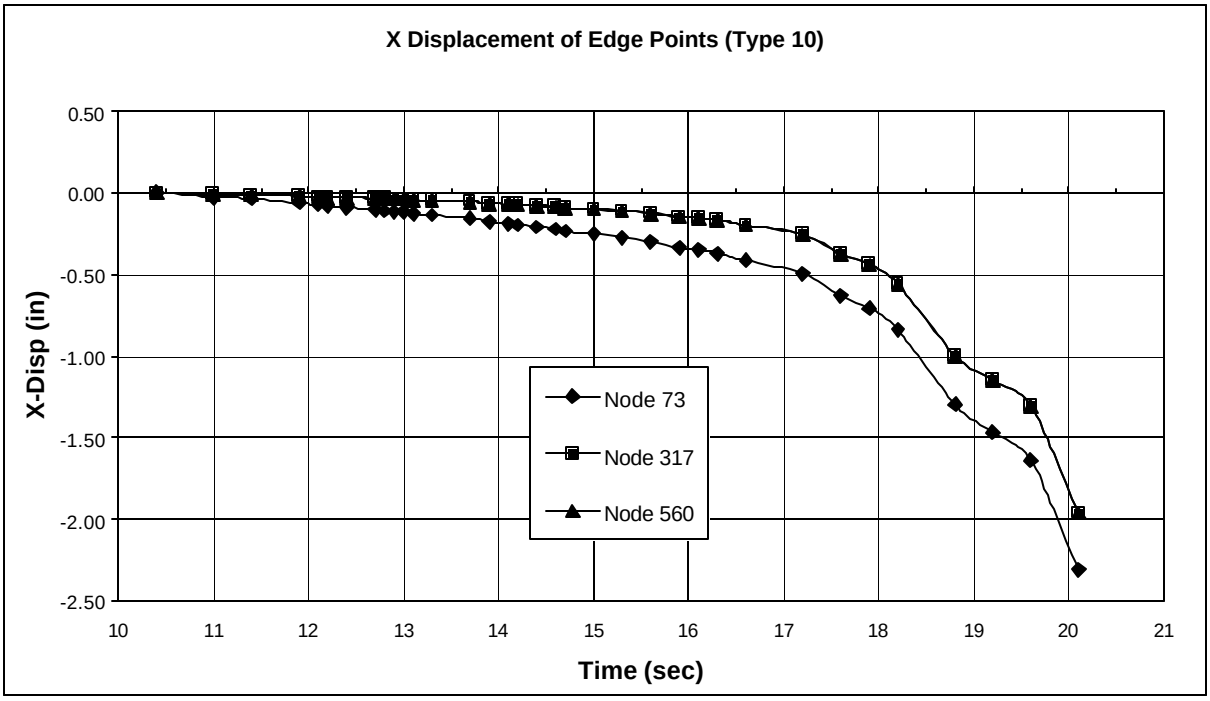


Figure 4.34 X Displacement time history of selected nodes (Type 10).

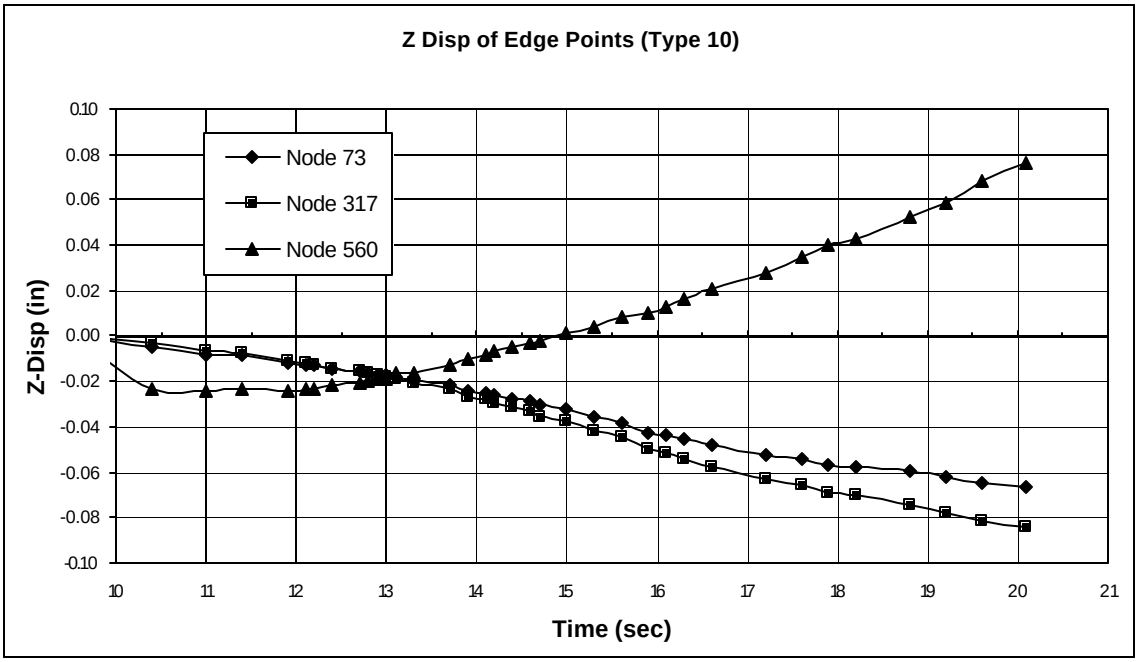


Figure 4.35 Z Displacement time history of selected nodes (Type 10).

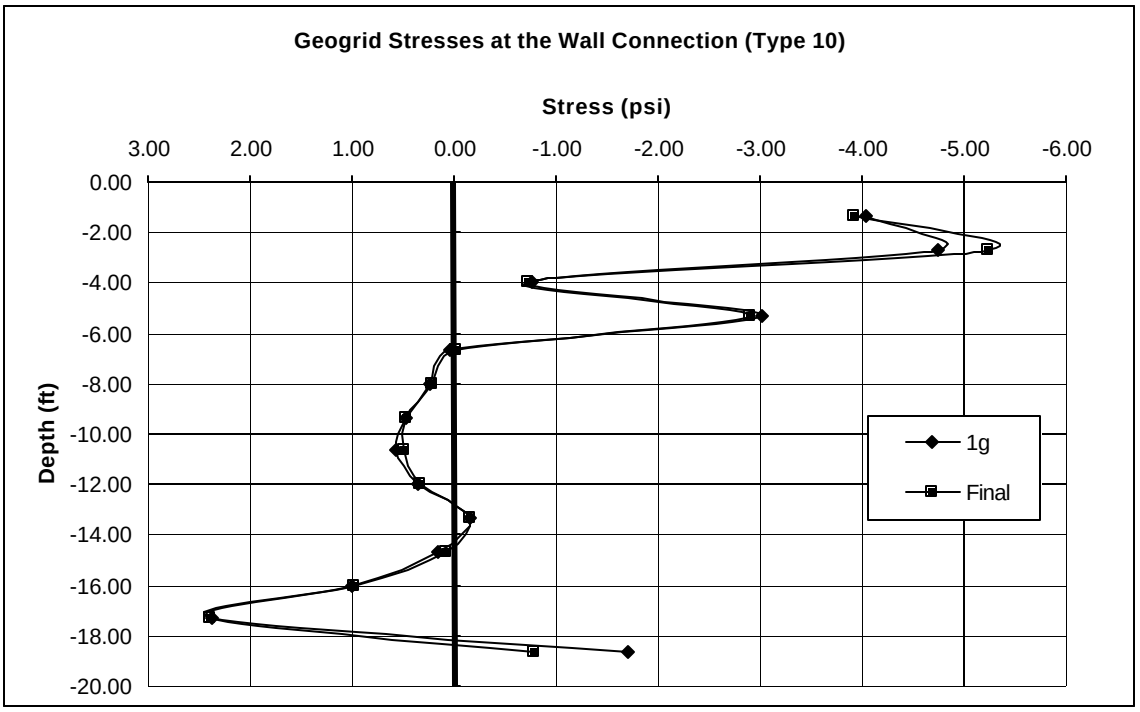


Figure 4.36 Geogrid stresses along the wall face (Type 10).

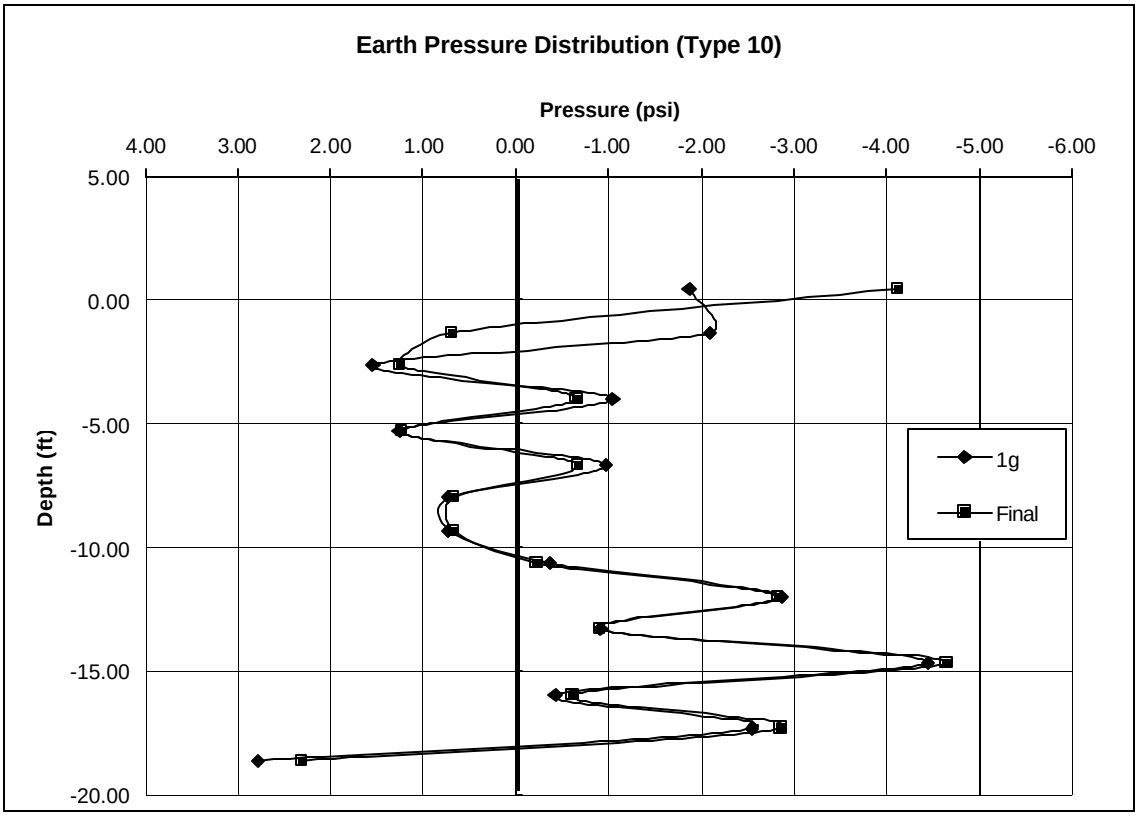


Figure 4.37 Earth pressure along the wall face (Type 10).

5.0 RECOMMENDATIONS FOR IMPLEMENTATION AT CDOT (FOR APPLICATIONS WITH TL4 AND TL5)

The current CDOT rail design practice for Colorado Type 7 and Type 10 uses the monolithic construction of the rail and 8-ft moment slab (termed rail system in this report) sitting directly on the natural ground or the backfill of an MSE wall. The analysis results in Chapter 4 show that, even in a 200-ft long rail system, the rail displacement can be excessive if the current CDOT practice is followed, particularly when the impact load is applied at the rail edge. This is caused mainly by the twisting and lifting of the rail system upon the application of the pseudo-static impact load, which in turn drastically reduces the interface frictional resistance between the base of moment slab and MSE wall backfill. Without any improvement or strengthening mechanism, the frictional resistance, a major source of the impact load resistance, becomes insufficient to resist the impact load. If the rail system were improved to resist the lifting and twisting, then the frictional resistance and inertia force would more effectively participate in the enforcement of rail safety. Besides, the length requirement can mostly likely be relaxed. So it is strongly recommended to adopt some rail system enhancement mechanisms to enhance performance and safety.

1. The appropriate length of a continuous wall-rail system (spacing between joints) is at least 200 ft. Designers need to pay attention to joints in anchor slab.
2. In the pseudo-static analysis of the rail systems, it is recommended to use an influence length of 200 ft (even if the continuous length is more than 200 ft) until new research findings are available to justify a shorter length.
3. In the TL5a areas, Type 7 rails are recommended.
4. All rails should, if possible, end at locations where no impact resistance is required. If the rail needs to end anywhere else including the joint area, then additional impact resistant measures are recommended. These can include pier or pile foundations.

5. To enhance the overall stability and safety of the rail-wall system, or to reduce the 200-ft length requirements of a continuous rail-wall system, the following mechanisms (or combination) are suggested:

    - Install continuous shear keys underneath the moment slab in the longitudinal direction, preferably where the moment slab ends.
    - Install micro piles from the moment slab into the wall backfill, or ground anchors at the toe of the rail system.
    - Monolithically integrate the rail system into the structural MSE walls.
    - Connect the moment slab to the adjacent concrete pavement, or increase the width of the moment slab.
    - Install appropriate foundation systems (piles or piers) at the end of rails to prevent excessive rail end movement.

To quantify the influence of these measures, additional research is needed. When funding is available, future research should cover the true dynamic analysis of the wall rail systems of any length, field crash tests, and their mutual calibration. Upon the proof of its effectiveness, the numerical analysis can generate a database required for the formulation of rail design guidelines.

6.0 SUMMARY, CONCLUSIONS, AND RECOMMENDATIONS

6.1 Summary

Many rail impact studies on record are either for the purpose of bridge deck overhang design or for the post and tube type roadside safety barrier design and very little information is available for the case with rail anchoring slabs on top of MSE walls. This study focuses on the stability of Colorado Type 7 (with Concrete Jersey barrier) and Type 10 (with Steel barrier) rails on MSE walls. Initially the CU-Denver research personnel and the CDOT study panel agreed to perform the finite element analysis on 20-ft rails on MSE walls. In all analyses, the rail impact load was applied to the rail system as specified by AASHTO in terms of magnitude and the point of application. In a pseudo static condition, the soil-moment slab interface frictional resistance, briefed as interface friction, and the moment resistance constitute the resistance to impact load, and under a dynamic impact condition, the rail-slab inertia force is added to resist the rail movement. The following analyses were performed in this study:

- Pseudo static analyses of 20-ft Type 7 and Type 10 rails under TL4 load.
- Pseudo static and impact analyses of 40-ft Type 7 and Type 10 rails under TL4 load.
- Pseudo static analyses of 400-ft Type 7 and Type 10 rails for influence length evaluation under TL5a.
- Pseudo static analyses of 200-ft Type 7 and Type 10 rails sitting on 20-ft MSE walls under TL5a. The analysis required a computation capacity larger than what SGI can offer and the task was accomplished on the Cray T90 super computer at the University of California at San Diego.

The analysis results showed gross instability of the 20-ft rails of both types under TL-4. The application of the pseudo-static impact load as specified in the AASHTO 2000 LRFD Bridge Design Specifications causes the rails to first rotate and twist about their

longitudinal axis and heels and eventually to gain momentum and fly off the MSE walls. The field test from Penn DOT (email communication between CDOT and Penn DOT) confirmed the finding.

To investigate the effect of the dynamic impact load, the analysis uses the time history of the impact load extracted from the results of the field crash tests performed at the Texas Transportation Institute (TTI). The results of analysis show that the rails suffer a similar fate to those under pseudo-static load.

The analysis was then redirected to the 40-ft rail systems. Both pseudo-static and impact load analyses were performed. The load was applied either at the mid-span or the edge of the rail. The analysis still shows the instability and excessive displacement of both rail types, particularly when the load is applied at the edge of the rails. A decision was then made jointly to assess the influence length under TL.5a using 400-ft rails sitting on 1-ft thick foundation soil. In the case of Type 7 rail, at 100 feet from the point of application of the pseudo-static impact load, both stresses and transverse displacements become negligible and the rails no longer fly off the wall and the transverse becomes tolerable when the load is applied at the mid-span. Thus, the length of 200 feet is chosen as the influence length for Type 7 Rail. Under the same loading condition, the Type 10 rail suffered a larger rotation, displacement and base lifting than the Type 7 rail.

When the impact load is applied at an end of either rail type, the rail rotation, twisting, transverse displacement, and lifting of the moment slab are found to be excessive. To maintain the consistency in analysis, the research group chose 200 feet as the influence length for both rail types and additional analyses were performed on the 200-ft rails sitting on 20-ft MSE walls. Pseudo static analysis results show that the rotation, twisting, transverse displacement, and base lifting displacement of the 200-ft Type 7 and Type 10 Rail systems sitting on 20-ft MSE walls are close to the tolerable magnitude and the rails no longer fly off the wall when the impact load is applied at the center of the rails. The rail-end application of impact loads still produces unacceptable rotation, twisting, displacement and base lifting. In all cases the displacement, rotation, twisting and lifting

were found to be more severe in Type 10 rail than in Type 7 rail. This is likely due to the difference in the stiffness of the two rail types. The Type 7 rail is stiffer and heavier than the Type 10 rail because of its massive Jersey-type concrete barrier. In the final analyses of 200-ft rails, the problems became too large for the SGI workstations at the University of Colorado at Denver. Thus, all analyses on the 200-ft rail-MSE wall systems were performed on the Cray T90 supercomputer at the San Diego Supercomputer Center.

6.2 Conclusions

The primary findings for 20-ft, 40-ft and 400-ft rails are outlined as follows:

1. Under TL4 impact load, the analysis result for the 20-ft Type 7 and Type 10 rails with monolithic anchor slab (or moment slab, sleeper slab) seating on the backfill of the supporting MSE retaining wall shows that the rail will gain momentum and fly off the wall.

2. The application of TL5a results in a large overturning moment leading to the rotation of the monolithic rail system about the heel, which, in turn, causes the partial separation of moment slab from backfill and the reduction of soil-slab interface frictional resistance and ineffective rail-backfill load transfer. There is an ample untapped resistance of MSE walls to restrain the impact-induced rail movement.

3. Under TL5a, the 400-ft continuous rails have an influence length of 200 feet when the impact load is imposed at the mid-span. When the load is applied at the end of the rails, the rotation, twisting, transverse displacement and anchor slab lifting remain excessive and some foundation system for the rail movement prevention is needed.

4. The application of TL4 to 20- and 40-ft rails and TL5a to 200- and 400-ft rails results in a large overturning moment causing the rotation of the monolithic rail-slab system about its heel, which causes the partial separation of moment slab from the backfill and the reduction of the frictional resistance because of the partial loss of contact area. In some cases the impact load caused the rail to gain momentum and set the rail in motion.

The primary findings of the numerical pseudo-static impact load analysis of continuous (no joints) 200 ft wall-rail (Type 7 and Type 10) systems sitting on a 20-ft high MSE walls under TL5a equivalent impact load are summarized as follows:

1. Small wall facing displacements and geogrid stresses, which suggest the ineffective rail-backfill load transfer and minimal resistance of MSE wall to impact load under current AASHTO specifications, which can be too conservative. The effect of a vertical load on the anchor slab needs to be investigated. With the vertical load and the enhancement mechanism as outlined in Chapter 5, the rail-backfill load transfer can be drastically enhanced.

2. Because of this inefficient load transfer in the current Colorado design, the effect of the TL5a load on the wall performance is minimal.

3. The displacements of the two systems are close to the tolerable magnitude and the rails no longer fly off the wall when the impact load is applied at the center of the rails. The displacements were more severe in Type 10 rail than in Type 7 rail. The Type 7 is stiffer and heavier than Type 10 rail because of its massive Jersey-type concrete barrier.

4. The rail-end application of high impact loads produced unacceptable displacements to the systems.

The above research findings can at least serve as a guide for further research in high impact load rail design. Abundant evidence in Colorado indicates that the field performance of rails and supporting systems already in place are better than what is estimated from the simple equivalent pseudo static analysis recommended by AASHTO. Crash tests coupled with real impact dynamic numerical simulation using powerful software like NIKE3D are the best way to resolve this issue and provide the average design engineer with the tools to implement and/or revise the recommendations of AASHTO 2000 LRFD specifications.

6.3 Recommendations for Further Study

The findings from this study have shed light on the performance of Colorado Type 7 and Type 10 rails under severe impact loads of TL5 and future research directions. Further research can be divided into two levels: Colorado's immediate interest and national interest with the former being the subset of the latter. To address Colorado's immediate interest, further research should include the following with limited budget:

- The effect of the participation of the inertia force on the stability of rails under severe impact loads. In the pseudo-static analyses of 200-ft rails, the rail displacements are resisted by the backfill-slab interface friction, stiffness of the rail system, and the resisting moment of the rail system about its heel under its own dead weight. The inertia force has not contributed to the resistance because of the nature of pseudo-static analysis. Thus, it is of great interest to assess the influence of the inertia force through dynamic analysis using time-dependent impact load.

- In the AASHTO LRFD specifications, no tire load application on the moment slab is recommended. This might be a bit over conservative and it may be more appropriate to apply a portion of the truck weight on the moment slab when analyzing the rail performance.
- The study on the effectiveness of each stability enhancement mechanism

recommended in this study is of paramount importance. While believing in a certain degree of effectiveness of each enhancement mechanism, its degree of improvement has not been evaluated and compared. Such evaluation is important before any is adopted and its associated design guidelines formulated.

- If the decision is to implement the use of piers or piles to support the rail end, then their capability in resisting lateral impact load will have to be assessed.

At the national level with a large multi-year budget, a comprehensive study can be carried out through both numerical analysis and field crash testing. The effectiveness of the numerical analysis is calibrated against the field test results. When found effective, the numerical analysis can be further performed to assess the performance of safety rails under large impact loads. Since the AASHTO 2000 LRFD Bridge Design Specifications lack the specifications for design details for the safety rails under severe impact load, further research is urgent to provide information greatly needed for the design of rails under high impact load. A problem statement (Problem Statement No.: 2002-C-11) was submitted for NCHRP funding by the CDOT Research and Bridge Branches in 2002. The major objectives of this national level research are six fold: 1) stress distributions for the structural design of rail cross-section, 2) assessment of displacements for assessing the rail stability, 3) 3-dimensional impact load transfer mechanism from rail to foundation to backfill and eventually to MSE walls, 4) formulation of the MSE wall design guidelines for supporting the top-mounted rails, 5) formulation of design guidelines for different rail types with different stability enhancement mechanisms under different impact loads, 6) recommendation for the revision of the AASHTO 2000 LRFD Bridge Specifications to include the findings from this research. It is envisioned that design charts could be developed based on the real impact dynamic analyses to replace the simplistic AASHTO 2000 LRFD equivalent pseudo static analyses. The research tasks to accomplish the above objectives are outlined in the NCHRP problem submitted by CDOT in 2002.

References

1. http://www.greatachievements.org/greatachievements/ga_11_3p.html
2. Ross, Jr., H.E, Sicking, D.L., Zimmer, R.A., and Miche, J.D., "Recommended Procedures for the Safety Performance Evaluation of Highway Features", NCHRP Report 350, 1993.
3. http://tti.tamu.edu/inside/factsheet/
4. http://tti.tamu.edu/inside/facilities/
5. http://tti.tamu.edu/inside/facilities/computing.stm
6. www.tfhrc.gov/about.htm
7. www.tfhrc.gov/pubrds/marapr00/concrete.htm
8. http://safety.fhwa.dot.gov/fourthlevel/hardware/pdf/Bridge.pdf
9. State of California Department of Transportation, Div. of New Technology, Materials and Research, "Vehicular Crash Tests of a Slip-Formed, Single Slope, Concrete Median Barrier With Integral Concrete Glare Screen"; Report Number FHWA/CA/ESC-98/02; December, 1997
10. Buth, C.E., Arnold, A., Campise, W.L., Hirsch, T.J., Ivey, D.L., Noel, J.S., "Safer Bridge Railings, Volume 1, Summary Report", Texas Transportation Institute, Texas A&M University, Final Report No. FHWA/RD-82/072, June 1984.
11. Buth, C.E., Arnold, A., Campise, W.L., Hirsch Hirsch, T.J., Ivey, D.L., Noel, J.S., "Safer Bridge Railings, Volume 2, Appendices A, B, D &E", Texas Transportation Institute, Texas A&M University, Final Report No. FHWA/RD-82/073, June 1984.
12. Buth, C.E., Arnold, A., Campise, W.L., Hirsch, T.J., Ivey, D.L., Noel, J.S., "Safer Bridge Railings, Volume 3, Appendices C, Part I", Texas Transportation Institute, Texas A&M University, Final Report No. FHWA/RD-82/074.1, June 1984.
13. Buth, C.E., Arnold, A., Campise, W.L., Hirsch, T.J., Ivey, D.L., Noel, J.S., "Safer Bridge Railings, Volume 4, Appendices C, Part II", Texas Transportation Institute, Texas A&M University, Final Report No. FHWA/RD-82/074.2, June 1984.
14. Buth, C.E., Williams, W.F., Menges, W.L., Schoeneman, S.K., "NCHRP Report 350 Test 4-10 of the Alaska Multi-State Bridge Rail", Texas Transportation Institute, Texas A&M University System, Report No. FHWA-RD-98, December, 1998.

15. American Association of State Highway and Transportation Officials, "Guide Specifications for Bridge Railings", Washington, D.C., 1989.

16. "Recommended Procedures for the Safety Performance Evaluation of Highway Appurtenances," NCHRP Report 230, 1979.

17. Ross, Jr., H.E, Sicking, D.L., Zimmer, R.A., and Miche, J.D., "Recommended Procedures for the Safety Performance Evaluation of Highway Features", NCHRP Report 350, 1993.

APPENDIX A Figures for 40-ft Type 7 Rail

Type 7, TL4, Static, Edge

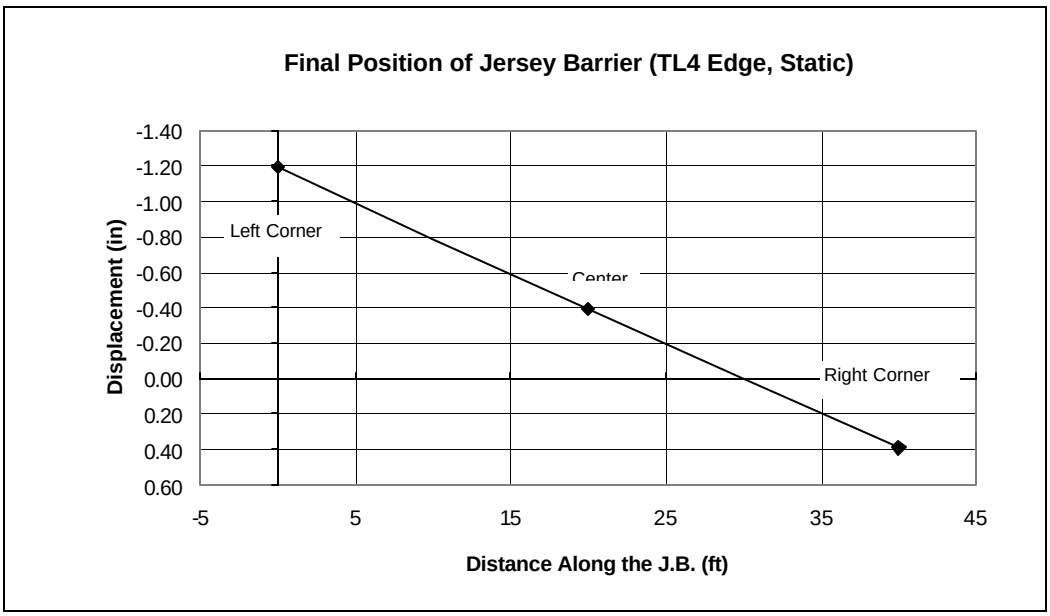


Figure A-1: Transverse displacement of edge and corner nodes of Type 7 barrier (TL4, Edge Hit, Static).

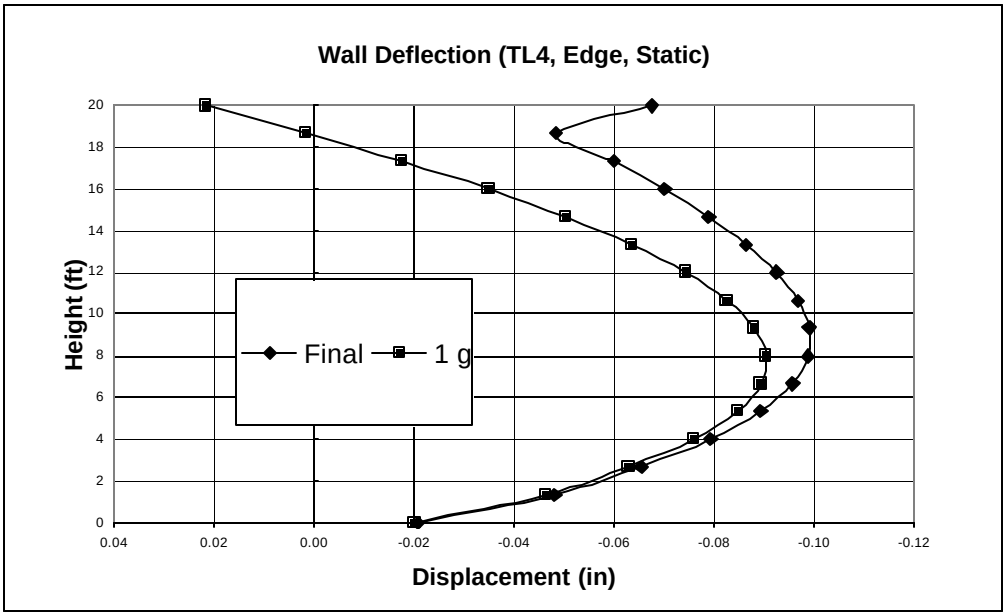


Figure A-2: Wall deflection (TL4, Edge Hit, Static).

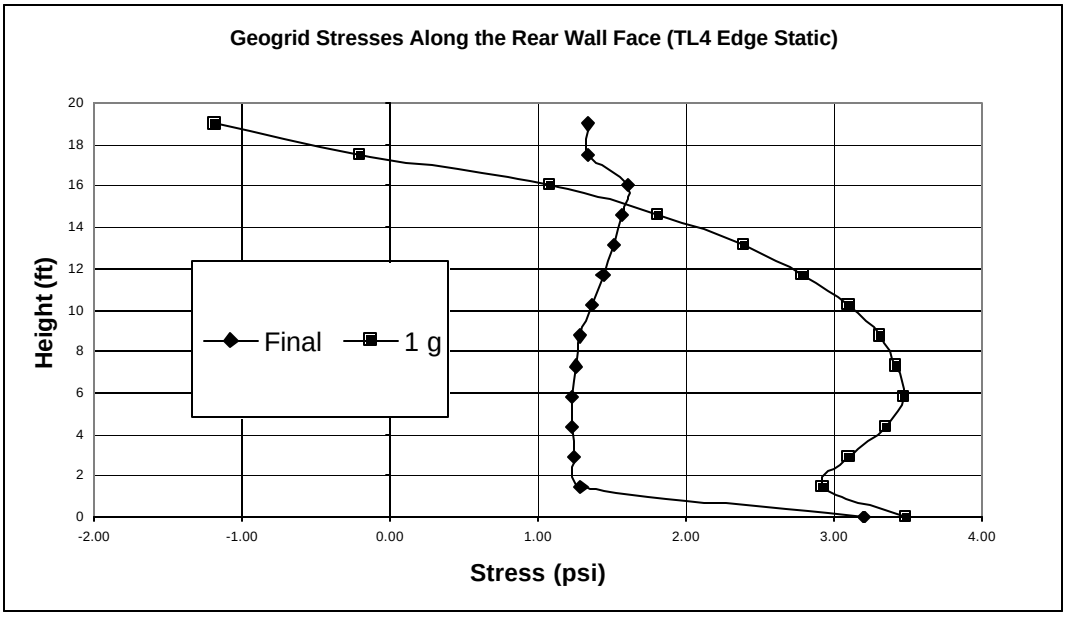


Figure A-3: Geogrid stresses along the wall connection (TL4, Edge Hit, Static).

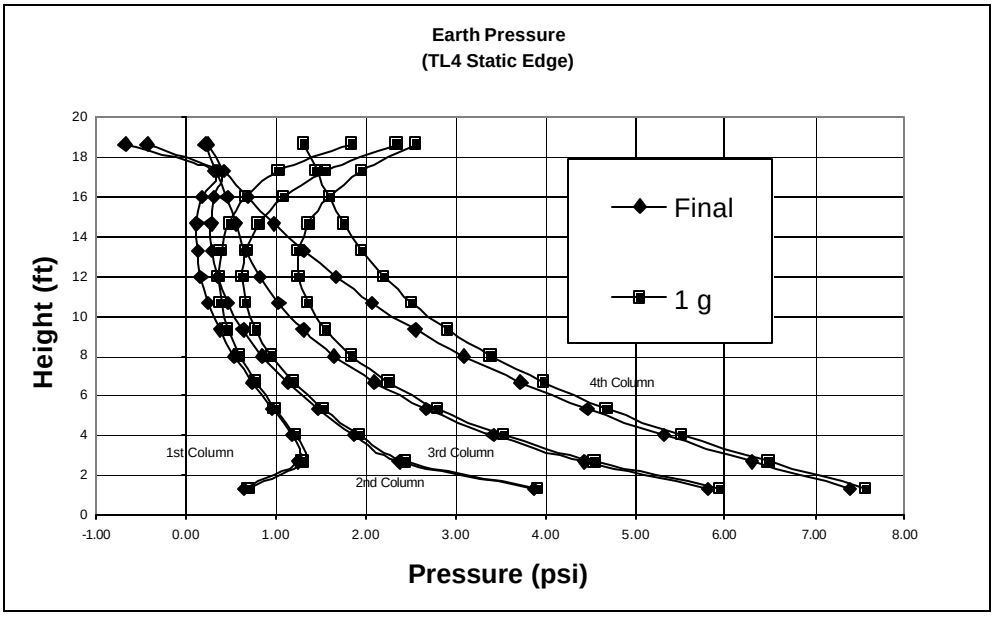


Figure A-4: Earth pressure distribution at four different locations (TL4, Edge Hit, Static).

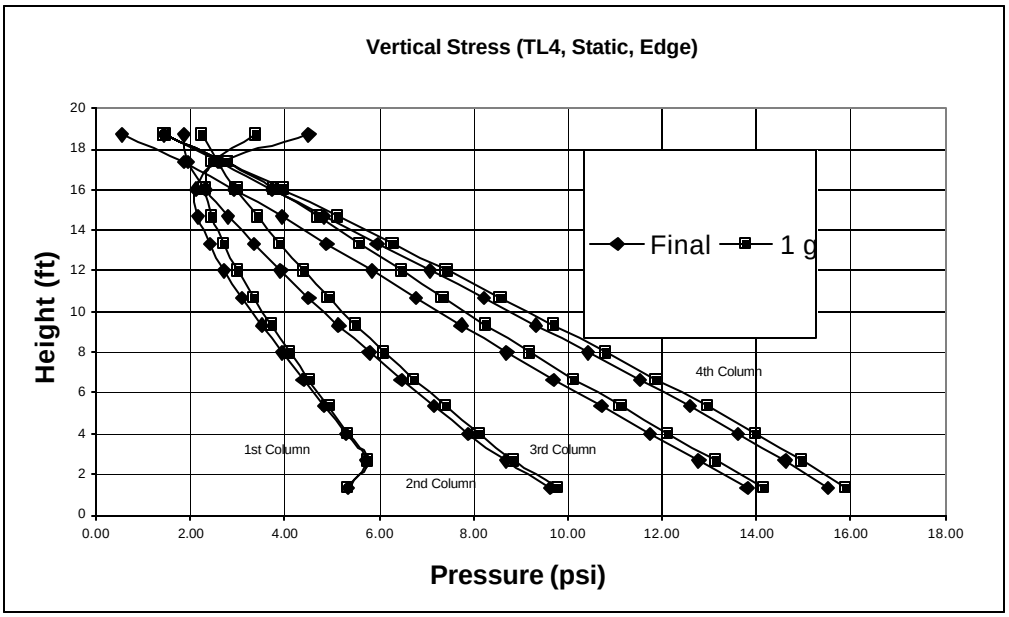


Figure A-5: Vertical soil pressure distribution at four different locations (TL4, Center Hit, Static).

Type 7, TL4, Impact, Edge

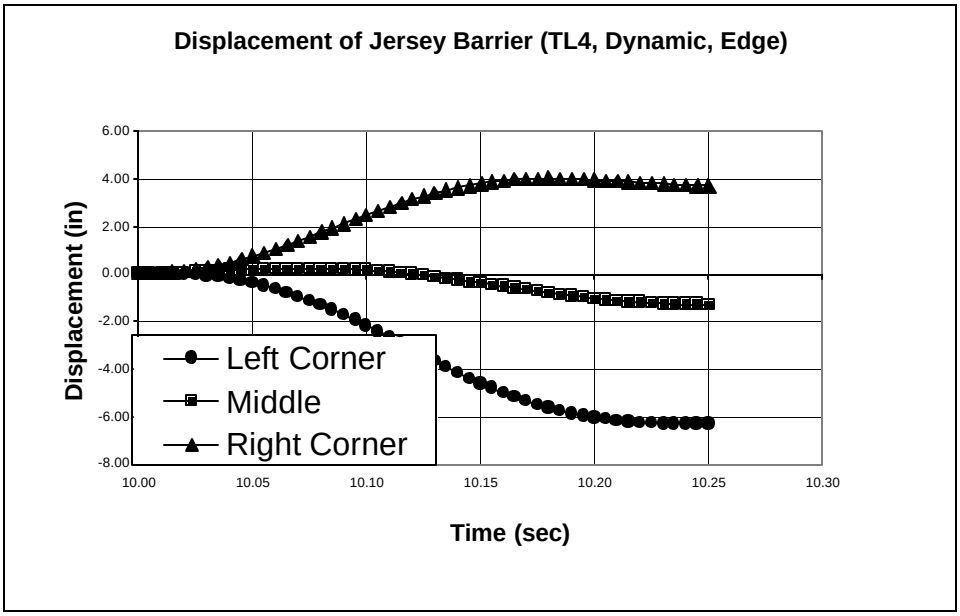


Figure A-6: Transverse displacement time history of edge and corner nodes of Type 7 barrier (TL4, Edge Hit, Impact)

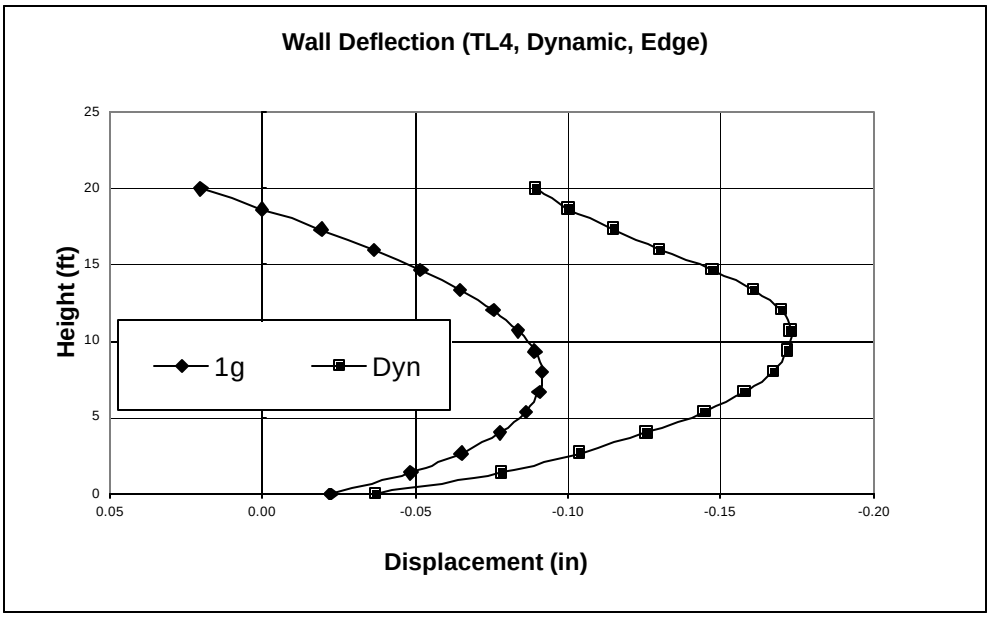


Figure A-7: Final wall deflection after impact load (TL4, Edge Hit, Impact)

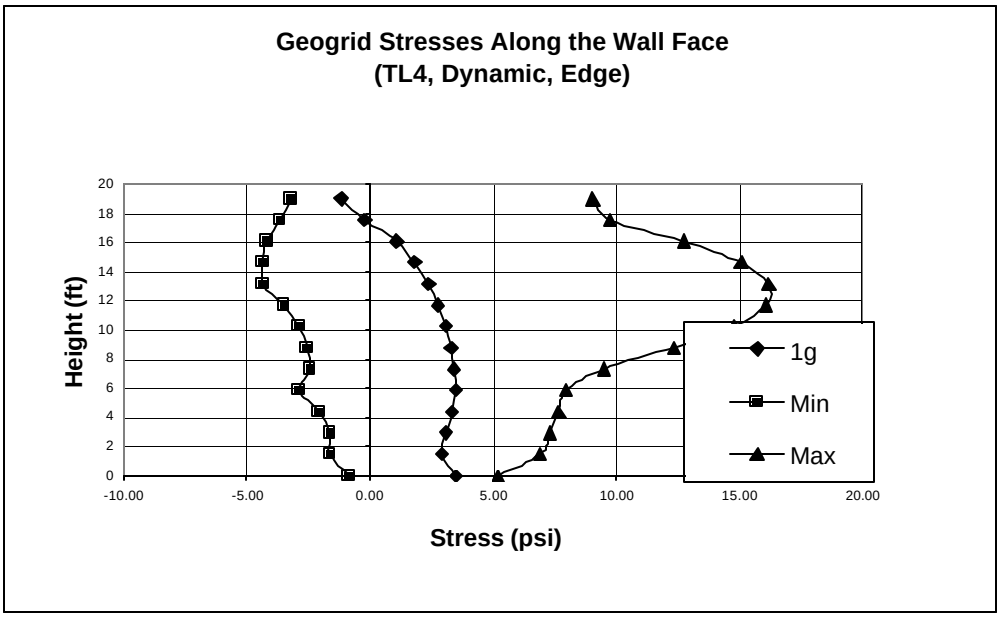


Figure A-8: Min, max and 1g geogrid stresses along the wall face (TL4, Edge Hit, Impact)

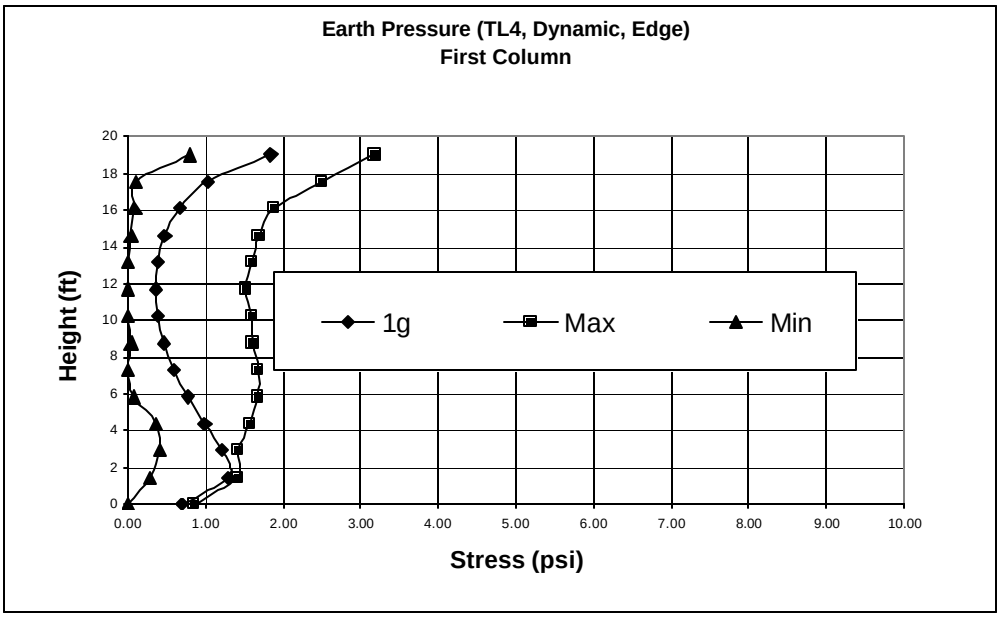


Figure A-9: Min, max and 1g earth pressure along the first column (TL4, Edge Hit, Impact).

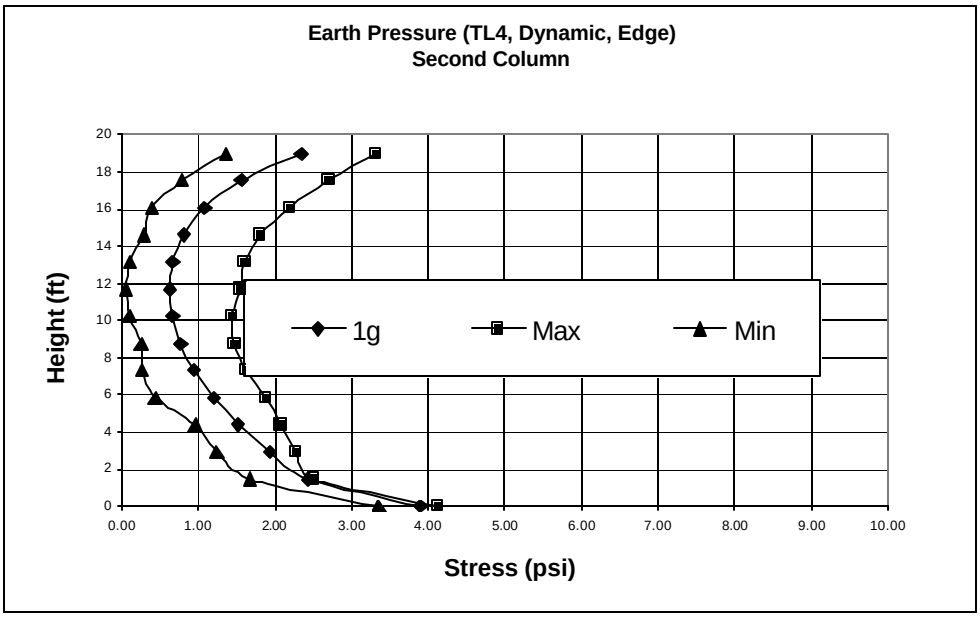


Figure A-10: Min, max and 1g earth pressure along the second column (TL4, Edge Hit, Impact).

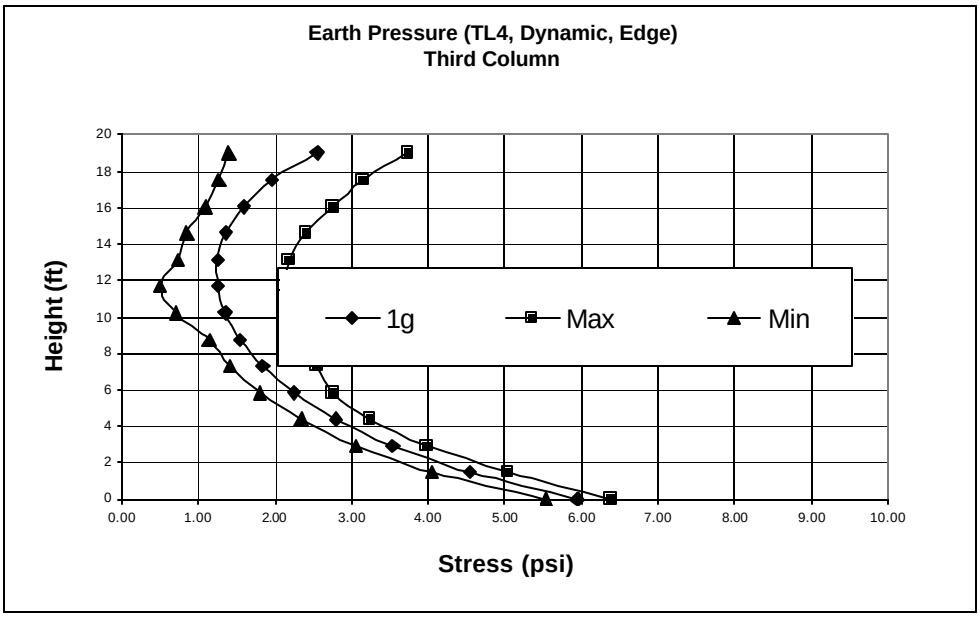


Figure A-11: Min, Max, and 1g earth pressure along the third column (TL4, Edge Hit, Impact).

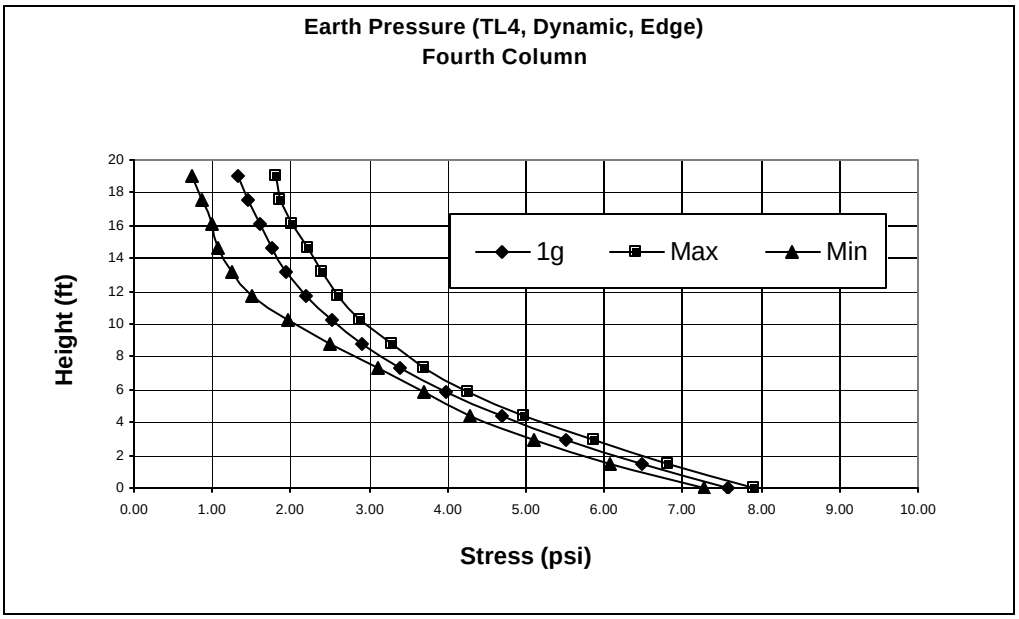


Figure A-12: Min, max and 1g earth pressure along the fourth column (TL4, Edge Hit, Impact).

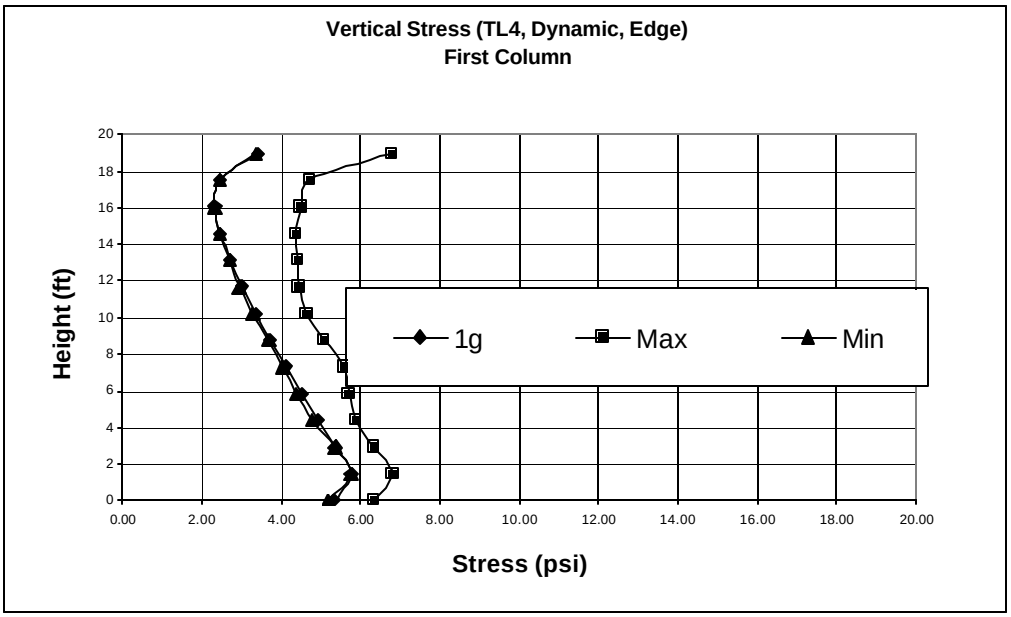


Figure A-13: Min, max and 1g vertical soil pressure along the first column (TL4, Edge Hit, Impact).

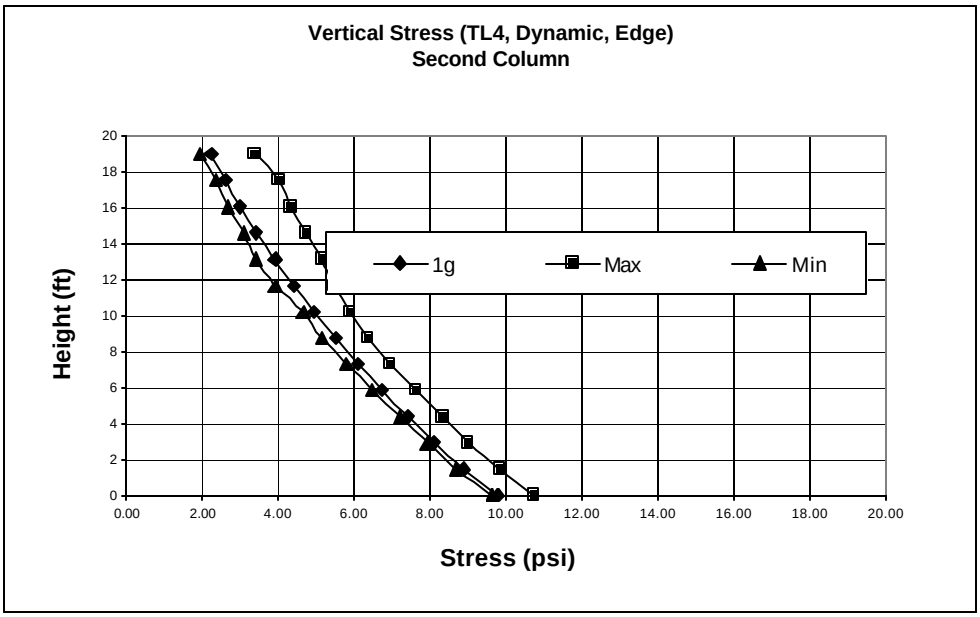


Figure A-14: Min, max and 1g vertical soil pressure along the second column (TL4, Edge Hit, Impact).

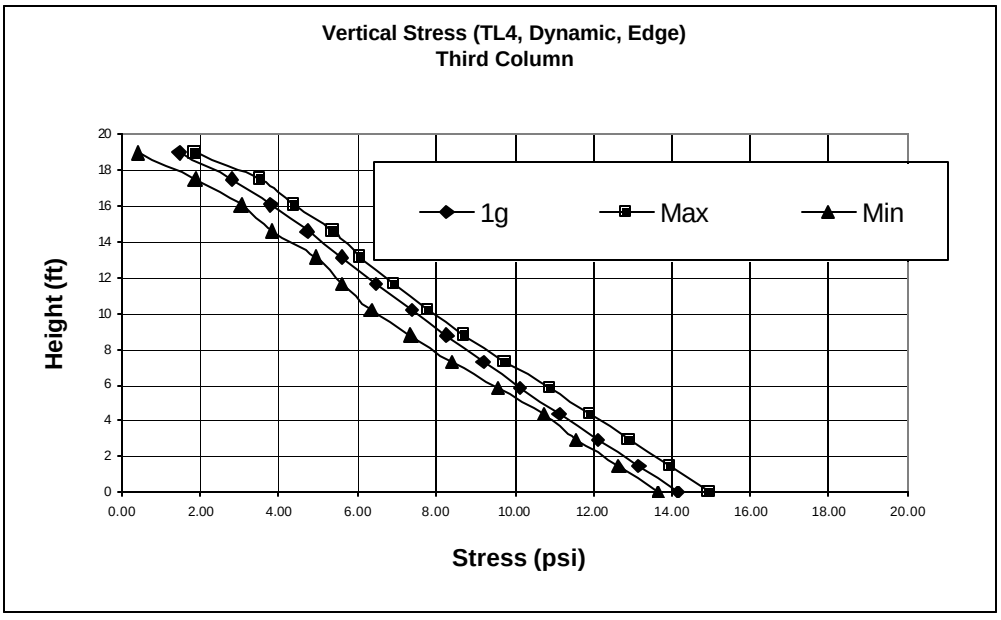


Figure A-15: Min, max and 1g vertical soil pressure along the third column (TL4, Edge Hit, Impact).

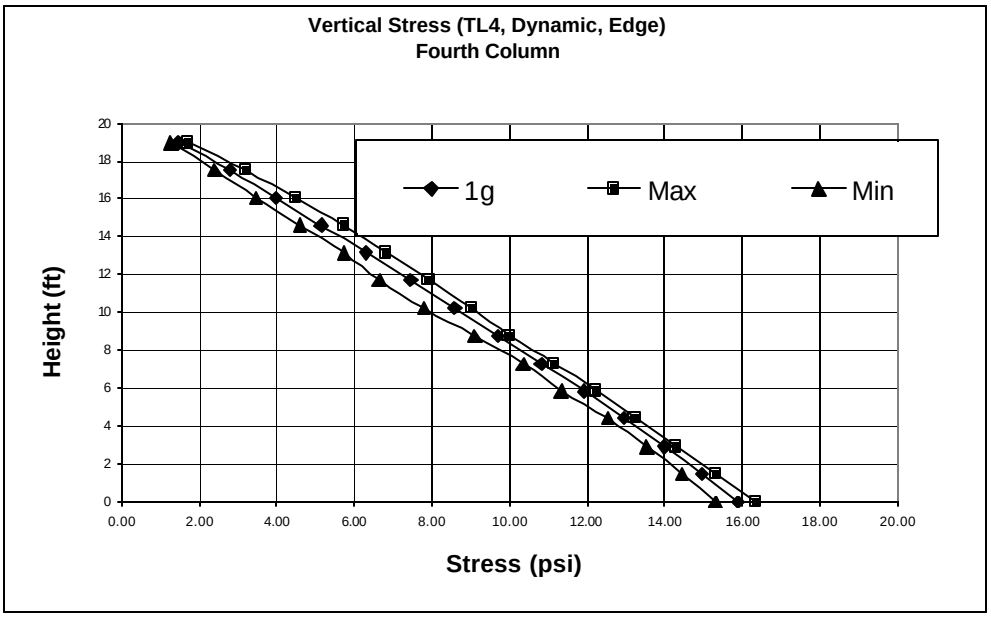


Figure A-16: Min, max and 1g vertical soil pressure along the fourth column (TL4, Edge Hit, Impact).

Type 7, TL5a, Static, Center

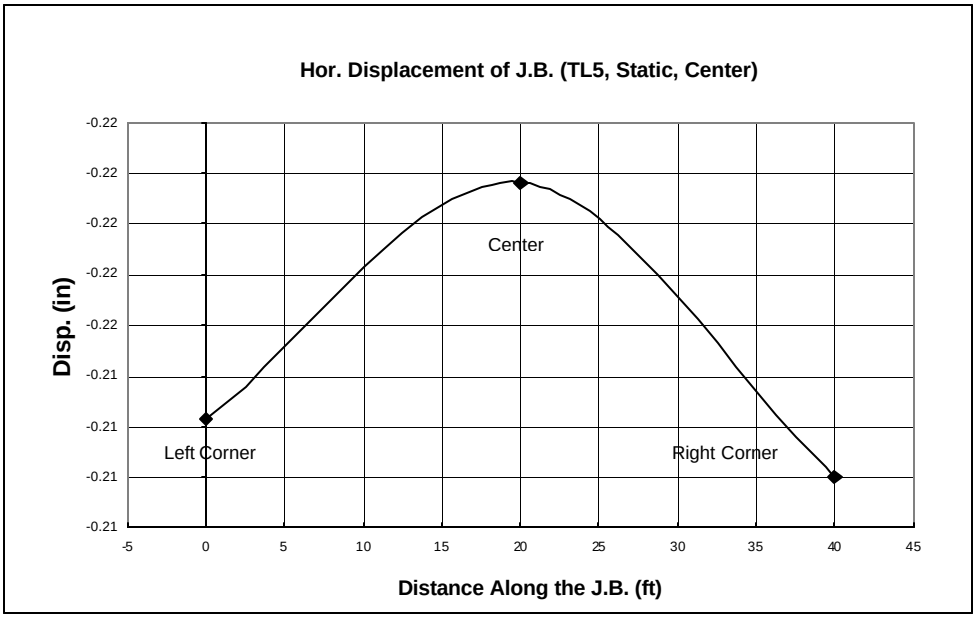


Figure A-17: Transverse displacement of edge and corner nodes of Type 7 barrier under TL5a

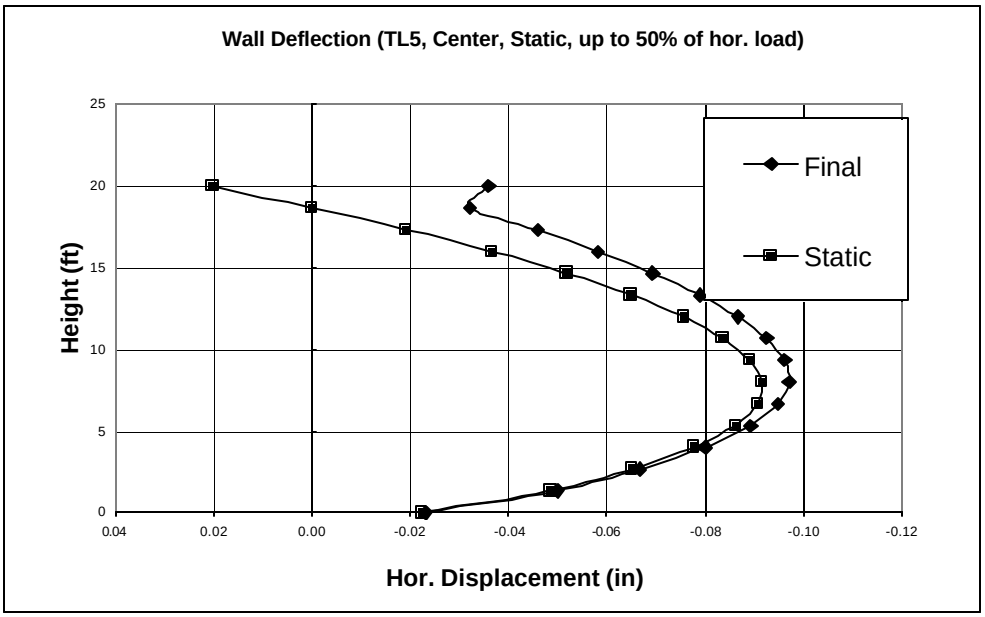


Figure A-18: Wall deflection (TL5a, Center Hit, Static).

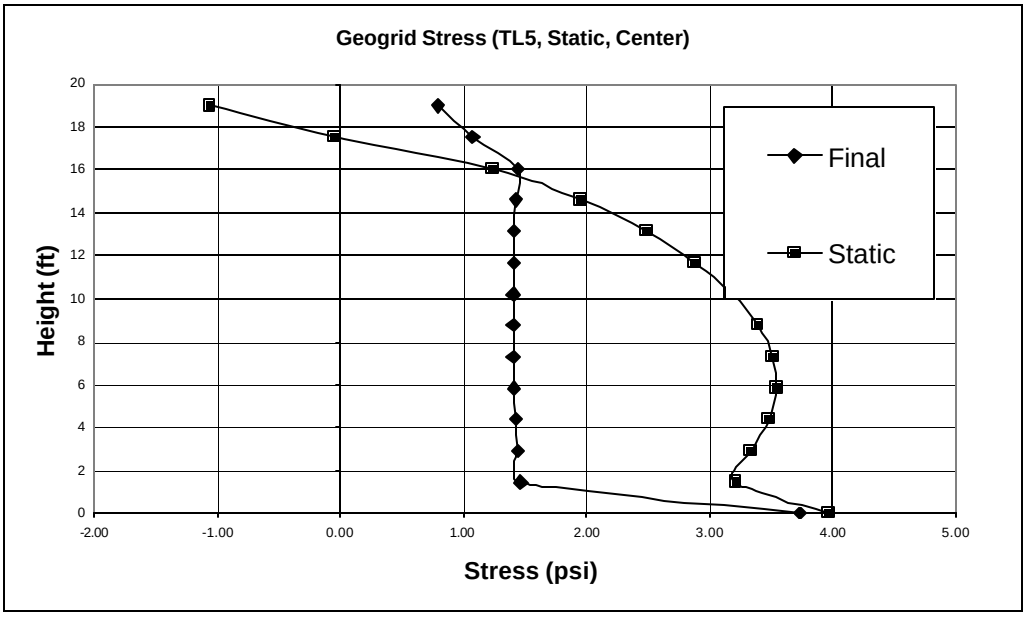


Figure A-19: Geogrid stresses along the wall connection (TL5a, Center Hit, Static).

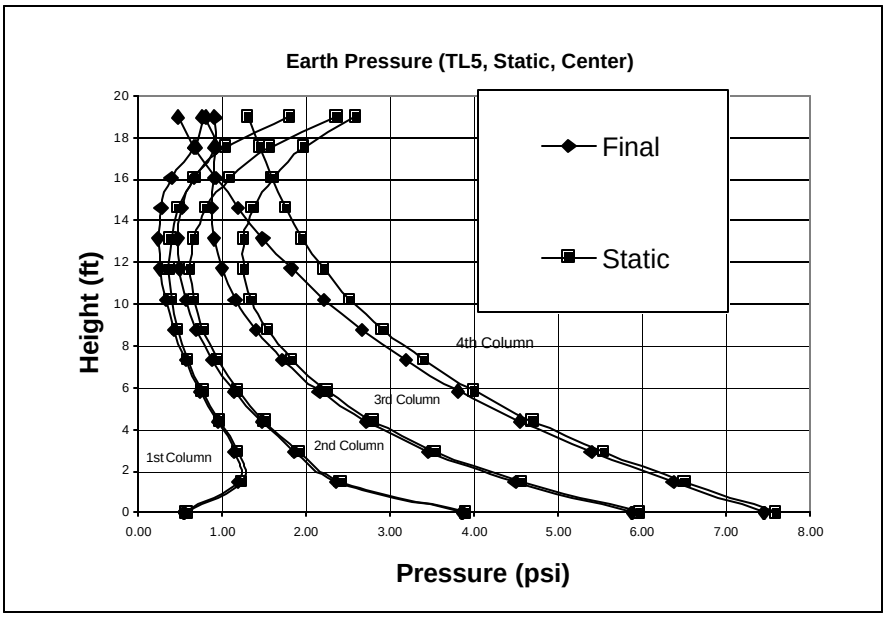


Figure A-20: Earth pressure distribution at four different locations (TL5a, Center Hit, Static).

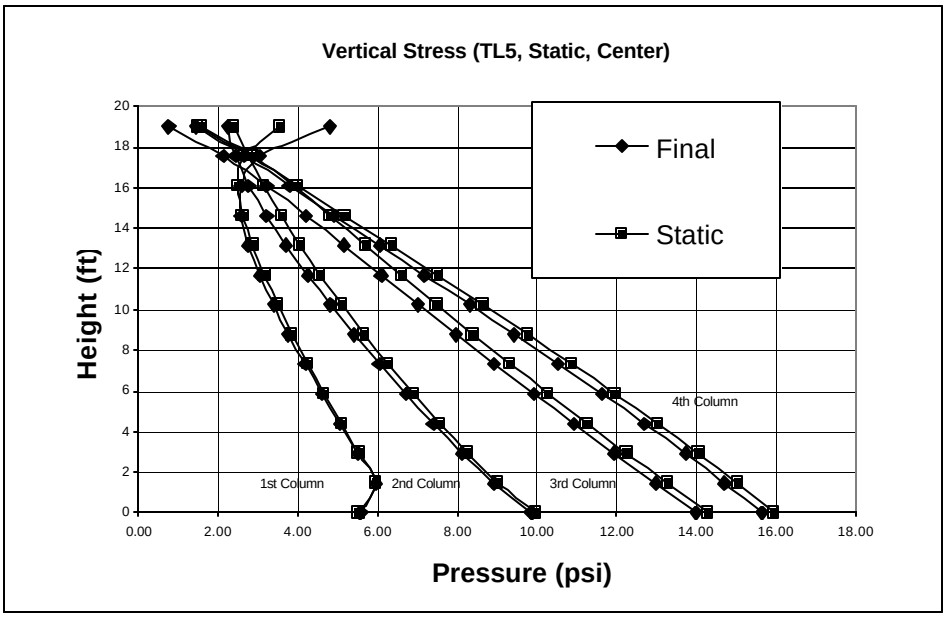


Figure A-21: Vertical soil pressure distribution at four different locations (TL5a, Center Hit, Static).

Type 7, TL5a, Static, Center

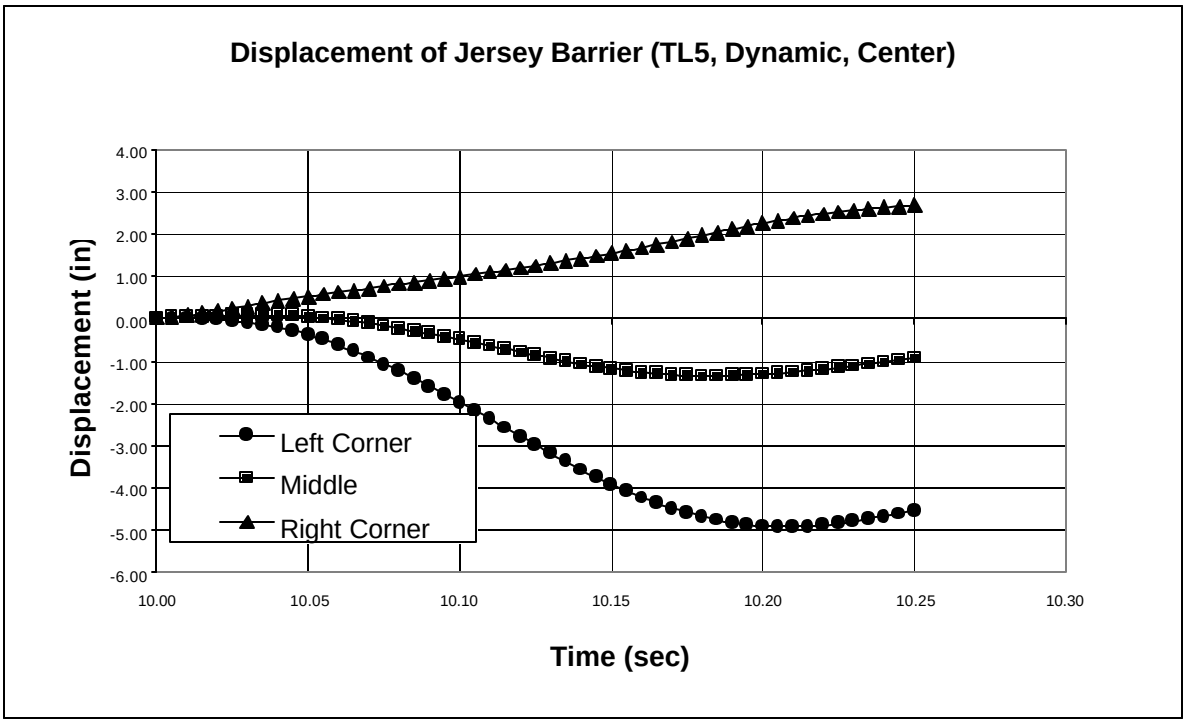


Figure A-22: Transverse displacement time history of edge and corner nodes of Type 7 barrier (TL5a, Center Hit, Impact)

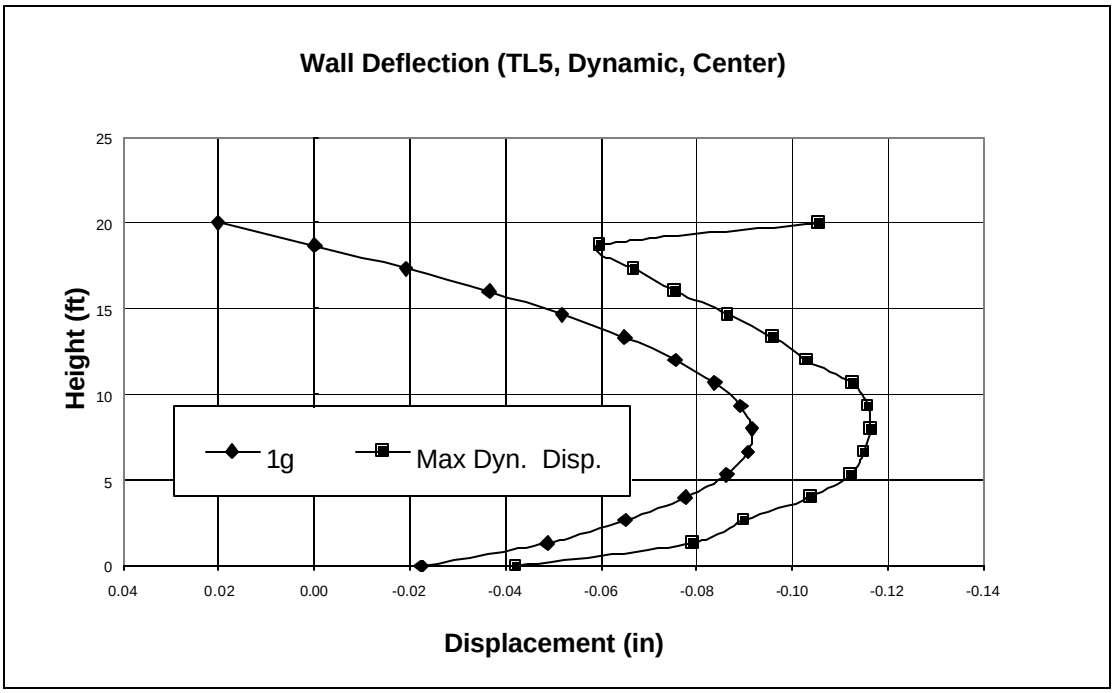


Figure A-23: Final wall deflection after impact load (TL5a, Center Hit, Impact)

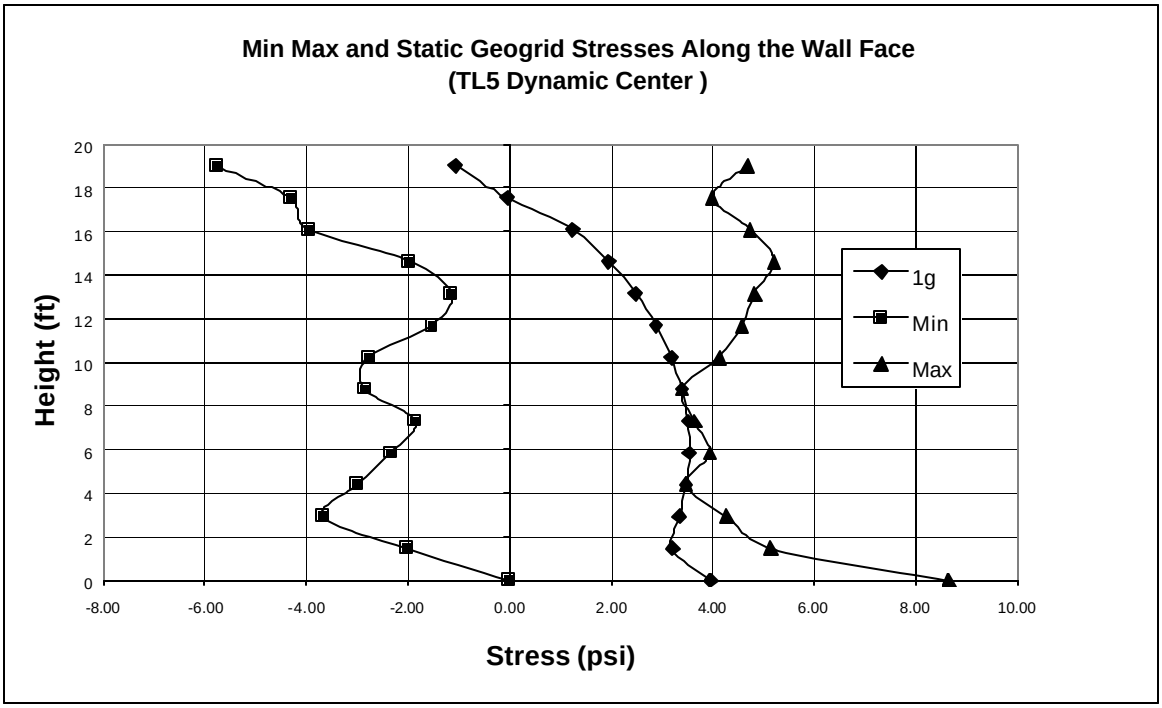


Figure A-24: Min, Max and 1g geogrid stresses along the wall face (TL5a, Center Hit, Impact)

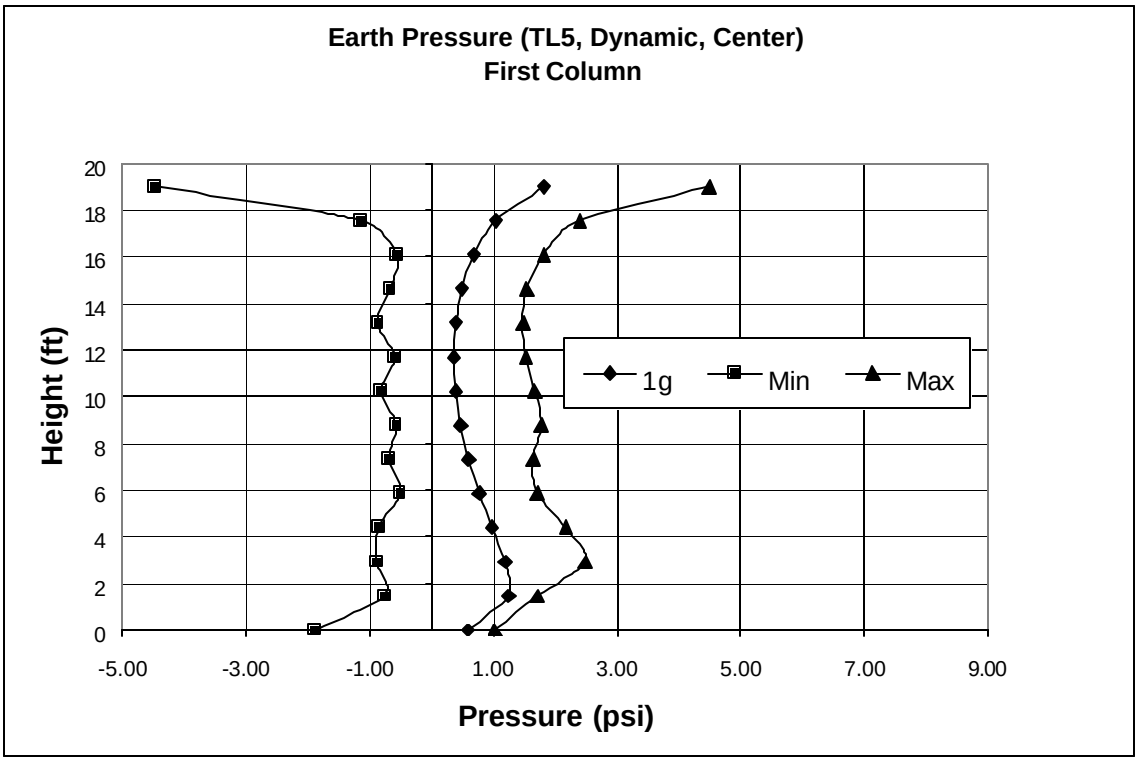


Figure A-25: Min, Max and 1g earth pressure along the first column (TL5a, Center Hit, Impact).

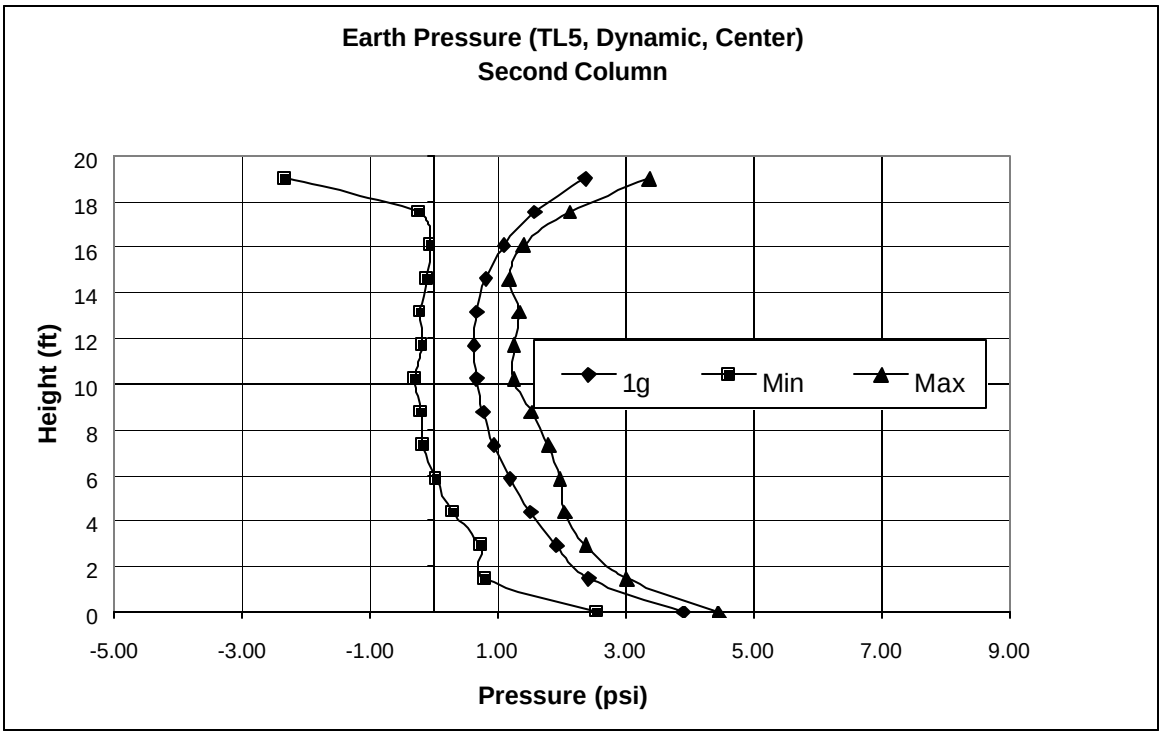


Figure A-26: Min, Max and 1g earth pressure along the second column (TL5a, Center Hit, Impact).

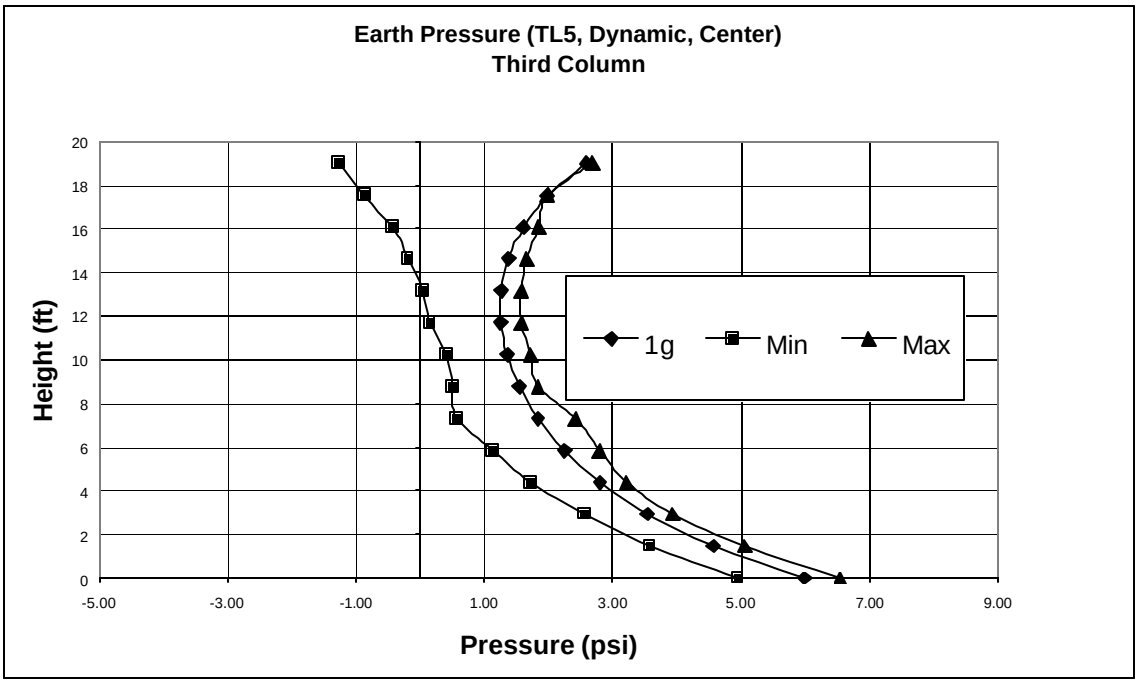


Figure A-27: Min, Max and 1g earth pressure along the third column (TL5a, Center Hit, Impact).

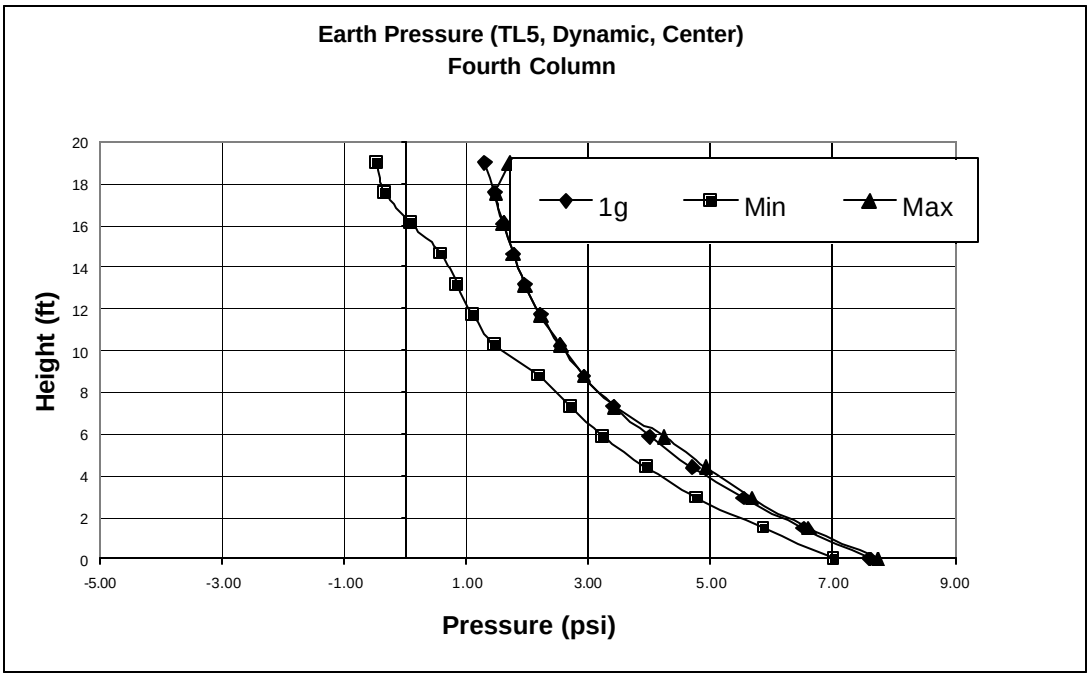


Figure A-28: Min, Max and 1g earth pressure along the fourth column (TL5a, Center Hit, Impact).

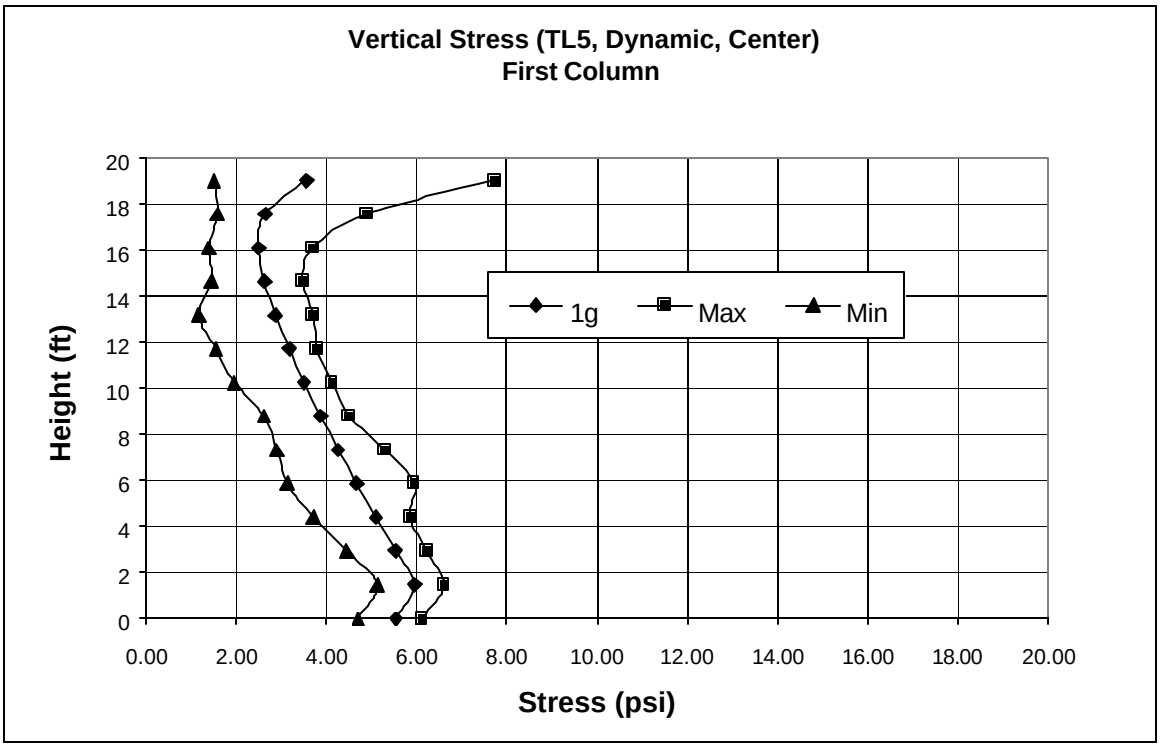


Figure A-29: Min, Max and 1g vertical soil pressure along the first column (TL5a, Center Hit, Impact).

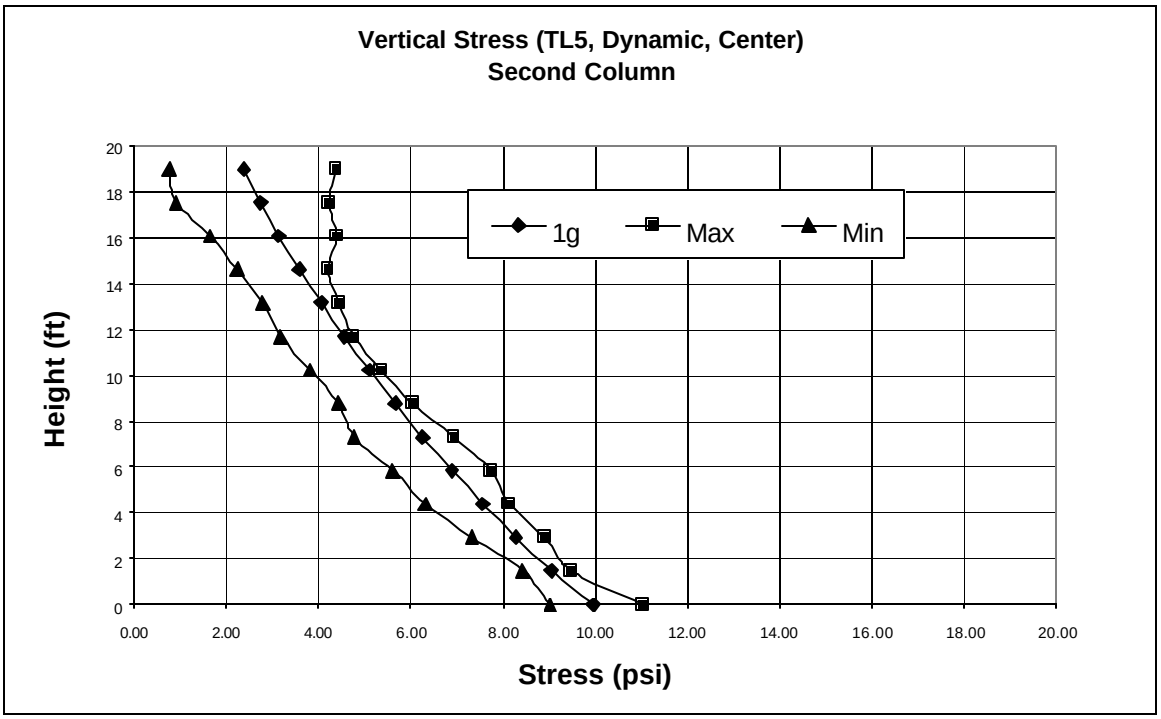


Figure A-30: Min, Max and 1g vertical soil pressure along the second column (TL5a, Center Hit, Impact).

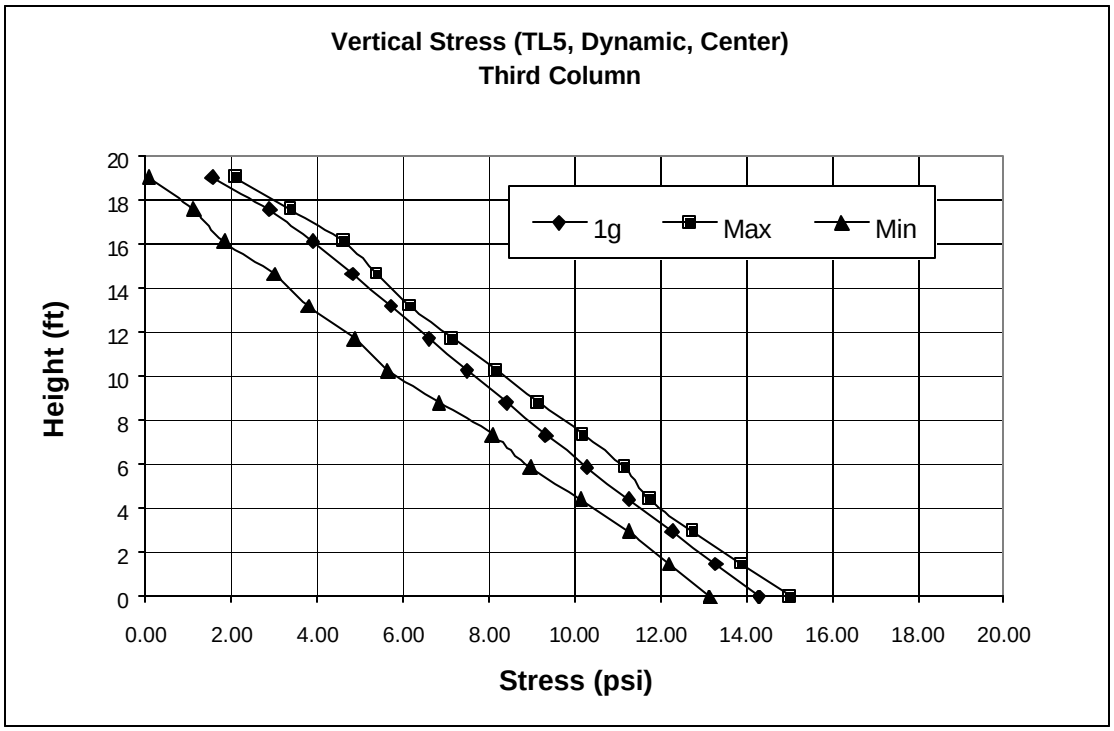


Figure A-31: Min, Max and 1g vertical soil pressure along the third column (TL5a, enter Hit, Impact).

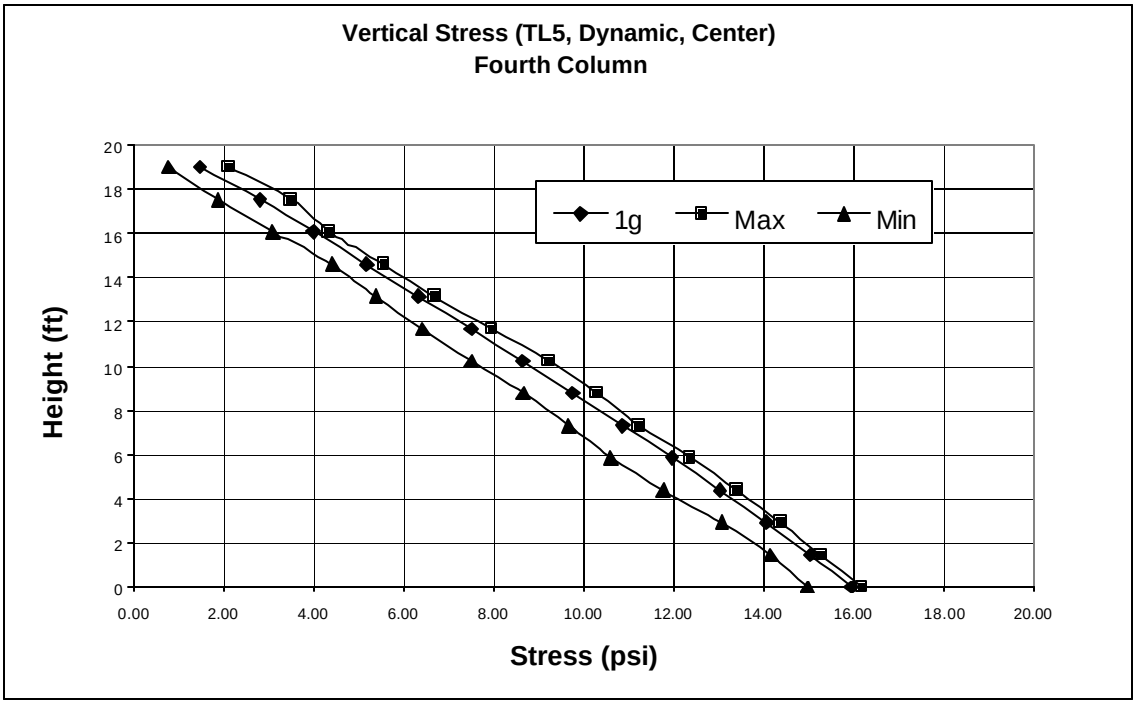


Figure A-32: Min, Max and 1g vertical soil pressure along the fourth column (TL5a, Center Hit, Impact).

APPENDIX B Figures for 400-ft Type 7 and Type 10 Rails

Type 7, Edge Hit, 400-ft, TL5a

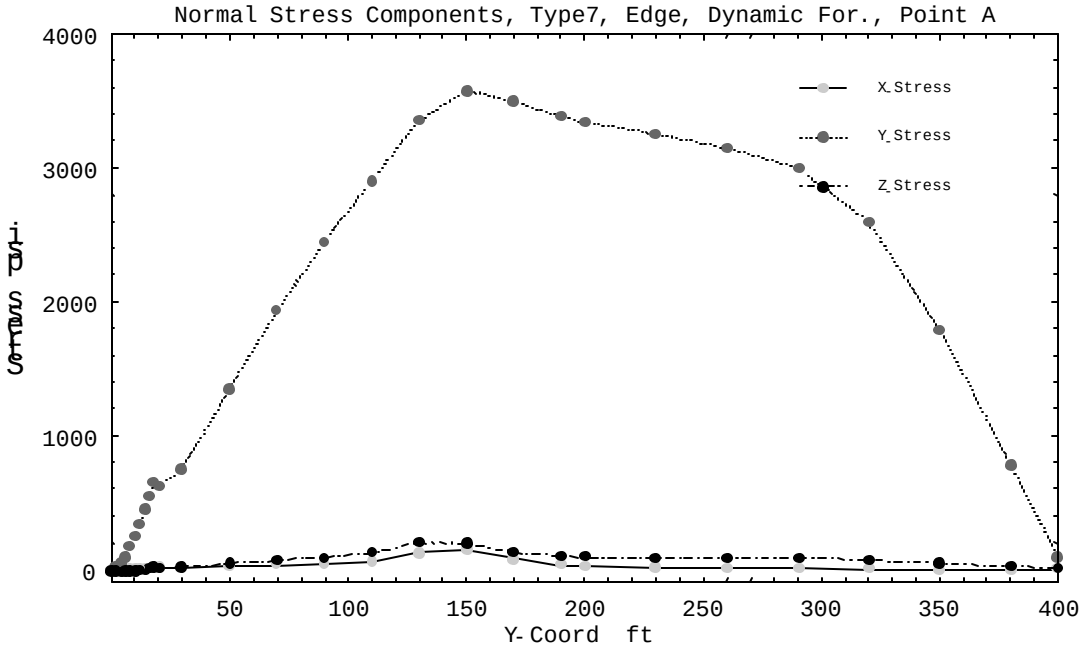


Figure B-1: Normal Stress components along point A of Type 7 Rail (400-ft, Edge Hit, Static, TL5a).

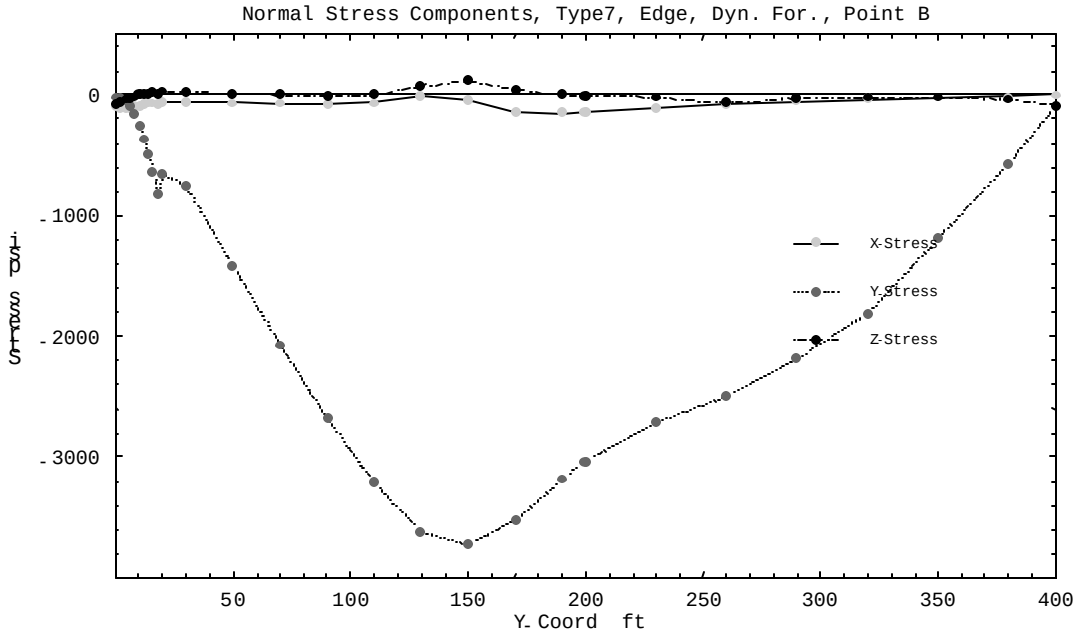


Figure B-2: Normal Stress components along point B of Type 7 Rail (400-ft, Edge Hit, Static, TL5a).

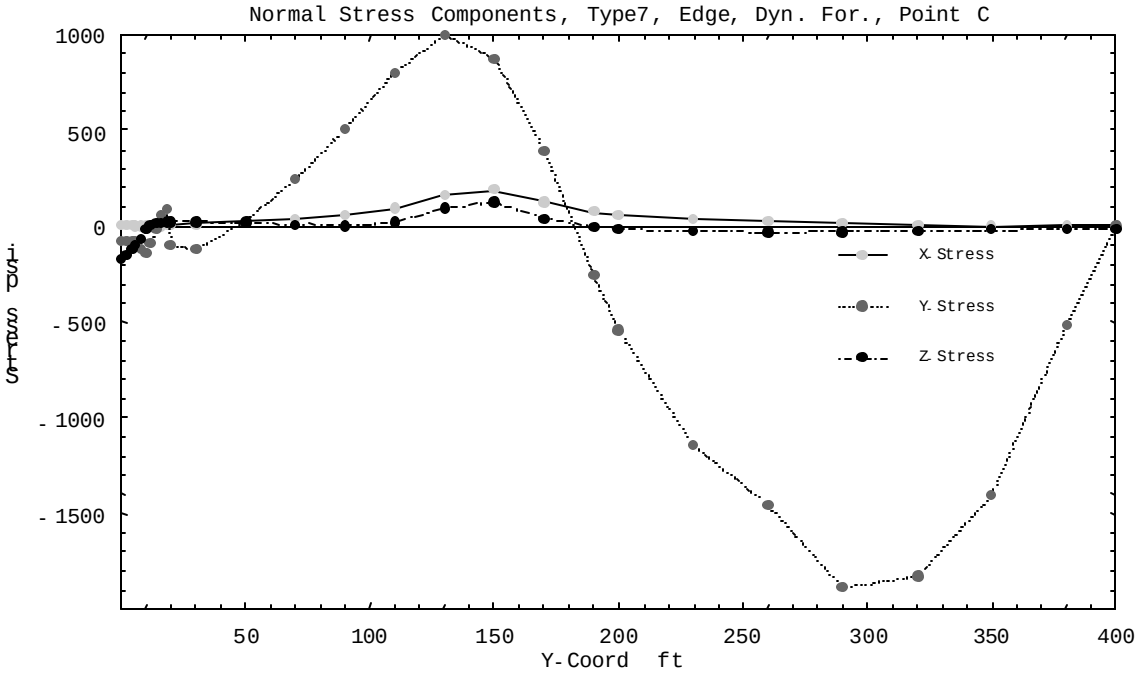


Figure B-3: Normal Stress components along point C of Type 7 Rail (400-ft, Edge Hit, Static, TL5a).

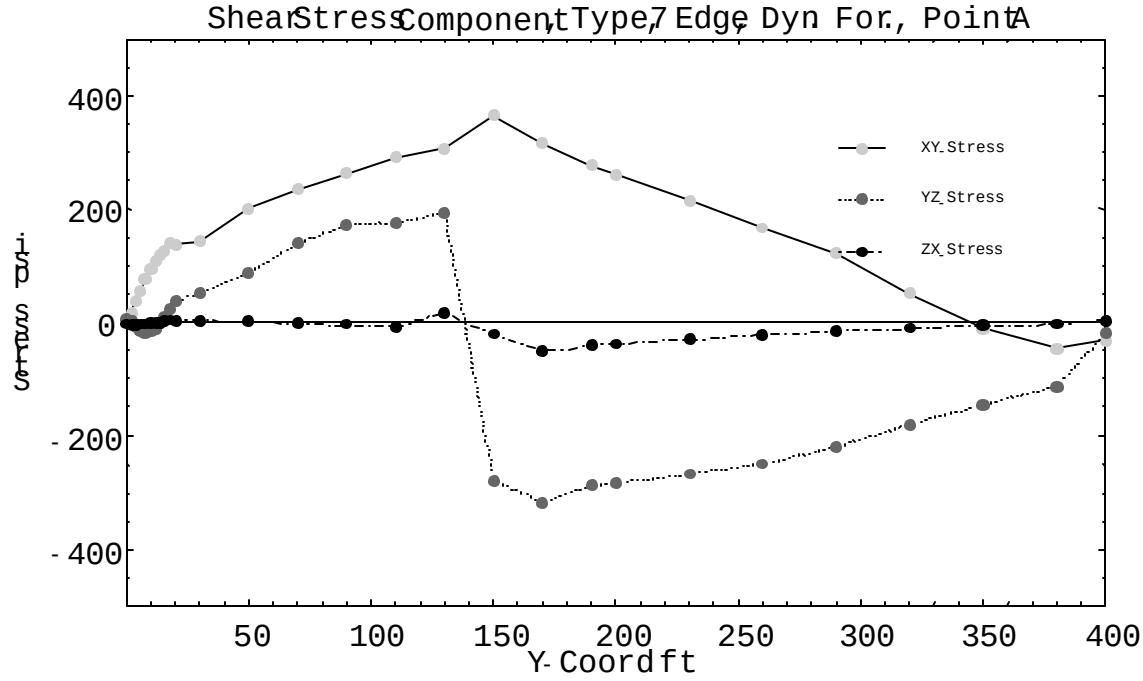


Figure B-4: Shear Stress components along point A of Type 7 Rail (400-ft, Edge Hit, Static, TL5a).

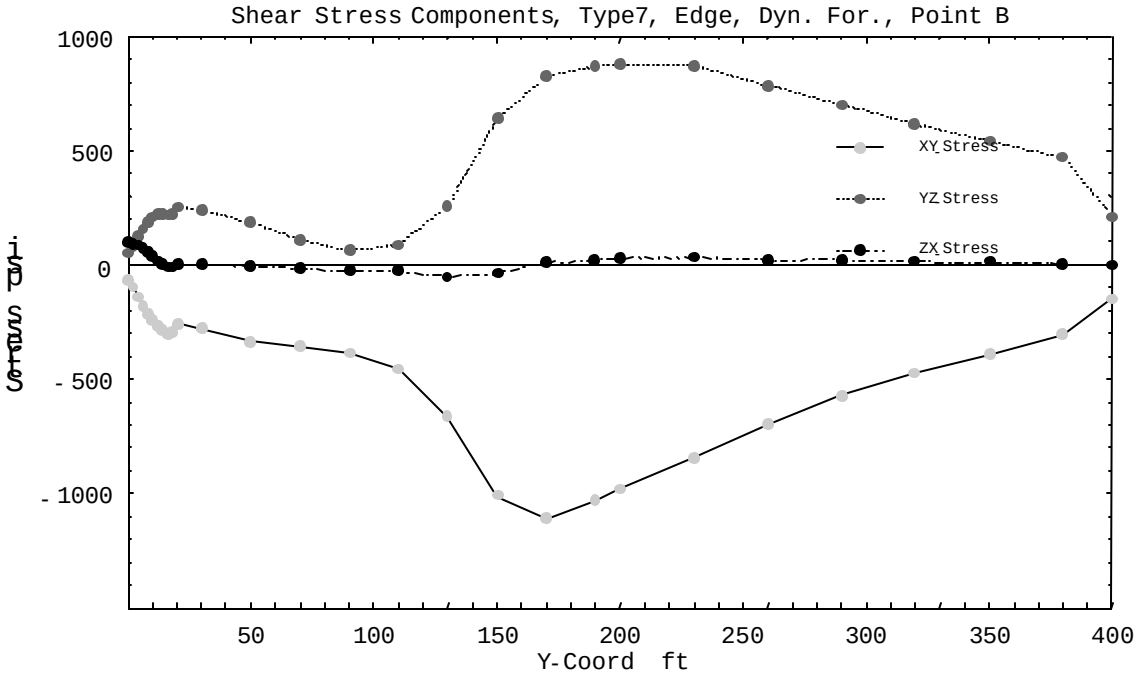


Figure B-5: Shear Stress components along point B of Type 7 Rail (400-ft, Edge Hit, Static, TL5a).

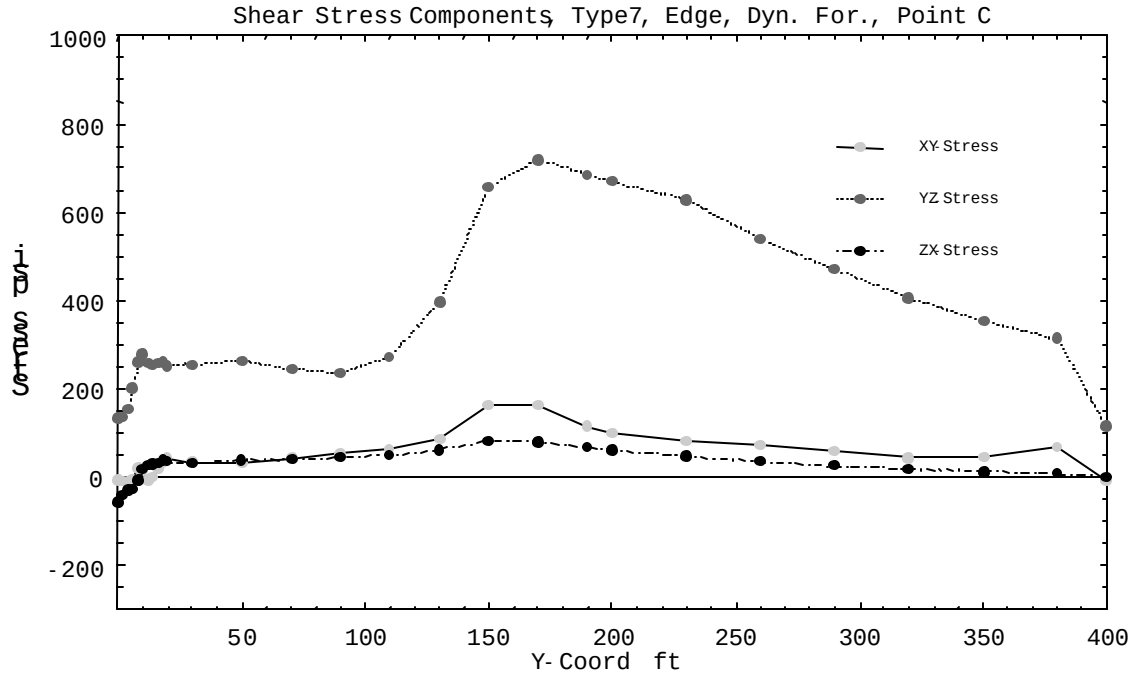


Figure B-6: Shear Stress components along point C of Type 7 Rail (400-ft, Edge Hit, Static, TL5a).

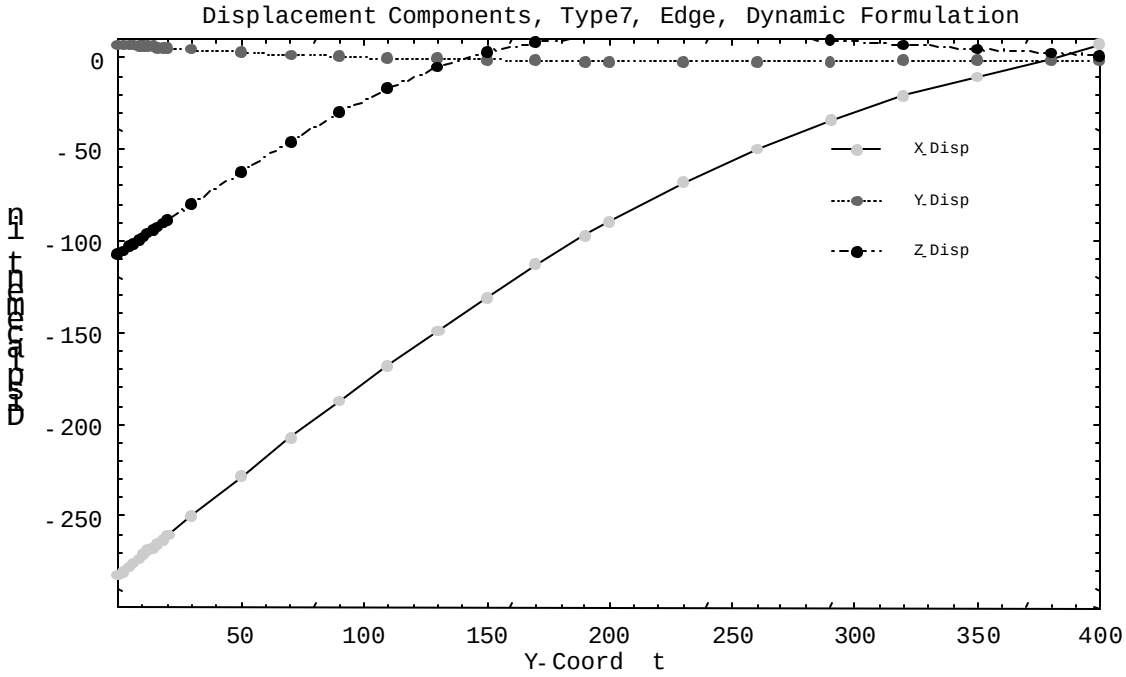


Figure B-7: Displacement components at point A of Type 7 Rail (400-ft, Edge Hit, Static, TL5a).

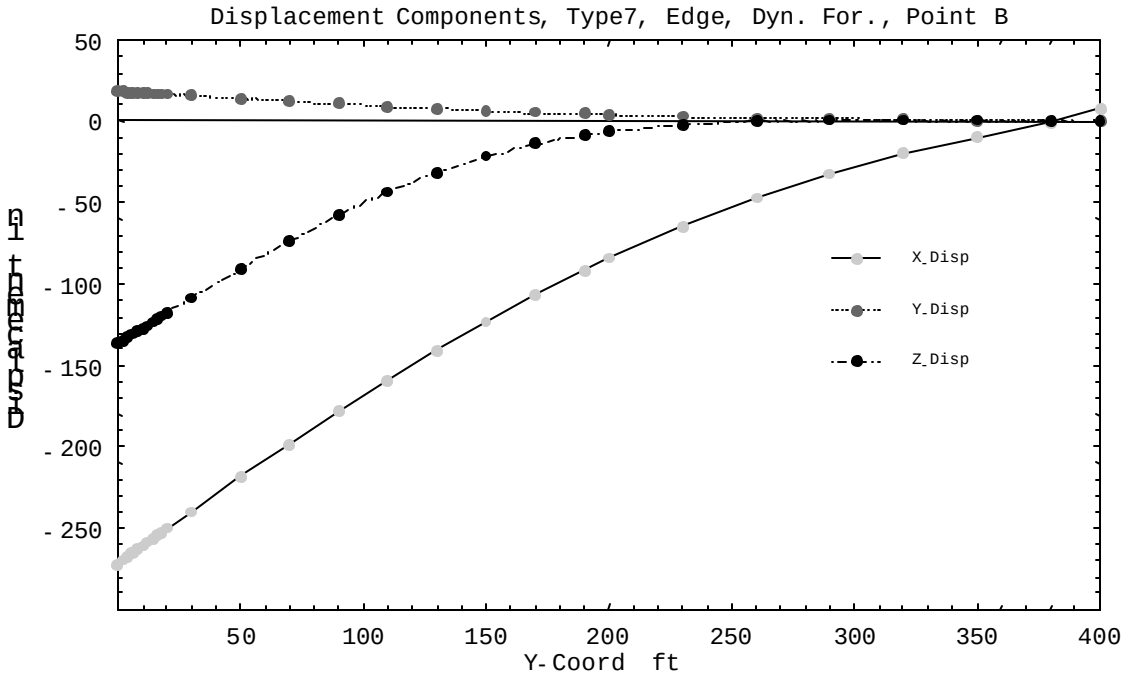


Figure B-8: Displacement components at point B of Type 7 Rail (400-ft, Edge Hit, Static, TL5a).

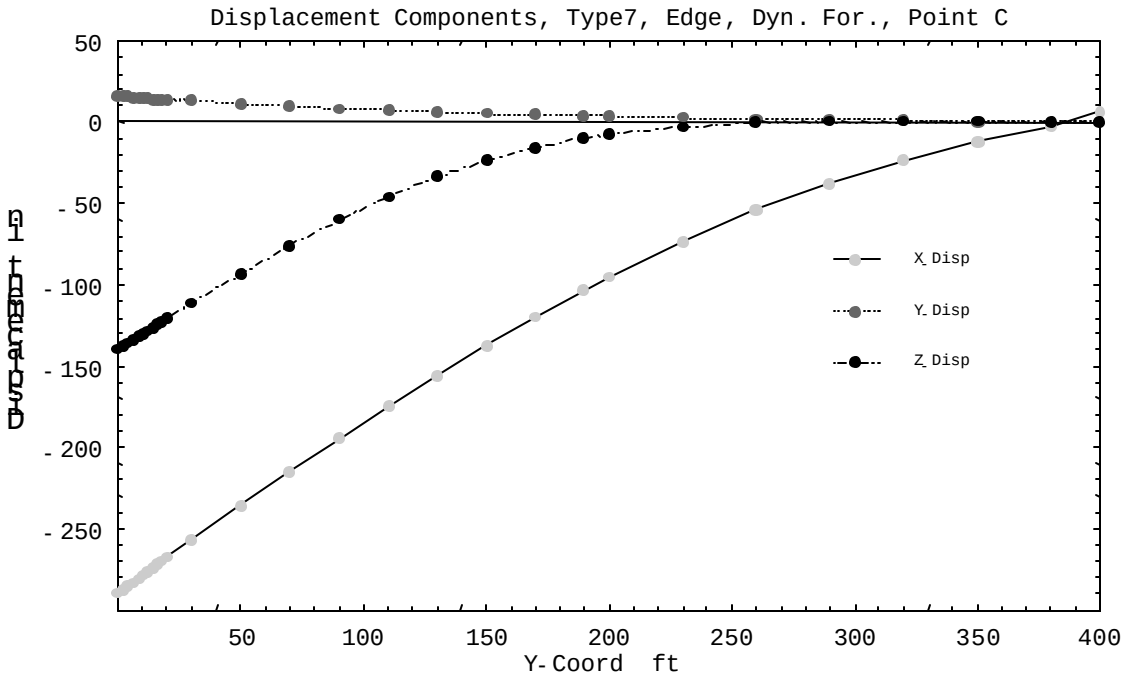


Figure B-9: Displacement components at point C of Type 7 Rail (400-ft, Edge Hit, Static, TL5a).

Type 10 Edge Hit

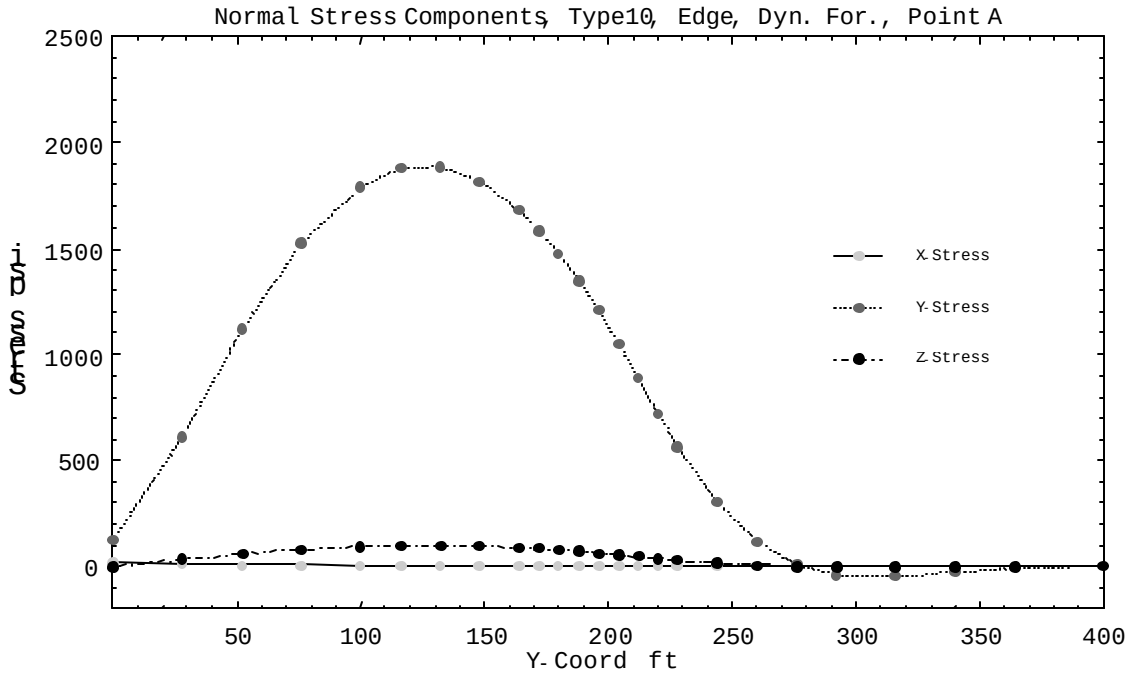


Figure B-10: Normal Stress components along point A of Type 10 Rail (400-ft, Edge Hit, Static, TL5a).

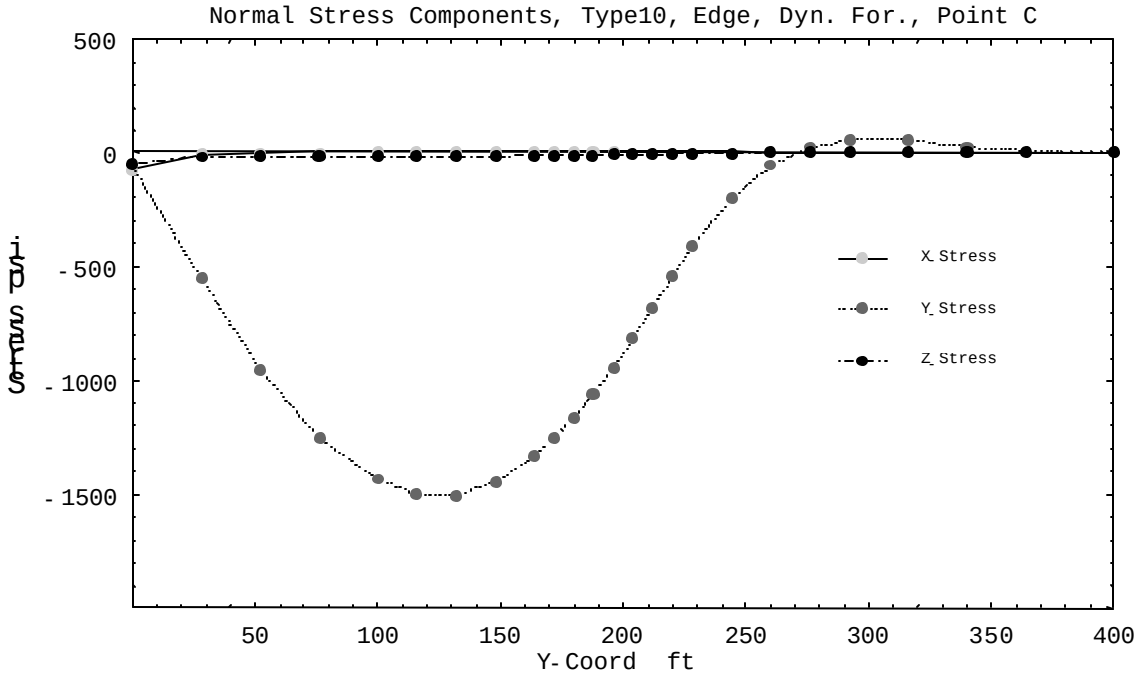


Figure B-11: Normal Stress components along point C of Type 10 Rail (400-ft, Edge Hit, Static, TL5a).

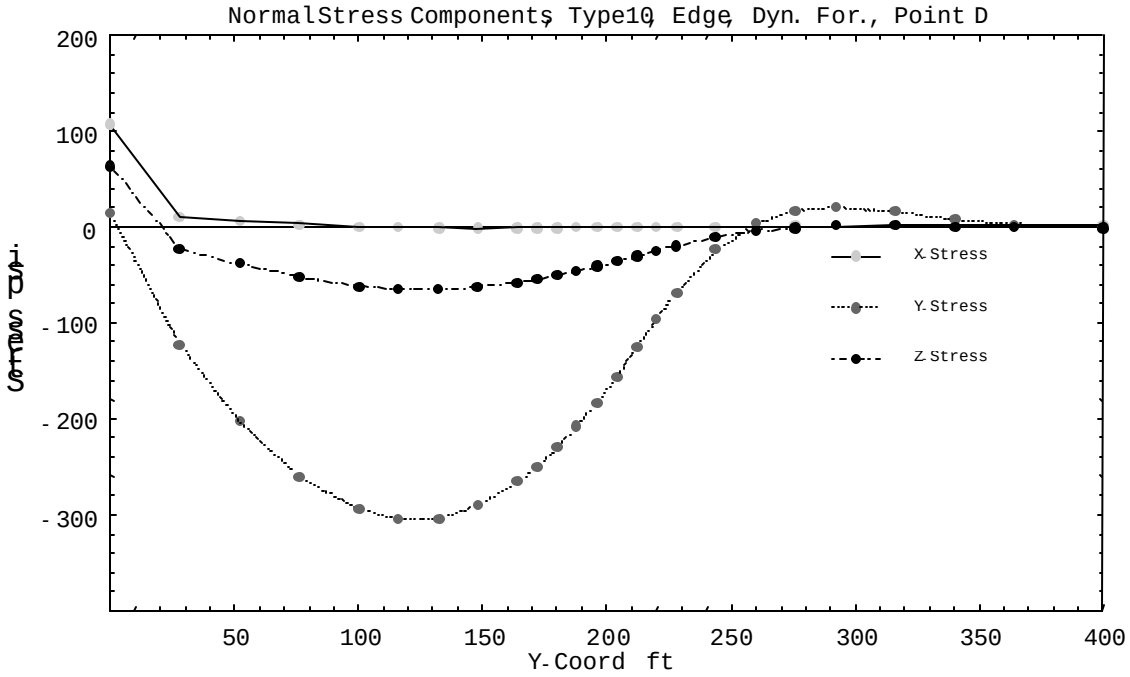


Figure B-12: Normal Stress components along point D of Type 10 Rail (400-ft, Edge Hit, Static, TL5a).

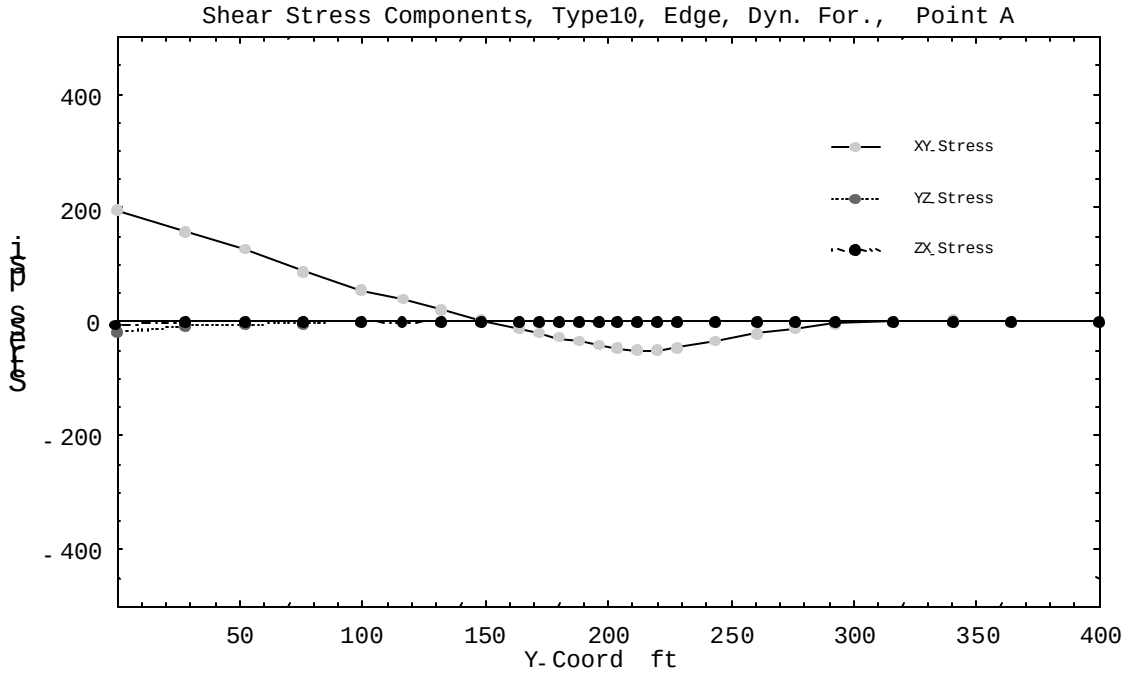


Figure B-13: Shear Stress components along point A of Type 10 Rail (400-ft, Edge Hit, Static, TL5a).

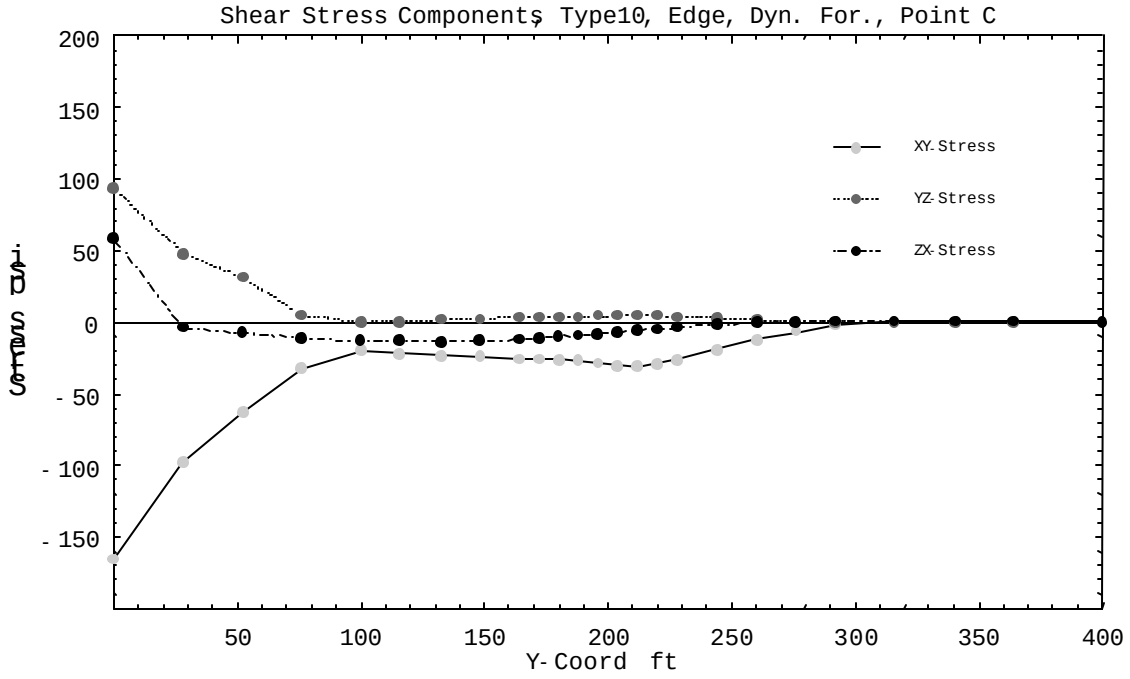


Figure B-14: Shear Stress components along point C of Type 10 Rail (400-ft, Edge Hit, Static, TL5a).

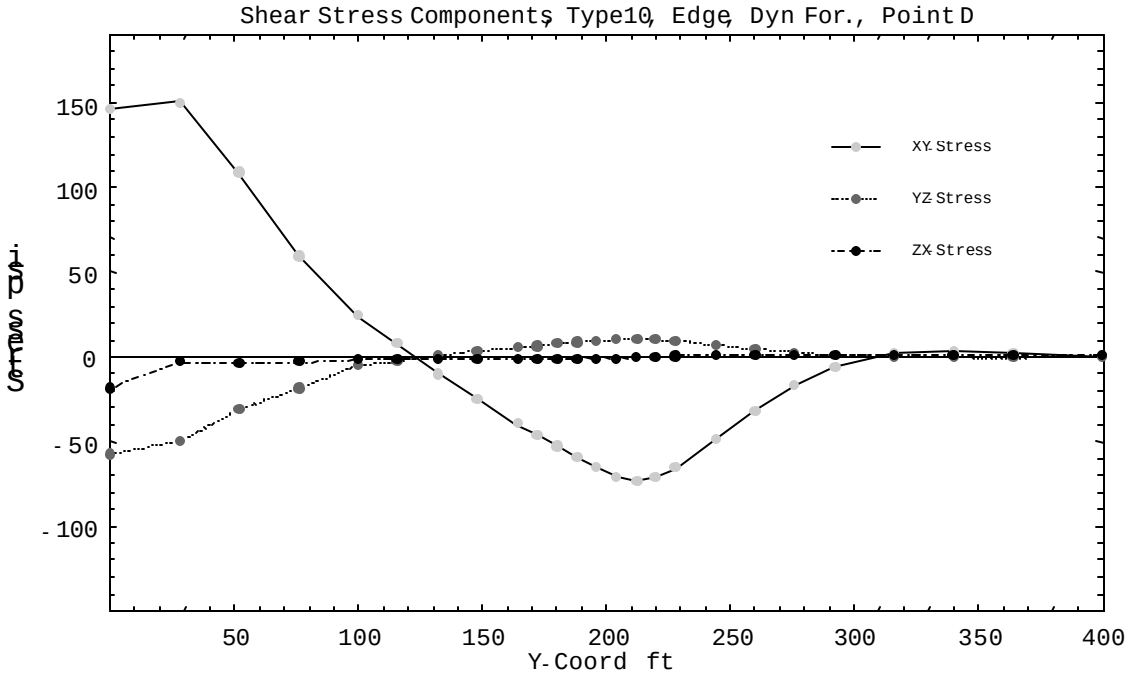


Figure B-15: Shear Stress components along point D of Type 10 RAil (400-ft, Edge Hit, Static, TL5a).

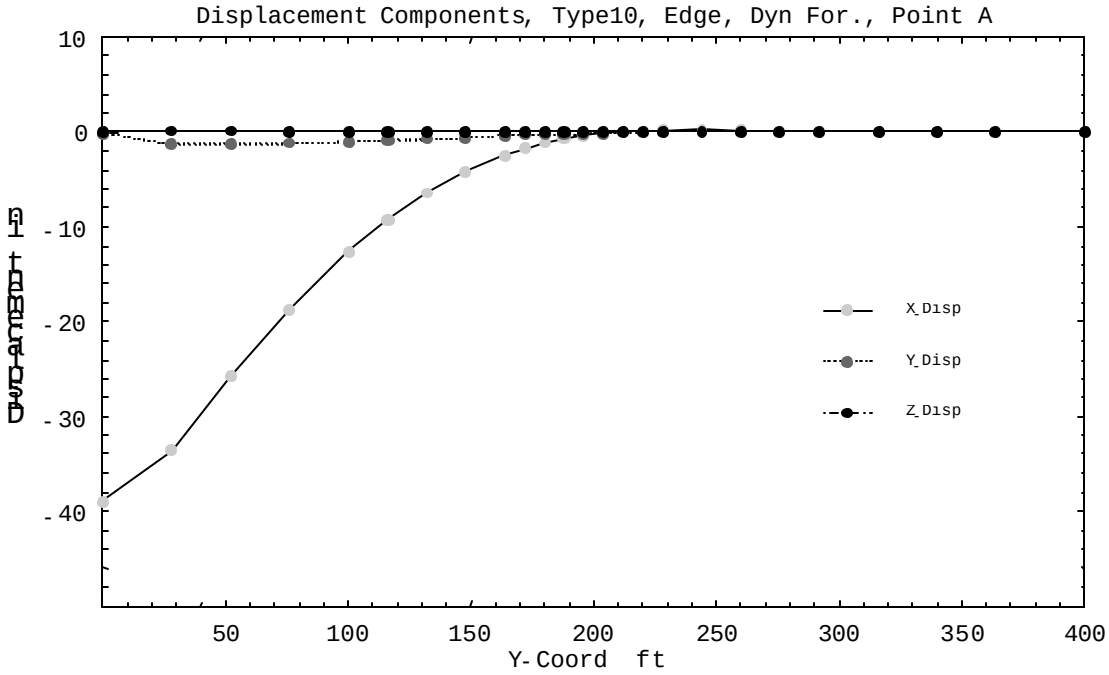


Figure B-16: Displacement components at point A of Type 10 Rail (400-ft, Edge Hit, Static, TL5a).

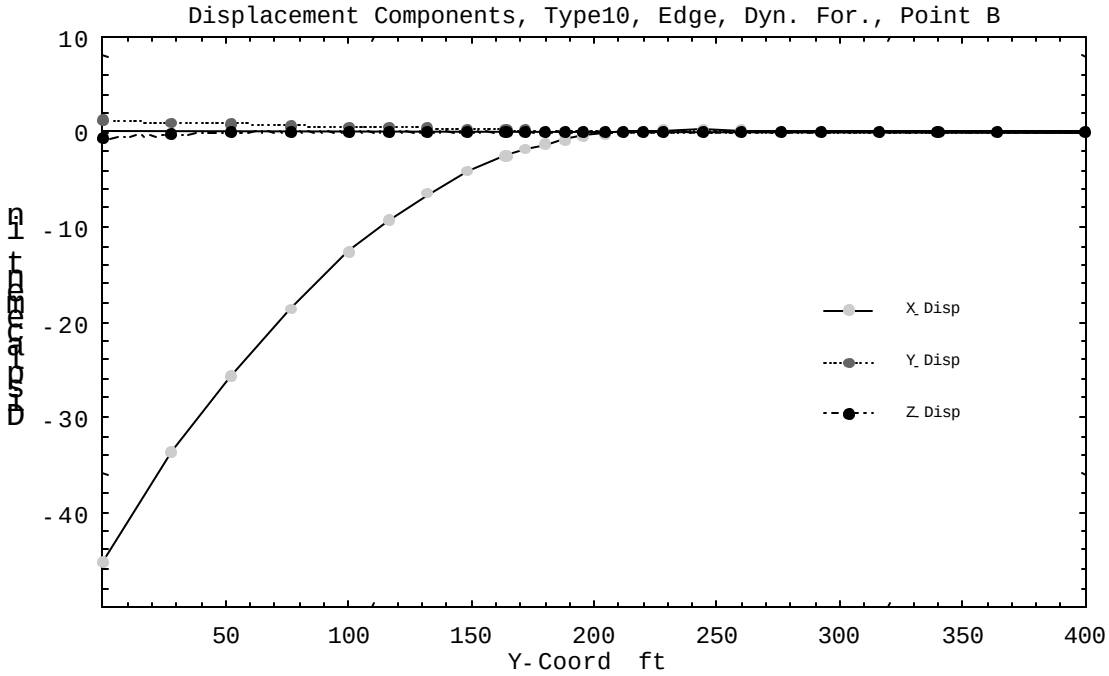


Figure B-17: Displacement components at point B of Type 10 Rail (400-ft, Edge Hit, Static, TL5a).

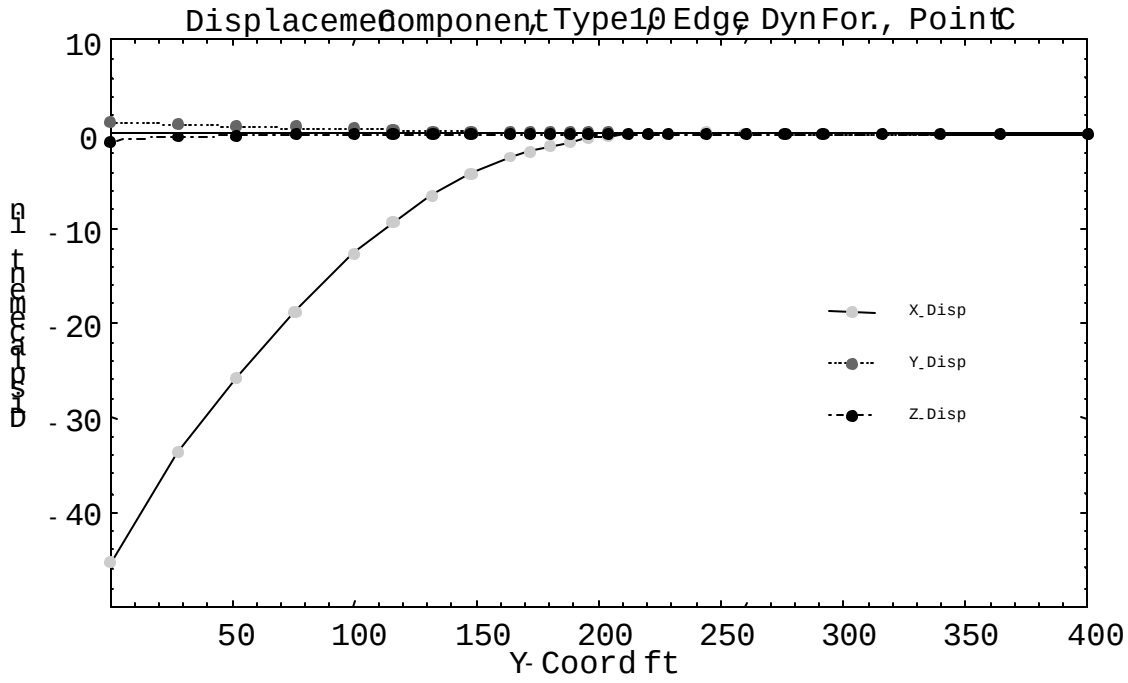


Figure B-18: Displacement components at point C of Type 10 Rail (400-ft, Edge Hit, Static, TL5a).

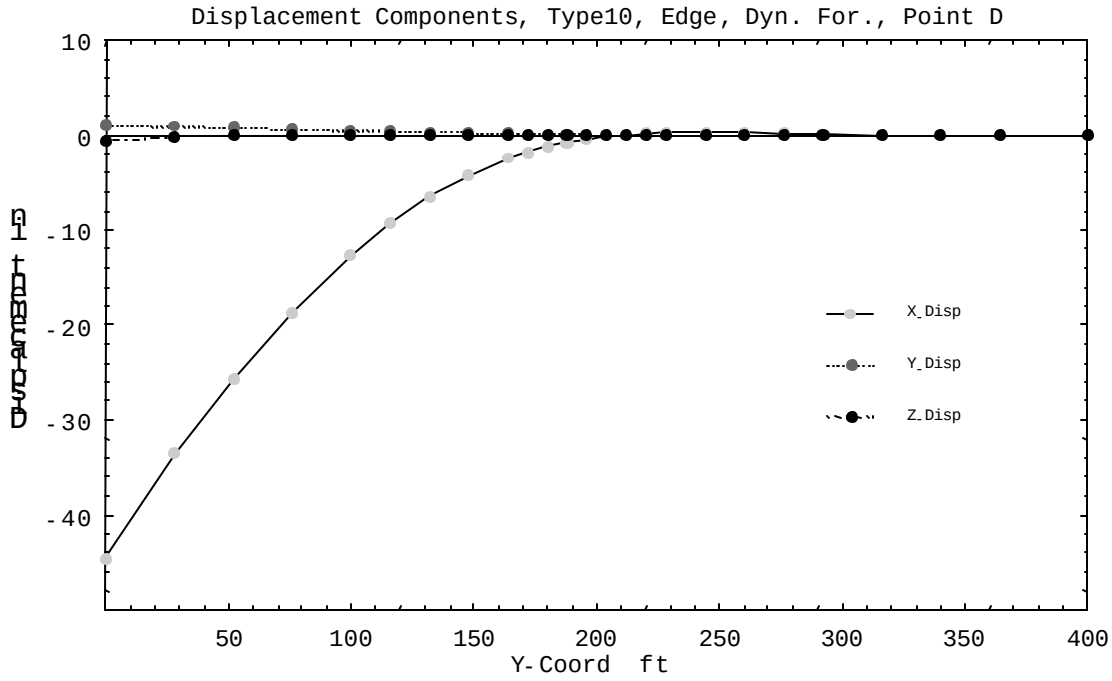


Figure B-19: Displacement components at point D of Type 10 Rail (400-ft, Edge Hit, Static, TL5a).

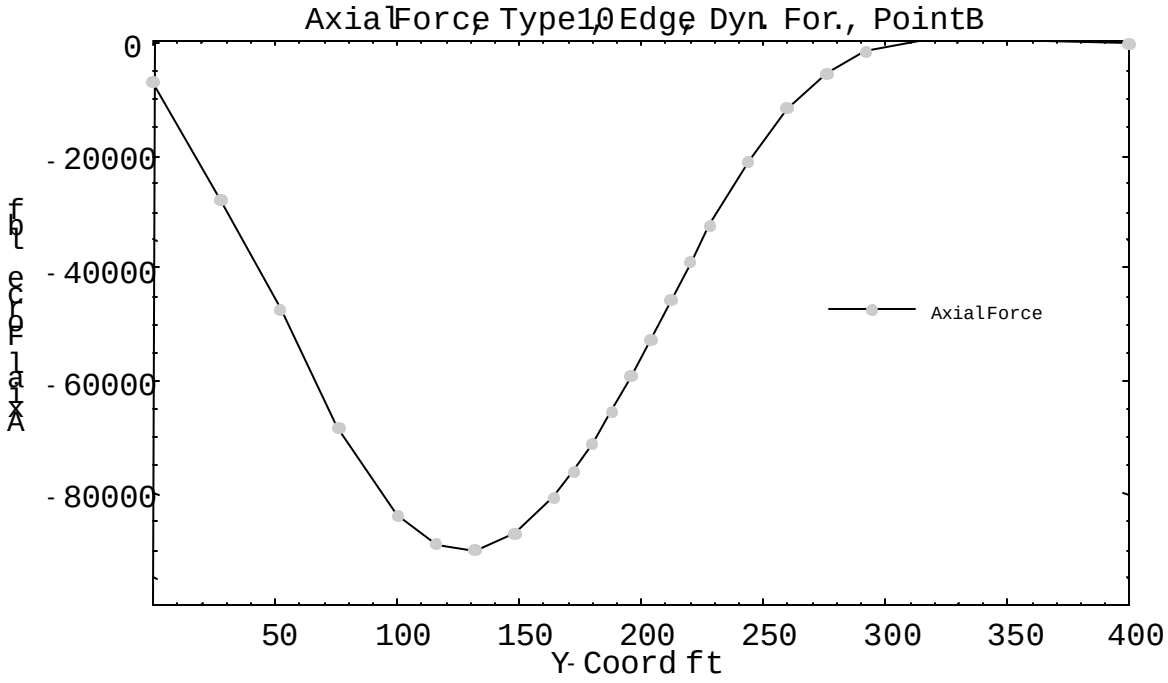


Figure B-20: Axial force distribution in the beam elements along point B of Type 10 Rail (400-ft, Edge Hit, Static, TL5a).

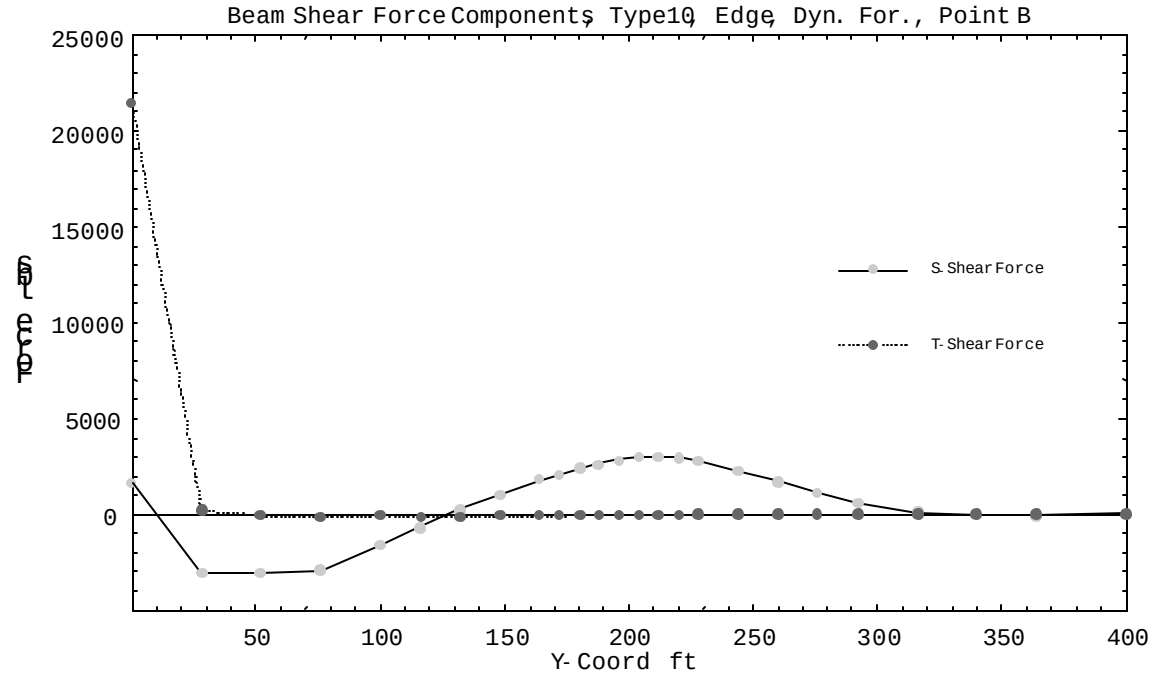


Figure B-21: Shear force components in the beam elements along point B of Type 10 Rail (400-ft, Edge Hit, Static, TL5a).